



FCTUC FACULDADE DE CIÊNCIAS
E TECNOLOGIA
UNIVERSIDADE DE COIMBRA

Joana Isabel Santos Paiva

Predicting lapses in attention: a study of brain oscillations, neural synchrony and eye measures

*Dissertation presented to the Faculty of Sciences
and Technology of the University of Coimbra to
obtain a Master's degree in Biomedical Engineering*

Supervisor:

Dr. Maria Ribeiro (Institute for Biomedical Imaging and Life
Sciences, Faculty of Medicine, University of Coimbra)

Coimbra, 2014

This work was developed with the collaboration with:

Institute for Biomedical Imaging and Life Sciences, Faculty
of Medicine, University of Coimbra



Faculty of Medicine, University of Coimbra



Esta cópia da tese é fornecida na condição de que quem a consulta reconhece que os direitos de autor são pertença do autor da tese e que nenhuma citação ou informação obtida a partir dela pode ser publicada sem a referência apropriada.

This copy of the thesis has been supplied on condition that anyone who consults it is understood to recognize that its copyright rests with its author and that no quotation from the thesis and no information derived from it may be published without proper acknowledgement.

Acknowledgements

Agradeço à minha orientadora, Dr.^a Maria Ribeiro, por toda a disponibilidade, apoio, pelos conhecimentos que me transmitiu e, especialmente, devido à confiança que depositou no meu trabalho.

Agradeço igualmente a todos os elementos da equipa do IBILI, pela forma como me receberam e pela ajuda que me prestaram ao longo de todo o projeto. Agradeço especialmente ao Gabriel Costa pelas discussões construtivas e pela ajuda prestada. Agradeço igualmente ao João Castelhana pela sua disponibilidade e por todas as dúvidas que me terá esclarecido.

Gostaria também de agradecer toda a ajuda prestada pela Professora Petia Georgieva da Universidade de Aveiro e por todos os seus conselhos relevantes para o desenvolvimento do projeto.

Agradeço também todo o acompanhamento dado pelo Professor Miguel Morgado, coordenador do Mestrado Integrado em Engenharia Biomédica, ao longo de todo o curso.

Devo um especial agradecimento aos meus avós por todo o esforço ao longo destes cinco anos, uma vez que sem eles o meu ingresso e permanência na Universidade não se teria concretizado. Agradeço igualmente aos meus pais, por toda a dedicação, paciência, preocupação, afeto e incentivo, especialmente durante este ano letivo. Igualmente sem eles, nada disto seria possível.

Desejo agradecer também ao João por toda a ajuda, apoio e paciência, especialmente durante o desenvolvimento do presente projeto, mas também ao longo de todo o curso. Por todo o afeto, carinho e compreensão prestadas. Agradeço-lhe igualmente todo o esforço e incentivo para que todos os meus objetivos fossem cumpridos.

Presto também um especial agradecimento à D. Olívia por todo o apoio e incentivo durante os momentos menos bons pelos quais terei passado.

Devo um agradecimento a todas as minhas amigas Sofia Prazeres, Daniela Martins, Diana Capela, Patrícia Santos, Sara Santos, Miriam Santos, Carolina Fernandes, Marta Pinto, por todos os momentos inesquecíveis durante a nossa vida académica. Por todo o apoio, carinho, amizade, companheirismo e, especialmente, sinceridade! Estaremos

sempre unidas. Agradeço igualmente aos meus amigos de Santa Maria da Feira por todo o apoio.

Expresso também agradecimento à Tânia Pereira e ao Pedro Vaz por toda a ajuda que me disponibilizaram, assim como pelas nossas interessantes conversas e por todo o trabalho que desenvolvemos em equipa durante estes dois últimos anos.

Por fim, tenho ainda a agradecer a todos os participantes deste estudo, pela sua colaboração e disponibilidade.

A todos um sincero obrigada,
Joana Isabel Santos Paiva

Abstract

Attention is defined as the maintenance of stable goal-directed behaviour during task performance. However, attention levels fluctuate with time due to internal (brain-driven) or external (stimulus-driven) events. Importantly, these moment-to-moment fluctuations in attention are exacerbated in disorders affecting brain function. In particular, enhanced fluctuations of attention levels are observed in children with Attention-Deficit/Hyperactivity Disorder (ADHD). The consequences of those fluctuations can be fairly benign such as not detecting a certain external stimuli; whereas in specific contexts, as driving scenarios or hazard situations, they can lead to tragedies. Notably, the detection of lapses in attention even before these happen, could avoid catastrophic consequences. Previous studies suggest that certain features of the electrophysiological (EEG) signal and of eye movement or pupil diameter are related to lapses of attention. The aim of this work was to determine if these parameters could be used for predicting attention lapses.

It has been shown that the state of attention is controlled by an activation trade-off between the attentional brain networks, which are responsible for the maintenance of sustained attention, during attentionally demanding tasks; and the Default-Mode Network (DMN), characterized by a set of brain regions active during resting states. Fluctuations in the activity of these two networks correlate with the occurrence of attention lapses. In addition, fluctuations in attention are associated with changes in brain oscillations. Furthermore, it has been established that changes in eye parameters, such as pupil diameter or gaze position, reflect changes related with brain activation events which underlie human sensory processing and cognition.

Twenty young healthy adults were recruited for this study. EEG signals and eye activity patterns were acquired during performance of a choice reaction time task. In these type of tasks fluctuations in reaction time (RT) are related to attention fluctuations. The parameters that most reliably predicted RT were studied through the analysis of high-density EEG signals and oculomotor parameters (gaze position and pupil diameter). Exploratory analyses were conducted in order to investigate if prestimulus brain activity parameters such as alpha amplitude in posterior brain areas; phase coherence in alpha, beta and gamma frequency bands; as also visual activity parameters, like pupil diameter and

gaze position, could predict subsequent task performance. A classification platform based on those features was also developed, using machine learning techniques, for predicting fluctuations in attention, on an intra-subjects basis. Three types of unimodal/simple classifiers (focused on eye parameters, alpha amplitude or phase coherence measures); and four hybrid classifiers, which took into account the output labels given by the three separate unimodal classifiers, were developed for each participant of the study.

The findings of this study showed that beta and gamma EEG phase coherence measures were capable of predicting fluctuations in subject's attention levels, i.e. intra-individual differences in reaction time. Increased frontal-parietal prestimulus phase coherence in beta and gamma frequency bands was associated with faster responses to stimulus' presentation, emphasizing the role of the attentional frontal-parietal networks for the maintenance of attention levels. In contrast, posterior alpha amplitude was not related to differences in RT. Pupil dilation was found to be a reliable pattern to predict fluctuations in subject's attention levels, while gaze position measures were not capable of predicting those fluctuations.

Relatively to the classification platform developed, only the unimodal classifiers based on eye activity parameters ensured a classification rate above chance level. EEG-based classifiers were not able to discriminate between attention states on a subject by subject basis, probably because the measures regarding the EEG signals were noisy and not so good at predicting fluctuations in task performance. Contrary to what was expected, hybrid classifiers did not improve the classification accuracy in comparison with the unimodal classification approach.

In conclusion, this study revealed that fronto-parietal EEG phase coherence and pupil diameter are related to moment-to-moment fluctuations in attention. Eye parameters were found to be useful to predict on a trial-by-trial basis the subject's attention level. This is important as pupil diameter and gaze position are easily accessible physiological markers that can be further explored in biofeedback systems to prevent attention lapses or to train attentional control.

Keywords: electroencephalography, visual attention, fluctuations in attention, spectral and phase coherence analysis, eye activity parameters, classifiers, predicting lapses in attention, machine learning techniques

Resumo

Quando estamos empenhados numa determinada tarefa, os nossos níveis de atenção não se mantêm constantes. Estes sofrem flutuações ao longo do tempo, as quais são mais acentuadas em patologias do foro neurológico, como por exemplo na perturbação de hiperatividade e défice de atenção. Flutuações nos níveis de atenção levam à ocorrência de lapsos de atenção, cujas consequências poderão ter um impacto pouco significativo como, por exemplo, a não deteção de um determinado estímulo; enquanto que, em determinados contextos (condução de veículos, atividades profissionais de risco, etc.) poderão desencadear acontecimentos trágicos. Por conseguinte, a deteção prévia da ocorrência destes lapsos poderá evitar consequências dramáticas. Estudos anteriores sugerem que certos padrões no sinal de eletroencefalograma (EEG) e de movimentos oculares, assim como flutuações no diâmetro da pupila poderão estar relacionados com os níveis de atenção. Neste trabalho pretendeu-se determinar quais desses parâmetros poderão ser empregues na previsão de lapsos de atenção.

Segundo a literatura, o estado de atenção é controlado por um compromisso entre a ativação das redes neuronais da atenção, as quais são responsáveis pela manutenção do estado de alerta durante tarefas que requerem concentração; e da *Default-Mode Network* (DMN), uma rede neuronal caracterizada por um conjunto de regiões cerebrais ativas durante o estado de repouso. A ocorrência de lapsos de atenção está associada a flutuações na atividade destas duas redes neuronais, assim como a alterações nas oscilações cerebrais. Evidências recentes sugerem que alterações em parâmetros oculares, tais como no diâmetro da pupila ou na posição do olhar, refletem alterações no estado cognitivo.

Para este estudo foram recrutados vinte jovens adultos saudáveis para a realização de uma tarefa visual, longa e monótona de forma a facilitar a ocorrência de lapsos de atenção, com aquisição simultânea de sinais de EEG e padrões de atividade ocular. Neste tipo de tarefas, flutuações no tempo de reação aos estímulos visuais apresentados aos participantes são associadas a flutuações no estado atencional dos sujeitos. Especificamente neste estudo, foram conduzidas análises aos sinais de EEG e parâmetros de atividade ocular adquiridos, de forma a identificar quais medidas mais fidedignamente preveem o tempo de resposta aos estímulos por parte dos sujeitos. Neste contexto, foram explorados

parâmetros de atividade cerebral pré-estímulo (amplitude das ondas alfa em zonas cerebrais posteriores e a sincronia de fase em três bandas de frequência: alfa, beta e gama), com o intuito de apurar se poderiam ser utilizados para prever o nível de desempenho subsequente do sujeito na tarefa. Parâmetros de atividade ocular, tal como o diâmetro da pupila e a posição do olhar foram igualmente estudados com o mesmo objetivo. Também se desenvolveram vários classificadores específicos para cada um dos participantes do estudo, tendo em conta características baseadas nos parâmetros anteriores, com recurso a técnicas de *machine learning*, para prever lapsos de atenção. Foram então desenvolvidos três tipos diferentes de classificadores unimodais (cada um deles baseado em parâmetros oculares, ou na amplitude das ondas alfa, ou em medidas de sincronia de fase entre sinais de diferentes regiões cerebrais); e quatro classificadores híbridos, tendo em conta os resultados da classificação retornados por cada um dos três classificadores unimodais separadamente, para cada sujeito em específico.

Os resultados obtidos neste estudo revelaram que medidas de sincronia de fase nas bandas de frequência beta e gama permitiram prever flutuações no estado atencional dos sujeitos, associadas a diferenças no tempo de reação dentro do mesmo indivíduo. Observou-se que um aumento da sincronia de fase entre as regiões frontal e parietal antes do surgimento de cada estímulo estava associado a respostas mais rápidas. Este resultado enfatiza o papel das redes neuronais da atenção com distribuição fronto-parietal na manutenção dos níveis de atenção. A amplitude das ondas alfa não mostrou estar relacionada com diferenças no tempo de reação. Os resultados obtidos revelaram, ainda, que o diâmetro da pupila é um parâmetro fidedigno para prever flutuações nos níveis de atenção dos sujeitos, contrariamente à posição do olhar.

Relativamente aos classificadores que foram desenvolvidos com o intuito de prever lapsos de atenção para cada indivíduo, apenas os classificadores unimodais baseados nos parâmetros oculares asseguraram taxas de classificação acima das que se obteriam tendo em conta uma classificação totalmente aleatória. Os resultados obtidos com os classificadores baseados em características extraídas dos sinais de EEG demonstram que este tipo de parâmetros não será adequado para a previsão de lapsos de atenção. Contrariamente ao que se esperava, não se obtiveram melhores taxas de classificação com os classificadores híbridos, em comparação com os classificadores unimodais.

Concluindo, os resultados obtidos neste estudo revelaram que medidas como a sincronia de fase entre as regiões cerebrais com distribuição fronto-parietal, assim como o diâmetro da pupila estão relacionadas com flutuações momentâneas dos níveis de atenção. Adicionalmente, foram encontradas evidências de que os parâmetros oculares estudados poderão ser úteis na previsão do estado atencional do sujeito em tempo real, tendo em conta os resultados obtidos nos classificadores baseados neste tipo de parâmetros. É de

evidenciar, portanto, a importância deste último resultado, uma vez que tanto o diâmetro da pupila como a posição do olhar são parâmetros fisiológicos que poderão ser facilmente adquiridos e empregues em sistemas baseados em *biofeedback*, desenvolvidos com o objetivo de prever lapsos de atenção ou para treino e controlo dos níveis de atenção.

Palavras-chave: eletroencefalograma, atenção visual, flutuações na atenção, análise espectral e de sincronia de fase, parâmetros de atividade ocular, classificadores, previsão de lapsos de atenção, técnicas de *machine learning*

Abbreviations

Acc	Classifier's Accuracy
ADHD	Attention-Deficit/Hyperactivity Disorder
AI	Anterior Insula
AUC	Area Under the Curve
BOLD	Blood-Oxygen-Level-Dependent
CV	Cross-Validation
DFT	Discrete Fourier Transform
DMN	Default-Mode Network
EEG	Electroencephalography
FDR	False Discovery Rate
FEF	Frontal Eye Field
FFT	<i>Fast Fourier Transform</i>
FIR	Finite Impulse Response
fMRI	Functional Magnetic Resonance Imaging
FN	False Negatives
FP	False Positives
IDF	iView Data File
IFG	Inferior Frontal Gyrus
IPS	Intraparietal Sulcus
ISI	Interstimuli Interval
KNN	<i>K-Nearest Neighbour</i> classification algorithm
MEG	Magnetoencephalography
MFG	Middle Frontal Gyrus
MPFC	Medial Prefrontal Cortex
PCA	<i>Principal Component Analysis</i> algorithm
PCC	Posterior Cingulate Cortex
PERCLOS	Percent Eye Closed
PET	Positron-Emission Tomography
PLV	Phase-Locking Value
PSQI	Pittsburgh Sleep Quality Index

RBF	Radial Basis Function
RT	Reaction Time
SMG	Supramarginal Gyrus
SPL	Superior Parietal Lobule
STG	Superior Temporal Gyrus
STS	Superior Temporal Sulcus
SVM	<i>Support Vector Machine</i> classification algorithm
TBI	Traumatic Brain Injury
TP	True Positives
TN	True Negatives
TPJ	Temporal-Parietal Junction
V4	Visual Area V4
VFC	Ventral Frontal Cortex
vMPFC	Ventromedial Prefrontal Cortex

List of Figures

1.1	Scheme illustrating differences about temporal and spatial resolutions of the four brain imaging methods addressed: EEG, MEG, fMRI and PET.	4
1.2	Relation between brain activation and functional PET and fMRI signals acquisition.	6
1.3	Scheme illustrating EEG technique.	7
1.4	Brain oscillations and the parameters which could provide information about the underlying neural processes - frequency, amplitude and phase.	9
1.5	Some examples of EEG waves which can be differentiated from the EEG signal in beta, alpha, theta and delta waves as well as spikes associated with epilepsy.	11
1.6	Scheme illustrating PLV calculation for a pair of electrodes, in the complex plane.	13
1.7	Definition of dorsal and ventral networks: their interactions and anatomical localizations.	16
1.8	Intrinsic correlations between the PCC - a task-negative region - and all other voxels in the brain for a single subject during resting fixation.	19
1.9	Results obtained by Van Dijk et al. about prestimulus alpha amplitude between hit and missed trials - trials in which subjects did and did not perceive the stimulus according with their visual discrimination ability, respectively.	22
1.10	Results obtained by Hanslmayr et al. about phase-locking in the alpha, beta and gamma frequency bands, for within-subjects analysis between perceived and unperceived trials.	25
2.1	Stimuli used in the task and their background.	34
2.2	Scheme illustrating the simple choice reaction time performed by subjects.	35
2.3	Behavioural Task. Subjects had to press response buttons with the index finger of their hand corresponding to the direction indicated by the target.	36
2.4	Participants characterization regarding daily habits in terms of drinking coffee, alcohol and smoking.	37
2.5	All materials required in the preparation phase were prepared in advance.	40
2.6	Electrode Layout for 64 Channel Quik-Cap TM from Compumedics Neuroscan. SynAmps2 64 Channel Quik-Cap, designed to interface to Neuroscan SynAmps2 TM amplifier.	42

2.7	The 10-20 international system is the standard naming and positioning scheme adopted for EEG applications. The scalp electrodes should be placed taking into account three bony landmarks: the nasion, theinion, and left and right pre-auricular points.	42
2.8	The simple visual display with impedance values for each electrode provided by the Acquire Data Acquisition software of the Neuroscan system used. Visual display is based on a grating colour system. Impedance testing is available without interrupting data acquisition.	43
2.9	Example of a participant being prepared for EEG acquisition.	44
2.10	Acquire Data Acquisition software layout (Compumedics NeuroScan, USA). 44	
2.11	RED Tracking Monitor from iView X TM Software.	46
2.12	Example of a participant prepared for EEG acquisition correctly positioned for the eyetracker monitoring his eyes.	46
2.13	Conceptual diagram explaining the criteria to characterize and count the behavioural responses.	48
2.14	Scheme illustrating how trials were divided in four bins (conditions) based on corresponding RT values.	49
2.15	Pre- and processing steps applied to EEG data for amplitude spectral and phase coherence analysis.	50
2.16	Graphic illustrating the Hamming window applied to a data segment of length SL.	52
2.17	Graphic representation of the procedure adopted for computing individual phase deviation, a measure for phase coherence on a single trial basis. . .	55
2.18	Scheme illustrating how the two vectors used for statistical correlation analysis between RT values and single trial phase deviation were generated. 56	
2.19	Scheme explaining how both group and individual eye parameters analysis were conducted.	58
2.20	Scheme illustrating how the four groups - RT_{Q1} , RT_{Q2} , RT_{Q3} and RT_{Q4} - used in the statistical analysis approach were aggregated into two classes - “Non Lapse” and “Lapse” - for the classification task.	63
2.21	Scheme illustrating the procedure adopted to develop a set of classifiers for predicting lapses in attention for each subject of the study.	64
2.22	Scheme illustrating how the temporal phase stability was obtained, a type of feature used in the classification platform developed here instead of single trial phase deviation, used in the statistical approach.	65
2.23	Scheme explaining how to obtain the output of the decision-level fusion approach adopted in this study, which takes into account the labels assigned to each instance by each unimodal classifier implemented.	71
2.24	Graphic illustration for the three-stage procedure adopted for evaluating the unimodal classifiers developed, for each prestimulus window, using as an example the classifier which used eye parameters as features.	73

2.25	All possible combinations tested for the hybrid classification approach, considering the three unimodal classifiers and the three classification algorithms implemented in this study, taking as example the output labels fusion of the classifiers for eye parameters (500 ms), alpha amplitude (500 ms) and temporal phase stability (500 ms).	74
3.1	Mean z -score for alpha amplitude (AUC) values, pooled over the electrodes within the parietal/parieto-occipital/occipital area, across subjects for each one of the four conditions (500 and 1000 ms prestimulus time windows).	79
3.2	An example of a subject (number 18) showing significant differences between fast (RT_{Q1}) and slow trials (RT_{Q4}) for alpha amplitude for 6 electrodes within the parietal/parieto-occipital/occipital area, and for the prestimulus time window of 500 ms length; and for 8 electrodes, considering the 1000 ms time window prior to stimulus onset. Spectral representations for one of those electrodes in common with the two sets (PZ) for each prestimulus window are also plotted.	81
3.3	Number of electrode pairs retained after the last step of the two-stage statistical test implemented for selecting those which showed a significant difference between the four conditions and which were associated with a higher or a smaller value for the mean phase coherence across subjects for fast trials in comparison with slow trials (conditions $RT_{Q1} > RT_{Q4}$ and $RT_{Q1} < RT_{Q4}$, respectively), for each frequency bin.	83
3.4	Results for group comparisons between the four conditions relatively to phase coherence analysis for beta frequency range (20-30 Hz).	85
3.5	Graphical representations of the results obtained for group comparisons between the four conditions relatively to phase coherence analysis regarding the gamma frequency range (30-45 Hz).	86
3.6	Single trial phase coherence analysis is plotted for subjects 15 and 16 and for alpha frequency range.	88
3.7	Results for single trial phase coherence analysis for subjects 15 and 16, regarding the beta frequency range.	89
3.8	Plot regarding the single trial phase coherence analysis, for subjects 15 and 16 and for gamma frequency range.	90
3.9	Graphical representation of the mean pupil diameter values across subjects - PD , in z -score values - for 500 ms and 1000 prestimulus windows, for each RT bin; and corresponding linear regression line.	92
3.10	Graphical representation of mean values for standard deviation of pupil diameter - $Std PD$, in z -score units - across subjects, for each RT bin and 500 ms and 1000 ms prestimulus windows.	93
3.11	Graphical representations of mean values for gaze position regarding the X and Y directions across subjects, for each RT bin and for 500 ms and 1000 ms prestimulus windows, considering the group analysis.	97
3.12	Graphical representations of mean values for standard deviation of gaze position in z -score units relatively to X and Y directions across subjects, for each RT bin and for 500 ms and 1000 ms prestimulus windows.	98

List of Tables

2.1	Participants characterization in terms of age, gender, academic degree, occupation and handedness (Age=mean \pm standard deviation)	37
2.2	Participants characterization in terms of sleep patterns during the five days prior to testing and sleep quality and disturbances regarding the month before testing (PSQI index); and caffeine and alcohol ingestion on the day before and on the test day.	39
2.3	Number of trials per condition for group analysis of EEG data.	60
2.4	Number of trials per condition used for analysis of eye parameters (pupil diameter and gaze position) relatively to the screen centre.	60
2.5	Percentage of data points removed from time segments after eye tracking data (pupil diameter and gaze position) were preprocessed.	61
2.6	Features used to develop the simple/unimodal classifiers.	67
2.7	Mean number of principal components/features chosen after applying the PCA algorithm across subjects for each unimodal classifier developed.	68
2.8	Simple/unimodal classifiers developed.	70
2.9	The four hybrid classifiers developed taking into account all possible combinations between unimodal classifiers.	71
2.10	Number of trials/samples across subjects per class used for training each simple classifier developed; and the corresponding number of trials set aside after PCA and used for assessing the accuracy of the classifier when it was submitted to “unseen” data ($\sim 10\%$ of the whole data set).	73
2.11	Number of trials/samples per class across subjects in common between the simple classifiers used in combination for the hybrid classification approach, both for training and for testing ($\sim 10\%$ of the whole data set in the last case).	75
3.1	Behavioural results for all the subjects in terms of median RT values for both left and right hands, percent of correct responses and missed trials.	78
3.2	Subjects and corresponding parietal/parieto-occipital/occipital channels which showed a statistically significant difference between the more extreme conditions (RT_{Q1} and RT_{Q4} , which corresponded to fast and slow trials, respectively), after correction for multiple comparisons.	80
3.3	Group analysis <i>p-values</i> for pupil diameter measures, considering 500 ms and 1000 ms prestimulus windows and comparisons between all conditions (RT_{Q1} , RT_{Q2} , RT_{Q3} and RT_{Q4}).	92

3.4	Individual comparisons for pupil diameter values, considering 500 ms and 1000 ms time windows.	94
3.5	Individual comparisons for standard deviation values of pupil diameter, considering 500 ms and 1000 ms time windows.	95
3.6	Group analysis <i>p-values</i> for gaze position measures, considering 500 ms and 1000 ms prestimulus windows and comparisons between conditions RT_{Q1} , RT_{Q2} , RT_{Q3} and RT_{Q4}	96
3.7	Individual comparisons for gaze position values relatively to the horizontal direction, considering 500 ms and 1000 ms prestimulus time windows.	100
3.8	Individual comparisons for gaze position values relatively to the vertical direction, considering 500 ms and 1000 ms time windows.	101
3.9	Individual comparisons for standard deviation of gaze position values relatively to the horizontal direction, considering 500 ms and 1000 ms time windows. Numbers in bold indicate values associated with statistically significant differences at the 0,05 level (two-tailed).	102
3.10	Individual comparisons for standard deviation of gaze position values relatively to the vertical direction, considering 500 ms and 1000 ms time windows.	103
3.11	Best classification algorithm for each type of unimodal classifier developed, considering each subject individually.	104
3.12	Accuracy values for the unimodal classifiers for each subject and considering the classification algorithms of the previous table.	106
3.13	<i>p-values</i> for the paired t-test conducted in order to compare the accuracy values obtained with each unimodal classifier.	106
3.14	Combination of classification algorithms that gave the best accuracy values for each subject in the hybrid classification approach.	107
3.15	Accuracy values for the hybrid classifiers developed for each subject and considering the combination of algorithms of the previous table.	108
3.16	<i>p-values</i> for the paired t-test conducted in order to compare the accuracy values obtained in the test stage using each unimodal classifier and each hybrid classifier developed.	109

Contents

1	Introduction	1
1.1	Motivation, Background and Objectives	1
1.2	Electroencephalography, Magnetoencephalography, Functional Magnetic Resonance Imaging and Positron Emission Tomography	3
1.2.1	Functional Magnetic Resonance Imaging and Positron-Emission Tomography	4
1.2.2	Electroencephalography and Magnetoencephalography	6
1.2.2.1	EEG/MEG Rhythms	8
1.2.2.1.1	Brain Oscillations: Frequency, Amplitude and Phase	8
1.3	The Neural Networks Underlying Attention	14
1.3.1	Attentional Networks and Task-Positive Brain Regions	14
1.3.2	Default-Mode Network and Task-Negative Brain Regions	16
1.3.3	Task-Positive and Task-Negative Brain Regions are Anticorrelated	18
1.3.4	The Behavioural Causes of Lapses in Attention	19
1.3.4.1	Sleep Patterns Influence Attentional States	19
1.3.4.2	Effects of Drugs Abuse, Nicotine, Caffeine and Alcohol Consumption on Attention	20
1.4	How To Predict Attentional Lapses	21
1.4.1	EEG-based Lapse Detection	21
1.4.1.1	Prestimulus Alpha Amplitude	21
1.4.1.2	Alpha Phase at Stimulus Onset	23
1.4.1.3	Phase-Coupling in Alpha Frequency And Higher Frequency Bands	24
1.4.2	fMRI Lapse Detection	25
1.4.3	Eye Parameters Predicting Attentional Fluctuations	26
1.4.3.1	Pupil Diameter Indicates Attentional Fluctuations	27
1.4.3.2	Gaze Position Dynamics as a Measure of Attention Levels	28
1.5	Management Systems for Predicting Vigilance Decline States	28
1.5.1	EEG/Eye Parameters-Based Machine Learning Algorithms For Predicting Lapses in Attention	28
1.5.2	Attention Management Devices	29
1.5.2.1	Classification of Subjects Attention Levels using Portable EEG Systems	29
1.5.2.2	Fatigue Detection using Smartphones	30

2	Materials and Methods	33
2.1	Visual Stimuli Paradigm and Behavioural Task	33
2.2	Participants	36
2.3	Surveys Performed	36
2.3.1	Sleep and Caffeine/Alcohol/Nicotine Consumption	38
2.3.1.1	Pittsburgh Sleep Quality Index	38
2.3.1.2	Sleep Patterns and Caffeine/Alcohol/Nicotine Ingestion During the Five Days Prior to Testing	38
2.4	EEG and Eye-Tracking Procedures	40
2.4.1	High-density EEG	40
2.4.1.1	Materials	40
2.4.1.2	Devices	41
2.4.1.3	EEG Recording Procedure	41
2.4.1.3.1	Subject Scalp Preparation and Positioning of the Cap	41
2.4.1.3.2	Testing Impedances	42
2.4.1.3.3	Data Acquisition	43
2.4.2	Eye-Tracking Method	45
2.4.2.1	Devices	45
2.4.2.2	Eye-Tracking Recording Procedure	45
2.4.2.2.1	Preparing Stimulation Computer and Eye-Tracking Device	45
2.4.2.2.2	Test Person Placement	45
2.4.2.2.3	Calibrating Eye-tracking Device	46
2.4.2.2.4	Data Acquisition	47
2.5	Data Analysis	47
2.5.1	Analysis of Behavioural Responses	47
2.5.2	Criteria to Select Conditions for EEG and Eye-Tracking Data Analysis	48
2.5.3	EEG Data	49
2.5.3.1	EEG Data Analysis	49
2.5.3.2	Frequency Domain Analyses of EEG data	51
2.5.3.2.1	Spectral Analysis	51
2.5.3.2.2	Analysis of Synchronization Between Elec- trodes	53
2.5.4	Eye-Tracking Data	56
2.5.4.1	Preprocessing of Eye Tracking Data	56
2.5.4.2	Pupil Diameter and Gaze Position Analysis	57
2.5.5	Statistical Analysis	58
2.5.6	Machine Learning Algorithms for Attentional Lapses Detection	62
2.5.6.1	Features Creation and Extraction of the Most Relevant Features	63
2.5.6.2	Classifiers	69
2.5.6.2.1	Classification Algorithms used to Develop the Unimodal Classifiers	69

2.5.6.2.2	Hybrid Classifiers	70
2.5.6.3	Performance Evaluation	71
3	Results	77
3.1	Behavioural Results	77
3.2	EEG Measurements	78
3.2.1	Prestimulus Alpha Amplitude	78
3.2.1.1	Group Comparisons	79
3.2.1.2	Individual Comparisons	79
3.2.2	Synchronization Between Electrodes	82
3.2.2.1	Group Comparisons: EEG Phase Coherence	82
3.2.2.2	Individual Comparisons: EEG Phase Deviation	87
3.3	Eye Measurements	91
3.3.1	Pupil Diameter	91
3.3.1.1	Group Comparisons	91
3.3.1.2	Individual Comparisons	93
3.3.2	Gaze Position	96
3.3.2.1	Group Comparisons	96
3.3.2.2	Individual Comparisons	99
3.4	Classifiers	103
3.4.1	Simple Classifiers	103
3.4.2	Hybrid Classifiers	107
4	Discussion and Conclusions	111
A	Appendix	123
A.1	Informed Consent	123
A.2	Socio-Demographic and Clinical Questionnaire	124
A.3	Pittsburgh Sleep Quality Inventory	129
A.4	Edinburgh Handedness Inventory	135
A.5	Sleep Patterns During the Four Days Prior to Testing	137
A.6	Sleep Patterns and Caffeine/Alcohol/Nicotine Ingestion On the Day Before and On the Test Day	139
	References	145

Chapter 1

Introduction

1.1 Motivation, Background and Objectives

Attention is defined as the maintenance of stable goal-directed behaviour during task performance. Momentary lapses in attention can affect the achieved sustained focus on a particular goal. Attention levels fluctuate with time. Indeed, the fatigue process is associated with gradual deterioration in perceptual, cognitive, and sensorimotor performance, but it is also common to observe rapid, temporary lapses of responsiveness, particularly in deeper fatigue states. In most cases, the consequences of attentional fluctuations are fairly benign such as responding more slowly to a certain external stimuli. However, in specific contexts, as driving scenarios or hazard situations, lapses in attention can lead to tragedies. The occurrence of these brief attentional lapses is perfectly normal in a healthy subject. In clinical syndromes such as Attention-Deficit/Hyperactivity Disorder (ADHD) focused attentional patterns can be altered. The understanding of the brain mechanisms that underlie the control of attention and its fluctuations can provide promising findings about the neural signatures which precede lapses. It has been established that there are specific brain activity patterns that occur before attention lapses which can be registered and analysed. However, little is known about these neural signals, although the detection of attentional lapses, even before these happen, could avoid catastrophic consequences of transient inattention episodes in real life.

In this line of research and trying to identify the neural correlates of attention, long monotonous visuomotor tasks, which facilitate the occurrence of attentional lapses, have been widely applied. In these experiments, behavioural measures such as reaction time (RT) and high-density electroencephalography (EEG) [1], magnetoencephalography (MEG) [2] or functional magnetic resonance imaging (fMRI) [3] signals are recorded. It is also usually acquired facial video recordings during the experiment [4, 5], for monitoring mind wandering or loss of vigilance states. Additionally, eye-tracking techniques

have been widely implemented in this context for predicting lapses in attention, by monitoring several eyes indices, such as eye blinks [6–8], saccadic movements [7], gaze fixations [7, 8], percent eye closure (PERCLOS) [8], pupil diameter [6, 7, 9] and gaze position [8, 10, 11]. The combination of several types of measures may be more sensitive to detection of attentional fluctuations. Indeed, several recent studies reported success in applying hybrid procedures based on EEG signals and eye parameters fused analysis to achieve accurate classification of responses to visual target detection related to the attentional state. Pupil measurements were proposed as a complementary modality that can really support improved accuracy of single-trial EEG signal analysis [12].

In the past few decades, efforts have been made to develop an effective and usable closed-loop attention management system, able to monitor an operator's attention via psychophysiological indicators, and then predict episodes of low vigilance and lapses in attention. Indeed, a warning system capable of reliably detecting lapses in responsiveness has the potential to prevent many fatal accidents. The development of a means of detecting human fatigue or behavioural lapse to prevent further growth in the number of fatalities caused by traffic accidents, for example, has increasingly attracted the attention of transportation safety administration, industry and the scientific community. Several imperative requirements for this type of technology have been established. The system must work only with minimal or no contact psychophysiological measures, being minimally invasive or constraining and unobtrusive. It must also provide an accurate and precise prediction of attention levels and task performance, and effective interface modifications, in near real-time, in order to support effective interventions. Such equipment could then prevent attention errors which could be lethal in several real world tasks, such as long distance driving, sonar monitoring for ship traffic or air traffic control and air defence warfare, supervision of semi-automated uninhabited vehicles, monitoring remote sensors, monitoring building security cameras, baggage screening, and many types of intelligence, reconnaissance, and surveillance tasks [13]. The aim of this project was to create knowledge that would facilitate the development of such a system.

Trying to explore a multimodal analysis, this work was conducted through measurements of brain and eye activity elicited by visual stimulation, by recruiting young healthy subjects to perform a simple task, with the aim to identify whether patterns in brain activity and eye parameters could predict the occurrence of attentional lapses. The identified neural and eye patterns most related with attentional decline states could be thereafter used in the development of novel closed-loop systems for detecting lapses in attention in a real-time manner or in the upgrading process of existing systems, leading to more accurate classification performances. Additionally, it was also intended to develop an algorithm to accurately predict attentional lapses in a single trial manner, for each one of

the participants of the study, using features based on both EEG measurements and eye activity parameters, and machine learning techniques. Several approaches were explored in terms of the type of features used to classify the subject's attentional state and the type of classification algorithms implemented. The final outcome was to determine the most robust option, taking into account the best classification accuracy. Note that this type of algorithms for classifying the subject's attention level can be used to develop not only drowsiness warning devices but also other systems which could help, for example, children suffering from ADHD or people with neurological disorders for training attention levels using biofeedback [14].

1.2 Electroencephalography, Magnetoencephalography, Functional Magnetic Resonance Imaging and Positron Emission Tomography

The neural correlates of attention have been studied with human neuroimaging techniques.

The diverse nature of cerebral activity, as measured using neuroimaging techniques, has been recognised long ago. Over the past few decades, several methods have been developed to allow mapping of the functioning human brain. In this context, two basic classes of mapping techniques have evolved: those that map (or localise) the underlying electrical activity of the brain; and those which map metabolic or local physiological consequences of altered brain electrical activity. Non-invasive neural electroencephalography technique (EEG) and magnetoencephalography (MEG) are included among the former. Both EEG and MEG are characterized by their exquisite temporal resolution of neural processes (typically over a 10-100 milliseconds time scale), but they suffer from poor spatial resolution (between 1 and several centimetres) - figure 1.1. Functional magnetic resonance imaging (fMRI) methods are included in the second category. They are sensitive to the changes in blood oxygenation that accompany neuronal activity, have good spatial resolution that is in the order of millimetres, and a temporal resolution of few seconds [15]. Positron-emission tomography (PET) modality is also included in the second group. PET is another noninvasive technique which can provide quantification of brain metabolism, receptor binding of various neurotransmitter systems, and as the fMRI, alterations in regional blood flow [16]. However, limitations are mainly due to the limited temporal resolution (figure 1.1), despite being an useful imaging technique for clinical purposes and in the neuroscience research field [16, 17].

Although this present study focuses only in EEG, those four brain imaging techniques (EEG, MEG, fMRI and PET) are described in the subsections below.

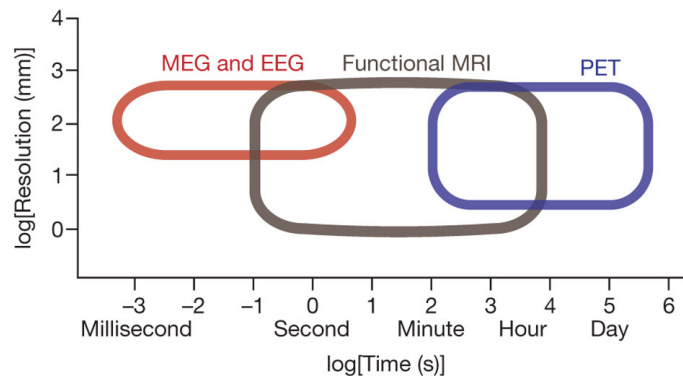


Figure 1.1: Scheme illustrating differences about temporal and spatial resolutions of the four brain imaging methods addressed: EEG, MEG, fMRI and PET [18]. The temporal resolution of both EEG and MEG methods can be on the order of milliseconds whereas their spatial resolution tends to be less that of fMRI and PET. However, fMRI and PET are limited in their temporal resolution to several 100 milliseconds (for fMRI) and minutes (for PET).

1.2.1 Functional Magnetic Resonance Imaging and Positron-Emission Tomography

Currently, functional MRI is considered the mainstay of neuroimaging in cognitive neuroscience research field. Indeed, the past two decades have witnessed the popularity of fMRI as an important tool for mapping human brain functions [19]. The fMRI imaging technique was developed in the early 1990s and had a real impact on basic cognitive neuroscience research. fMRI is routinely used in humans not just to study sensory processing control of action, but also to investigate the neural mechanisms of cognitive functions, such as recognition or memory [20].

The underlying principle of fMRI is that changes in regional cerebral blood flow and metabolism are coupled to changes in regional neural activity related with brain function, such as remembering a name or memorizing a phrase [21].

The blood-oxygen-level-dependent functional magnetic resonance imaging (BOLD fMRI) is the most widely used among fMRI techniques [21]. It is based on the detection of oxygen levels in the blood, point by point, throughout the brain. In other words, it relies on a surrogate signal, resulting from changes in oxygenation, blood volume and flow, not directly providing a measure of neural activity. More specifically, increased neural activity in a local brain region increases blood flow in that specific region. This change in blood flow is accompanied by an increase in glucose utilization, but smaller

changes in oxygen consumption [22]. Therefore, when blood flow increases it leads to a decrease in the amount of oxygen extracted from blood and, therefore, to an increase in the amount of oxygen available in the area of activation (supply transiently exceeds demand). In contrast, when blood flow diminishes, increases the amount of oxygen extracted from the blood, leading to smaller decreases in the amount available in such area. Thus, changes in blood flow accompanying local changes in brain activity are associated with significant changes in the amount of oxygen used by the brain, which accounts for the BOLD fMRI signal generation. Therefore, fMRI modality uses hemoglobin as an endogenous contrast agent, relying on the difference in the magnetic properties of oxyhemoglobin - the form of hemoglobin that carries oxygen - and deoxyhemoglobin - the form of the molecule without oxygen - thus measures a correlate of neural activity - the haemodynamic response [23].

The principal advantages of fMRI lie in its ever-increasing availability, relatively high spatial resolution, noninvasive nature and its capacity to demonstrate the entire network of brain areas involved when subjects perform particular tasks. However, fMRI provides measurements with poor temporal resolution [20].

The signal used by functional PET to map changes in neural activity in the human brain is also based on local changes in blood flow, similarly with fMRI, being also an indirect measure of brain activity [17]. In PET, a short-lived radioactive tracer is introduced into the human bloodstream, usually via an intravenous injection [16]. A radioactive tracer is a biomolecule labelled with a positron-emitting isotope such as Carbon-11 (^{11}C), Nitrogen-13 (^{13}N), Oxygen-15 (^{15}O), and Fluorine-18 (^{18}F), which are obtained in a cyclotron, a particle accelerator that generates static magnetic and electric field between specifically designed electrodes within a vacuum chamber. After intravenous administration, the radioactive tracer can be monitored in the brain in order to acquire structural and kinetic information regarding the distribution of the tracer in the brain. The PET signal is generated by a detector system which acquires radiation emission profiles of the radioactive tracer [16]. Depending on the particular brain function in which investigators are interested in, specific tracers are chosen. A radioactive tracer commonly used in brain imaging, specially in neuroscience research areas is the ^{18}F -FDG - *fludeoxyglucose* - which distributes according to regional glucose utilization, recording an indirect measure of the local neural activity [21]. Note that as was mentioned above, neural activation is characterized by an increase in local blood flow and in glucose consumption. The scheme of the figure 1.2 explains the relation between the origin of both PET and fMRI signals.

Similarly to fMRI, PET is limited in its temporal resolution but provides a better spatial resolution than EEG and MEG techniques [18]. Additionally, due to its ability to

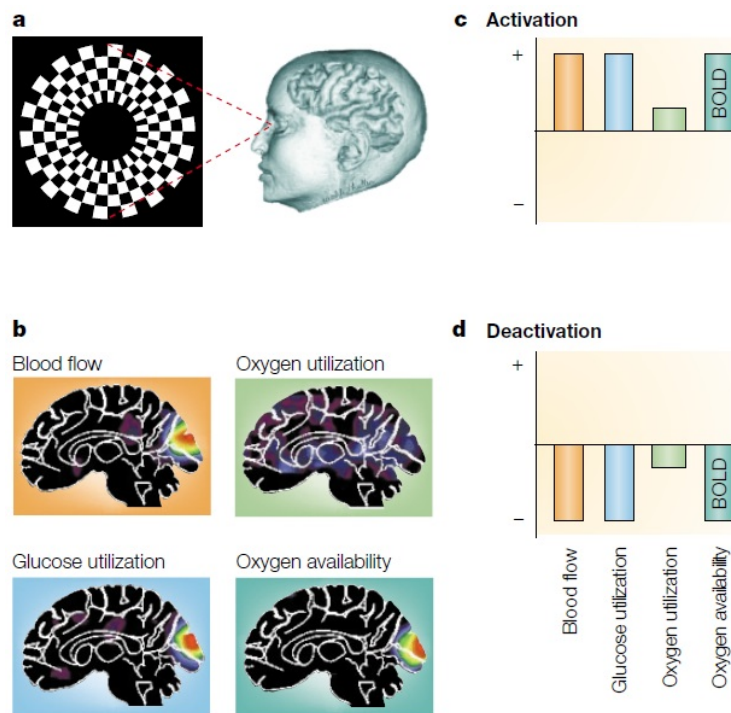


Figure 1.2: Relation between brain activation and functional PET and fMRI signals acquisition [22]. **(a)** Brain activation can be achieved experimentally, for example, by submitting a subject to a task in which a certain visual stimuli - here, a reversing annular chequerboard - is presented at certain instances within a blank screen. **(b)** Compared with viewing the blank screen, when the subject see the stimulus, marked changes are observed in activity in visual areas of the brain, as shown in PET images. These changes are characterized by an increase in local blood flow and in glucose utilization, but smaller changes in oxygen consumption. As a result, the amount of oxygen available in the area of activation increases (supply transiently exceeds demand), which accounts for the BOLD fMRI signal generation. **(c)** As was referred in the text above, an activation of a certain brain region is characterized by an increase in blood flow, glucose consumption, oxygen usage - being this change much more subtle than the others - and oxygen availability. Changes in glucose utilization and oxygen availability are the main underlying mechanisms for the origin of functional PET and BOLD fMRI signals, respectively. **(d)** In contrast, brain deactivation represents the opposite spectrum of circulatory and metabolic changes to those observed in the activation state.

measure tiny concentrations of the radioactive tracer used, PET modality provides physiological measurements exquisitely sensitive [21].

1.2.2 Electroencephalography and Magnetoencephalography

The electroencephalography or EEG became accepted as a method of analysis of brain functions in health and disease since Berger demonstrated that the electrical activity of the brain can be recorded from the human scalp, in the 1920s. Over the ensuing decades, EEG proved to be very useful in both clinical and scientific applications [24]. In fact, during more than 100 years of its history, EEG has undergone massive progress [25].

The EEG is defined as a procedure that measures the summed electrical activities of populations of neurons. Neurons produce electrical and magnetic fields, which can be recorded by means of electrodes placed on the scalp. In EEG, because from neuronal layers to electrodes current penetrates through skin, skull and several other layers, the weak electrical signals detected by the electrodes located on the scalp are massively amplified [25]. Magnetoencephalography (MEG) is usually recorded using sensors which are highly sensitive to changes in the very weak neuronal magnetic fields. These are placed at short distances around the scalp, similarly to the EEG procedure [26].

Only large populations of neurons in activity can generate electrical signals recordable on the head surface. The physiological phenomenon underlying EEG signal is based on that neurons generate time-varying electrical currents when activated, which are generated at the level of cellular membranes, consisting in transmembrane ionic currents. A summary of the ionic currents produced by a neuron is shown in figure 1.3.

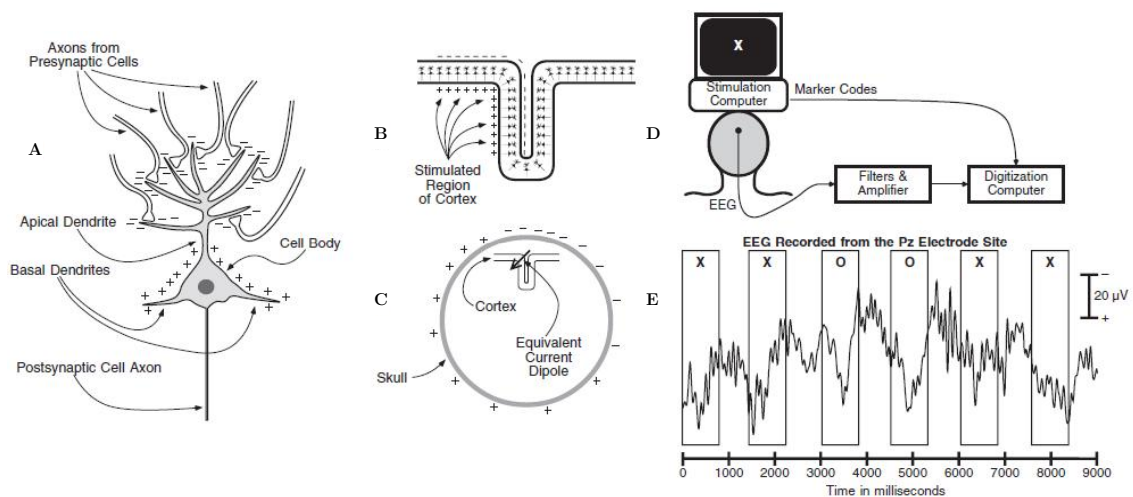


Figure 1.3: Scheme illustrating EEG technique (adapted from [24]). (A) The neurotransmission phenomenon - an excitatory neurotransmitter is released from the presynaptic terminals causing positive ions to flow in the postsynaptic neuron, which creates a net negative extracellular voltage in the area of other parts of the neuron. (B) Cerebral cortex contains many neural cells. Here, it is presented a schematic folded sheet. When a certain region is stimulated, the electrical activities from the individual neurons summate. (C) The summated dipoles from the individual neurons can be approximated by a single equivalent electrical current, shown as an arrow. (D) This electrical current can be recorded using EEG technique. Here, it is represented a scheme for an EEG signal acquisition example from a midline parietal electrode site, while the subject response to a certain stimulus presented on a computer screen. This signal must then be filtered and amplified, making it possible to observe the EEG signal. (E) The rectangles show an 800-ms EEG-segments following each stimulus in the EEG.

EEG is a non-invasive procedure which can be applied repeatedly to healthy adults, patients, and children with virtually no risk or limitation [25]. EEG has poor spatial

resolution. This limitation has been solved by combining anatomical/physiological with biophysical/mathematical concepts and tools, in order to build models that incorporate knowledge about cellular/membrane properties with those for the local circuits, their spatial organisation and organisation patterns. Thus, the difficulty involved in estimating the complex networks of generators suggests that functional imaging techniques such as fMRI combined with EEG can play a significant role in improving the understanding of human brain functioning [26]. Taking into account its temporal resolution, complex patterns of brain electrical activity can be recorded occurring within fractions of a second after a stimulus has been showed, being this one of the greatest advantages of EEG modality [25]. Additionally, EEG is much less expensive than other imaging techniques such as fMRI or PET.

1.2.2.1 EEG/MEG Rhythms

Recent studies have reported that fluctuations in attention are related with changes in brain oscillations¹ [1, 2, 28, 29]. Specific patterns of cyclic brain fluctuations correlate with the subject's performance in visuomotor tasks.

Brain oscillations have been studied by analysing the temporal dynamics of electrocortical signals acquired with EEG or MEG equipments. Usually, in studies about lapses in attention, EEG signals of participants are recorded while they perform a monotonous visuomotor task during long periods of time. Frequency analyses of EEG data are frequently performed, after acquisition of electrophysiological signals. To detect neural signatures of lapsing attention, it is being currently investigated how far back in time a lapse is foreshadowed in EEG [28]. One of the main current objectives of studying high-dense EEG signals obtained during a goal-directed task is to extract specific neural patterns that could be used to predict the occurrence of lapses even before these happen. Indeed, identifying the electrophysiological signatures of such brain states, and predicting whether or not a sensory stimulus will be perceived, are two of the main goals of modern cognitive neuroscience [29]. Several EEG studies suggest a fundamental role of ongoing oscillations for shaping perception and cognition. However, at first, it is necessary to understand how different parameters of oscillatory activity might provide information about the underlying neural processes.

1.2.2.1.1 Brain Oscillations: Frequency, Amplitude and Phase

Brain oscillations reflect rhythmic fluctuations in local field potentials, being generated by the summed electrical activities of several thousand of neurons. By applying

¹**Brain oscillations** - Transient, rhythmic variations in neuronal activity. They can be detected as fluctuations in the electric field created by the summed synaptic activity of a local neuronal population [27].

spectral analysis to the raw EEG signal, which contains various different brain oscillations, information about frequency, amplitude and phase about each brain oscillation can be obtained (figure 1.4). Spectral analysis can be performed using, for example, *Fourier* analysis or *wavelet* transforms [29]. *Fourier* analysis is based on the principle that stationary waveforms may be represented as a sum of sinusoidal waveforms, each one of different frequency and having an associated amplitude and phase. Alternatively, *wavelet* transforms perform a local analysis of non-stationary signals in the time-frequency domain. Providing simultaneously the frequency content of the signal in the vicinity of each time point, *wavelet* transforms can be used to analyse short-lasting changes in the frequency spectrum of the EEG signal over time. Basically, it is a method of converting a signal into another form which either makes certain features of the original signal more amenable to study.

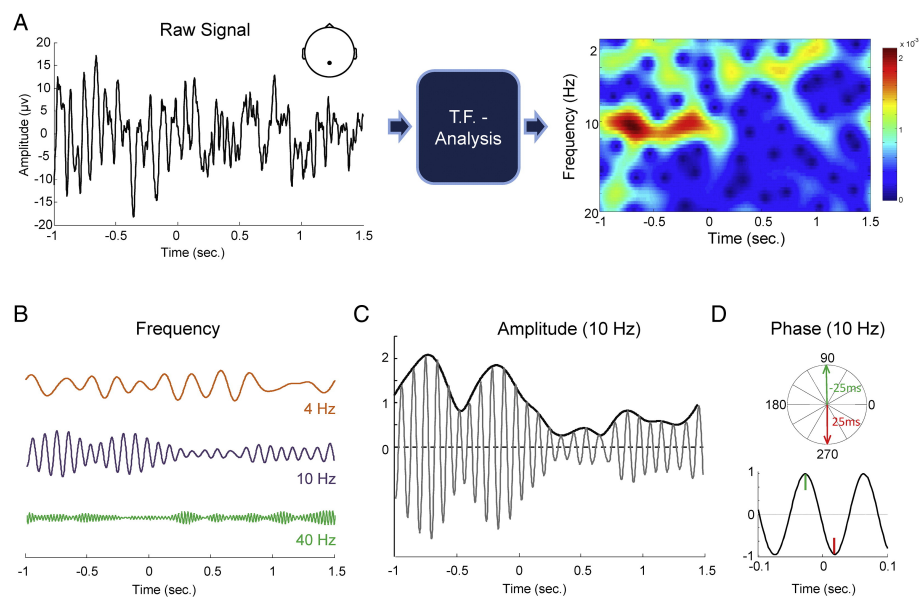


Figure 1.4: Brain oscillations and the parameters which could provide information about the underlying neural processes - frequency, amplitude and phase [29]. **(A)** On the left is represented an EEG signal recorded using a parietal electrode. A stimulus was presented at instance 0. The results of time-frequency analysis using *wavelet* transform of the corresponding signal are plotted on the right. Spectral amplitude is depicted for each time-point (X-axis) and frequency band (Y-axis). **(B)** By applying a band-pass filter, theta (4 Hz), alpha (10 Hz) and gamma (40 Hz) oscillations were extracted from the above raw signal. **(C)** Amplitude time-course for 10 Hz oscillation component. **(D)** Alpha phase at two different time points: 25 ms prior, and 25 ms after stimulus presentation.

Frequency

It is already known that electrical brain activity exhibits an oscillatory behaviour. Despite the wide range of neuronal population sizes generating each type of signal, distinct frequency bands were identified across different signal types which exhibit characteristic changes in response to sensory, motor and cognitive events [30]. Different frequency bands were then established to classify distinct neuronal rhythms as slow oscillations (<1 Hz), delta (0,5-4 Hz), theta (4-8 Hz), alpha (8-13 Hz), beta (13-30 Hz) and, finally, gamma activities (>30 Hz) [30, 31] (see figure 1.5). Further subdivisions are becoming more common. Note that different rhythms are associated with different temporal windows for processing, spatial scales and cell population sizes. Indeed, it has been suggested that low frequencies are responsible for the modulation of brain activity over large spatial regions considering long temporal windows, while high frequencies modulate activity over small spatial regions and short temporal windows [30]. These different types of rhythmical activities can be recorded from the brain using EEG. Some prominent activities are frequently the object of neurocognitive EEG studies, such as sleep rhythms, activities in the alpha frequency range and beta/gamma rhythms [26] and also pathological brain patterns, such as spikes associated with epilepsy [31].

The alpha rhythm is the best-known and most widely studied brain rhythm (figure 1.5). It can be mainly observed in the posterior and occipital regions. Alpha activity can be induced by closing the eyes and by relaxation, and abolished by eye opening or alerting by any mechanism, such as thinking and other types of mental processing, thus alpha reduction is a marker of attentive, focused state. EEG is sensitive to several mind states such as stress, alertness, hypnosis, periods of rest and sleep. For example, beta waves are dominant during normal state of wakefulness with open eyes [25].

Synchronization Between Sources

Differences in synchronization of brain signals (also termed phase coherence) from different sources have been linked to fluctuations in attention. The methods used to study synchronization will be described next.

The brain oscillates and synchronization of these oscillations have been linked to the dynamic organization of communication in the central nervous system, being task-dependent neural synchronization a general phenomenon. Currently, the study of oscillatory rhythms and their synchronization in the brain is a subject of growing interest [32].

Calculation of synchronization between neural sources using EEG or MEG measurements is a recent technique populated by several competing methods. Indeed, a considerable number of different approaches have been employed for the calculation of this

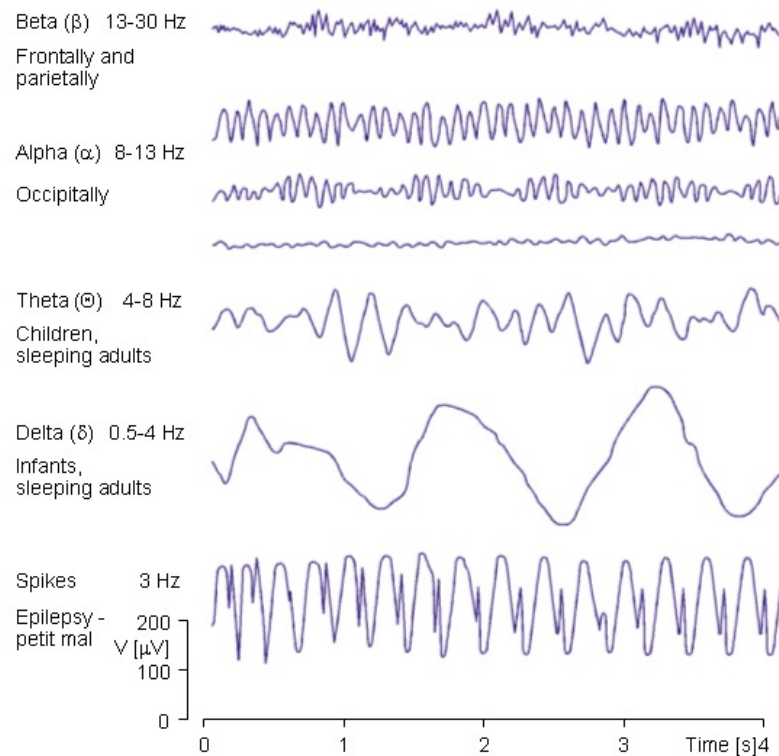


Figure 1.5: Some examples of EEG waves which can be differentiated from the EEG signal in beta, alpha, theta and delta waves as well as spikes associated with epilepsy [31]. Note that alpha waves are mainly detectable from the occipital region and beta waves over the parietal and frontal lobes. Delta and theta waves are frequently detectable in sleeping adults and children.

measure. Most widely and successfully employed among these are the phase-locking value (PLV) [33] approach and phase-coherence analysis [34]. Such methods aim to assess synchronization between pairs of neural sources (neurons or neural populations) or scalp electrodes by quantifying the stability of the phase relationship between the two.

For PLV calculation, given two series of signals m and n and a frequency of interest f , the procedure computes for each latency a measure of phase-locking between the components of m and n at frequency f . This needs the extraction of the instantaneous phase of every signal at the target frequency. The most frequently employed method to obtain the phase of an oscillator using EEG or MEG data is *wavelet* analysis, although it can also be done using the analytic signal. Using the former approach for time frequency analysis, the signal is decomposed into various versions of a standard *wavelet*, defined as a short version of a cosine wave. The output of this analysis, which are the *wavelet* coefficients, represents the similarity of a particular *wavelet* to the signal considering defined frequency bands and time instants [32].

It is usually to use the Morlet *wavelet*, which is defined by the product of a sinusoidal wave with a Gaussian or normal probability density function [32].

For instantaneous phase calculation, the MEG or EEG signal, $h(t)$, must be filtered, at first, into small frequency ranges using a digital band-pass filter. Thereafter, the *wavelet* coefficients, $W_h(t, f)$, which are complex numbers, are computed as a function of time, t , and center frequency of each band, f , from:

$$W_h(t, f) = \int_{-\infty}^{+\infty} h(t) \Psi_{t,f}^*(u) du \quad (1.1)$$

where $\Psi_{t,f}^*(u)$ is the complex conjugate of the Morlet *wavelet* defined by:

$$\Psi_{t,f}(u) = \sqrt{f} e^{j2\pi f(u-t)} e^{-\frac{(u-t)^2}{2\sigma^2}} \quad (1.2)$$

Note that the complex conjugate of a number $z = x + jy$ is defined as $z^* = x - jy$. The *wavelet* is then passed along the signal from time point to time point, with the *wavelet* coefficient for each time point being proportional to the match between the signal and the *wavelet* in the vicinity of that time point, which is closely related to the amplitude of the envelope of the signal at that instant. Additionally to the envelope's amplitude of the signal at each time instant, *wavelet* transform also supplies the phase at each time point available. The phase difference (Δ phase) between two signals, m and n (being each one from different neural sources or scalp electrodes), can then be computed using *wavelet* coefficients for each time and frequency point by taking:

$$e^{j(\phi_m(t,f) - \phi_n(t,f))} = \frac{W_m(t, f) W_n^*(t, f)}{|W_m(t, f) W_n(t, f)|} \quad (1.3)$$

where $\phi_m(t, f)$ and $\phi_n(t, f)$ are the phases of sources/scalp electrodes m and n at time point t and frequency f .

From this point, the PLV can be computed across the N trials of an experiment, being a measure of the relative constancy of the phase differences between two signals along the considered trials. These trials are considered epochs time-locked to a particular stimulus or response in the original signals.

The PLV can be obtained, for each time point t by:

$$PLV_{m,n,t} = \frac{1}{N} \left| \sum_N e^{j[\phi_m(t) - \phi_n(t)]} \right| \quad (1.4)$$

where $\phi_m(t)$ and $\phi_n(t)$ are the phases of sources m and n at time point t for each of the N epochs considered.

PLV measures the intertrial variability of the phase difference between the two sources (m and n), ranging from a maximum of 1, when the phase differences have maintained constant across all N epochs to minimum of 0, when the phase differences have varied randomly across the different trials. PLV is the length of the resultant vector when each phase difference (Δ phase) is represented by a unit-length vector in the complex plane [32]. The length of this resultant vector is proportional to the standard deviation of the distribution of phase differences (see figure 1.6 for an explanation).

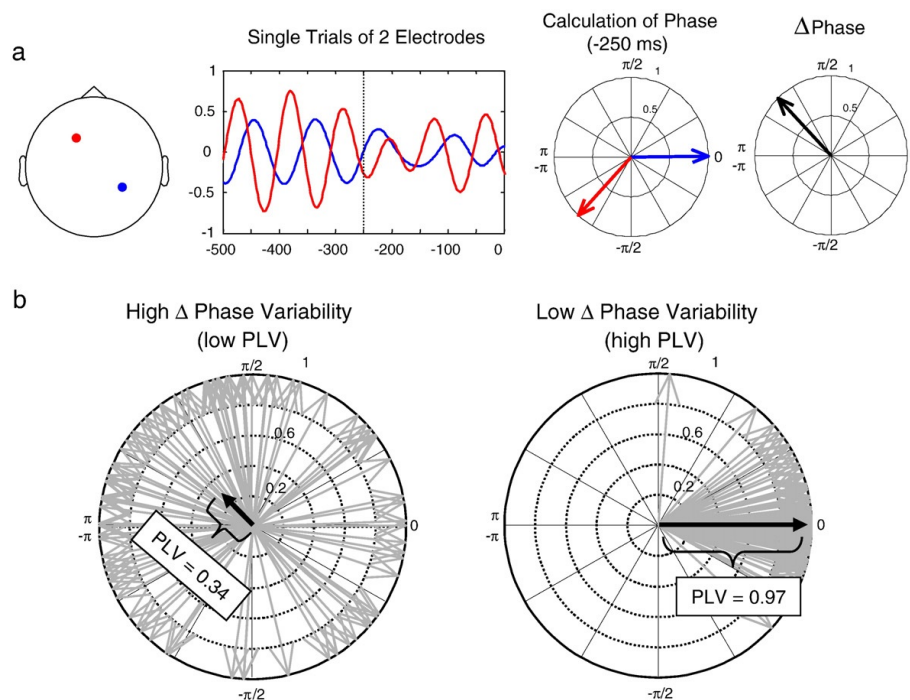


Figure 1.6: Scheme illustrating PLV calculation for a pair of electrodes, in the complex plane [35]. **(a)** Two filtered single trials signals (10 Hz) for a frontal (red line) and a parietal electrode (blue line) are shown for a given interval (in this case, -500 to 0 ms prestimulus). Then, the phase of these two signals is extracted for each time point (e.g. -250 ms). The phase difference (Δ phase) between those signals is thereafter calculated (black arrow). **(b)** The PLV can be then obtained by computing the circular mean of phase differences (grey arrows) across all single trials. This yields a vector with a certain direction, representing the mean phase difference (black arrow), and a certain length, representing the PLV. Phase differences (grey arrows) and the mean phase difference (black arrow) is plotted for two sets of single trials. The example on the left depicts a set of single trials with high phase difference variability, resulting in a short mean vector (low PLV); and the example on the right represents a dataset with low phase differences variability and a long mean vector (high PLV).

Phase coherence techniques for phase synchronization analysis between two signals providing from two different sources/scalp electrodes have been also implemented. An

example for phase coherence calculation is the formula developed by Delorme et al. [34], defined in terms of *wavelet* coefficients as:

$$C_{m,n}(f,t) = \frac{1}{N} \sum_{i=1}^N \frac{W_{m,i}(f,t)W_{n,i}^*(f,t)}{|W_{m,i}(f,t)W_{n,i}(f,t)|} \quad (1.5)$$

where, N is the number of trials, and C an index indicating the phase coherence between two different signals m and n , varying between 1 (for perfect phase-locking) and 0 (for random phase-locking).

The following sections describe how neuroimaging has revealed the neural correlates of attention.

1.3 The Neural Networks Underlying Attention

1.3.1 Attentional Networks and Task-Positive Brain Regions

Using functional brain imaging studies as PET and fMRI, it was possible to observe task-induced increases in regional brain activity during attentionally demanding tasks in certain cerebral areas. These alterations in brain activation patterns can be observed when comparisons are made between a task state, designed to place demands on the brain, and a control state, with a set of demands that are uniquely different from those of the task state [17].

According to biased-competition models of attention, brain frontal regions responsible for the control of attention bias sensory regions to favor the processing of behaviourally relevant stimuli over that of irrelevant stimuli [36–39]. The increase on sensory cortical activity is a consequence of this biasing, which results in high-quality perceptual representations that can be fed forward to other brain regions that determine behaviour. It has been established that brief attentional lapses are originated from momentary reductions of activity in frontal control regions, just before a relevant stimuli is presented. This reduced prestimulus activity leads to impairments in suspending irrelevant mental processes, during task performance [17].

Specifically, recent studies have suggested that attention is thought to be controlled by two anatomically nonoverlapping brain networks: the dorsal and ventral fronto-parietal networks [40]. The first one controls goal-oriented top-down deployment of attention, while the ventral fronto-parietal network mediates stimulus-driven bottom-up attentional reorienting. Anatomically, the dorsal attention network is comprised of bilateral frontal eye field (FEF) and bilateral superior parietal lobule (SPL)/intraparietal sulcus (IPS) [37, 41–44]. On the other hand, the ventral fronto-parietal network, which is right-lateralized, contains right ventral frontal cortex and right temporal-parietal junction

(TPJ) [41–43, 45, 46]. Anatomically, TPJ is defined as the posterior sector of the superior temporal sulcus (STS) and gyrus (STG) and the ventral part of the supramarginal gyrus (SMG) and ventral frontal cortex (VFC), including parts of middle frontal gyrus (MFG), inferior frontal gyrus (IFG), frontal operculum, and anterior insula (AI) [47].

It is generally believed that the effective interaction between ventral and dorsal fronto-parietal networks underlies the maintenance of sustained attention, during attentionally demanding tasks [40]. It is believed that input from the ventral to the dorsal network impairs task goal-oriented performance [48]. This evidence suggests that the two attention networks interact by suppressing each other. The neuronal mechanisms of this interaction remain not well understood [40]. Although, Corbetta et al. [47] have proposed a hypothesis to explain it. As reviewed by these authors, top-down signal from the dorsal attention network to the ventral attention network suppress and filter out irrelevant distracter information so that goal-oriented sensorimotor processing can proceed unimpeded. While this information is being transferred from the dorsal network to the ventral network, bottom-up signals circulate in the opposite direction to disrupt the sensorimotor processing enabled by the dorsal attention network (figure 1.7). Support for this hypothesis has mainly come from studies of brain lesions. For example, in accordance with Meister et al. [49], permanent lesions or damage caused by temporary interference in areas belonging to the ventral attention network adversely impacts the ability to disengage from an existing attentional focus. These findings suggest a breakdown in communication between the orienting system and the dorsal fronto-parietal structures as the main cause for the deterioration on attentional control functions. Indeed, fluctuations in goal-directed sustained task performance are frequently observed. Notably, it has been shown that these behavioural fluctuations are related with fluctuations in the activity of the two fronto-parietal networks, which modulate attention. Fluctuating levels of information transfer from the ventral into the dorsal attention network are intrinsically involved with performance variability and with the oscillatory activity of the two networks [40].

Regarding the role of frontal regions on controlling attention mechanisms, the study of Weissman et al. [3] using fMRI modality provides new insights about this relation. They found that momentary lapses in attention are associated with the reduced activity in frontal control regions. This finding suggests a failure of frontal control regions to fully enhance the perceptual processing of behaviourally relevant stimuli. They also conclude that, probably, momentary lapses in attention result in a relatively low-quality perceptual representation of behaviourally relevant stimuli, due a reduction of top-down biasing signals to the sensory cortices. Interestingly, negative relationships between attention lapses and target-related activity in frontal control regions were reported, although positive relationships were observed after such lapses. This evidence suggests a compen-

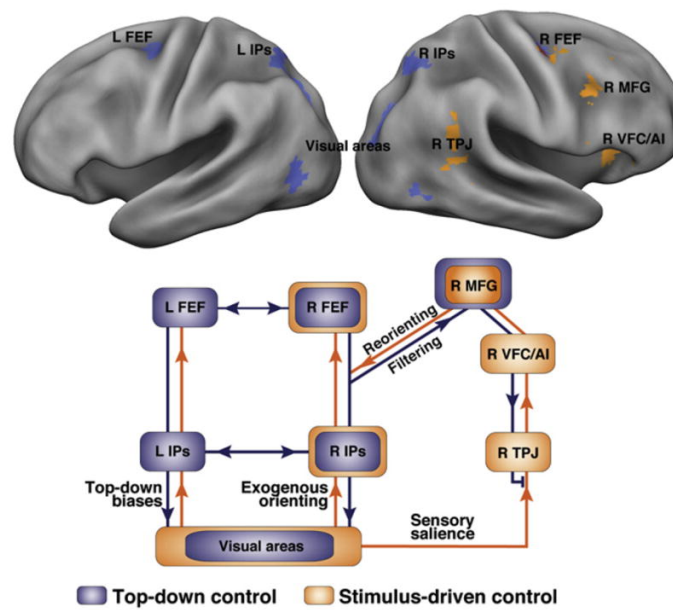


Figure 1.7: Definition of dorsal and ventral networks: their interactions and anatomical localizations [47]. **(Top panel)** Brain regions in orange are activated when attention is reoriented to a behaviourally relevant object that appears unexpectedly. Regions in blue are consistently activated by central cues, which indicate what is the feature of an upcoming object or where a peripheral object will subsequently appear. **(Bottom Panel)** Interactions between dorsal (blue) and ventral (orange) networks during stimulus-driven reorienting. Dorsal network regions FEF and IPS restrict ventral activation to behaviourally important stimuli, by sending top-down biases to visual areas and via MFG to the ventral network (filtering signal). Globally, the dorsal network coordinates stimulus-response selection, being FEF and IPS regions also important for exogenous orienting. When a salient stimulus occurs during stimulus-driven reorienting, a reorienting signal is sent by the ventral network to the dorsal network through MFG region.

satory recruitment of control mechanisms, which possibly helps the brain to cope with increased processing demands, after a disruption on attention. Weissman et al. [3] have also studied the reorienting of attention mechanisms. They investigated whether the ventral fronto-parietal network is implicated in these processes, as was previously proposed. Notably, they found that an increased right TPJ and IFG activities are both associated with faster RT in the following trial of a goal-directed task. Broadly, their results illustrate that important questions about the neural signatures of behaviour can be addressed through a trial-by-trial comparative study between RT and brain activity.

1.3.2 Default-Mode Network and Task-Negative Brain Regions

According to several models [1,3,50], lapses in attention have been associated with increases in activation within the default-mode network (DMN). The DMN is a set of brain regions responsible for the high metabolic demands and brain activity required at resting state [17]. Supporting internally directed mental activity is one of its functions [51, 52].

The DMN is composed by the posterior cingulate cortex (PCC), precuneus and parts of the ventromedial prefrontal cortex (vMPFC); regions with dense white matter connections [50]. It has been established that those components form part of the brain's structural core [53]. Abnormalities related with the disruption of the DMN network are observed in various psychiatric and neurological disorders, enhancing its clinical importance and impact [50, 54]. Its involvement in cognitive control and in regulation of the attention focus has been also investigated. Indeed, it has been established that the DMN network could control attentional mechanisms by promoting a coordinated balance between internally and externally directed thought [55]. Conditions as Traumatic Brain Injury (TBI), which frequently produces failures to maintain consistent goal-directed behaviour, are associated with abnormalities in DMN function. Diffuse axonal injury is a hallmark of TBI, which can lead to cognitive impairment by disconnecting nodes in distributed brain networks [50].

The impact of the DMN activity on the occurrence of attentional lapses during a goal-directed task has been widely discussed by several authors [1, 3, 17, 56]. Daydreaming, recalling previous experiences from memory or monitoring the external environment are mental activities without a defined goal that were linked with the activation of the DMN. When a behaviourally relevant stimulus is presented, a deactivation in this network must occur. According to Weissman et al. [3], during a lapse of attention subjects may not fully reallocate attentional resources toward behaviourally relevant processes, leading to an inefficient DMN deactivation. They emphasize a tight relation between the DMN deactivation's magnitude and the RT across trials in a goal-directed task, which is frequently considered a good criterion to define the occurrence of a lapse in attention [5, 50]. Longer RTs (considered attention lapses) were associated with an increased activity in several regions related with the DMN, including the PCC, the precuneus and the middle temporal gyrus. Weissman and colleagues [3] also reported an impaired performance accuracy with the global/local selective-attention task² performed by participants. Additionally, their results revealed an evident activation trade-off between the DMN and the attentional networks, which control the maintenance of sustained attention. According with these authors, both reduced spontaneous activity in the attentional networks and greater spontaneous activity in the DMN leads to a disruption on attentional state, facilitating the occurrence of attentional lapses. The findings of Yordanova et al. [1] also reinforce the relation between the DMN and attention lapses. They were able to identify specific patterns by

²**Global/local selective-attention task** - Task in which, normally, subjects are asked to response to a visual stimulus that consisted of a large character/symbol (the global level) made out of small characters/symbols (the local level). It is often used to explore the idea that global structuring of a visual scene precedes analysis of local features [57].

analysing the distribution of error occurrence, which corresponded to behavioural oscillations with a frequency of 0,08 and 0,05 Hz in ADHD patients. This evidence seems to be in accordance with the concept of the DMN in the brain, because this network is characterized to manifest intrinsic oscillations at very low frequencies - approximately less than 0,1 Hz [17, 22, 58] - detectable in both EEG and fMRI recordings. Also according with these authors, one possible source of subconscious interference which determines both correct and error human actions may be the DMN. Moreover, others studies also reported evidence that there might be an organized mode of brain function that is present as a default state and suspended during specific goal-directed behaviours, being the magnitude of its deactivation possibly directly related with the occurrence of perturbations in attention [17, 56].

Concluding, during periods of mind wandering, small but consistent increases in brain activity occur in a specific set of regions called the default-mode network (DMN), which can be intrinsically correlated with perturbations of subject's attention state. Although much is known about the topological and connectional properties of the DMN, its functions remain a matter of debate.

1.3.3 Task-Positive and Task-Negative Brain Regions are Anticorrelated

Taking into account the above cited studies, during performance of goal-directed tasks, certain regions of the brain routinely increase activity, whereas others routinely decrease activity. Indeed, there is increasing evidence that during performance of attention-demanding cognitive tasks, two opposite types of responses are observed: task-positive regions exhibits increased activations, whereas task-negative regions or associated with the DMN routinely exhibit activity decreases. This dichotomy becomes more pronounced, as the attentional demand of the task is increased: activity in task-positive regions is further increased, whereas activity in task-negative regions is further decreased. In this context, through the study of spontaneous fluctuations in the BOLD fMRI signal, Fox et al. [59] have examined resting state correlations associated with six predefined seed regions, three regions routinely exhibiting activity increases - task-positive regions or regions belonging to the attentional networks - and three regions routinely exhibiting activity decreases - task-negative regions, or regions related with the DMN (figure 1.8). Specifically, they observed anticorrelations between a region in the premotor cortex, part of a task-positive network, and the PCC and medial prefrontal cortex (MPFC), regions belonging to the task-negative network. According with Fox et al. [59], an inefficient DMN deactivation in combination with a disproportionately low activation of the attentional network can lead to error-precursor states.

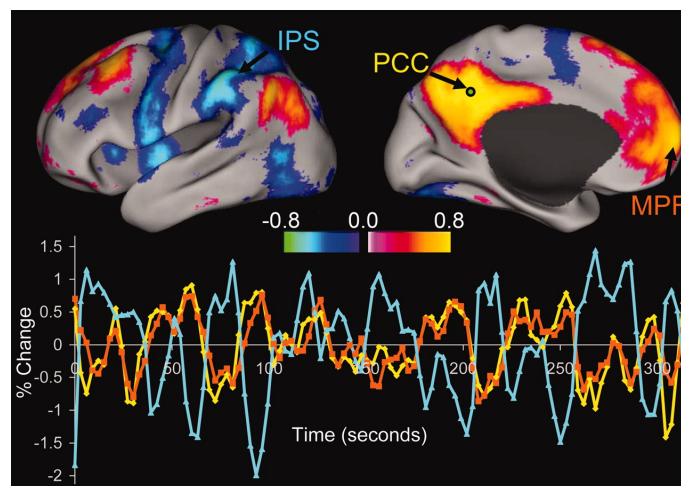


Figure 1.8: Results obtained in the BOLD fMRI study performed by Fox and colleagues [59]: intrinsic correlations between the PCC - a task-negative region - and all other voxels in the brain for a single subject during resting fixation. **(Top Panel)** The spatial distribution of correlation coefficients shows both correlations (positive values) and anticorrelations (negative values). **(Bottom Panel)** The time course for a single run for the seed region (PCC, yellow), a region positively correlated with this seed region in the MPFC (orange), and a region negatively correlated with the seed region in the IPS (blue) is shown.

Globally, the above cited findings indicate that momentary lapses in attention are associated with both reduced activity in task-positive regions and greater activity - or less task-induced deactivation - in the DMN.

1.3.4 The Behavioural Causes of Lapses in Attention

Because subject's attentional state can be influenced by many factors such as sleep quality patterns, illicit drugs, alcohol, caffeine and nicotine consumption, some studies which explored the effects of those conditions on attention will be reviewed in the subsections below.

1.3.4.1 Sleep Patterns Influence Attentional States

Usually, drowsiness at work is associated with insufficient or poor-quality sleep mainly because sleep disorders or irregular sleep patterns. Note that drowsiness states are intrinsically correlated with lapses in attention. In fact, impairments on daytime performance due to sleep loss are frequently experienced by humans and associated with a significant human, social, and financial cost. *Microsleeps*³, sleep attacks, and lapses in attention increase with sleep loss as a function of wake state instability. It has been established that

³*Microsleeps* - The term *microsleep* is usually used to describe brief episodes, between 1-15 and 14-30 seconds of EEG-defined sleep [4].

specific neurocognitive domains, such as executive attention, working memory, and other cognitive functions are notably vulnerable to sleep loss [60].

According to several authors, hallmarks of sleep deprivation during task performance have been associated with increased errors, slowing of RTs and increased RT variability [5, 60]. Cognitive performance variability involving those hallmarks in sleep-deprived subjects has been hypothesized to reflect wake state instability [60].

In fact, numerous groups have demonstrated lapses of responsiveness under monotonous task conditions with sleep deprivation, adopting a variety of auditory and visual sustained attention tasks, and mental tasks [4]. For example, Chee et al. [61], by conducting a BOLD fMRI study, concluded that although lapses in attention can occur even after a normal night's sleep, they are longer in duration and more frequent in sleep deprivation conditions. Their findings suggest that performing a certain task while sleep deprived involves periods of apparently normal neural activation alternated with periods of depressed cognitive and sensory functions, such as visual perception.

Sleep deprivation condition has proven to be an useful experimental paradigm for studying the neurocognitive effects of sleep disturbances on cognitive performance. Recent studies have investigated also the effects of sleep restriction on cognitive performance. According to several authors, repeated days of sleep restriction to between three and six hours time in bed has been observed to increase daytime sleep and *microsleep* occurrence propensity, decrease cognitive accuracy and speed, and increase the occurrence of lapses in attention [60].

Concluding, both sleep deprivation and sleep restriction conditions influence subject's task performance, being important to monitoring sleep patterns when studies about the neural correlates of lapses in attention are being conducted.

1.3.4.2 Effects of Drugs Abuse, Nicotine, Caffeine and Alcohol Consumption on Attention

According to several authors [62, 63], regular use of illegal drugs is suspected to cause cognitive impairments, and it has been linked to symptoms of inattention and deficits in learning and memory. For example, recent research trends are to specify the relation between patterns of ecstasy use and side effects, specifically long term neurocognitive damage. Raznahan et al. [64] have reported long term neurocognitive damage and mood impairment with ecstasy use.

Nicotine enhances reorienting of attention in visuospatial tasks [65], and there are indications that its effects are largest on processes of selective attention or on disengaging attention from irrelevant events and shifting it to behaviourally relevant stimuli [66].

Regarding the behavioural effects of caffeine, it has been established that caffeine improves performance on simple and complex attention tasks, and affects brain networks responsible for the alerting, and executive control. However, there is inconclusive evidence about the influence of habitual caffeine consumption on subject's task performance [67].

Presently, alcohol is the dominant drug contributing to poor job performance. Evidence from public roadways and work accidents provides an example for work-related risk exposure and performance lapses. Alcohol reduces the scope and focus of attention, such that behaviours are determined only by highly salient environmental cues. According with the Alcohol Myopia Model, alcohol rather than disinhibit, produces a myopia effect that causes users to pay more attention to salient environmental cues and less attention to less salient cues [68].

Indeed, regular or sporadic consumption of illicit drugs, alcohol, caffeine and/or nicotine affects attention levels, being also important to monitoring the ingestion's patterns of these substances when it is intended to study the neural and eye activity signatures of lapses in attention.

1.4 How To Predict Attentional Lapses

EEG measures have been widely used to predict the occurrence of lapses in attention and momentary changes in vigilance. Analysis of fMRI data are being also conducted to identify patterns of haemodynamic activity which could predict events of transient inattention, although EEG modality be more adequate for this purpose, mainly due to its better time resolution. Many other behavioural and psychophysiological indices have also been used to assess and quantify a loss of vigilance. An example is the measure of several eyes indices (eye blinks [6–8]; gaze fixations [7,8]; PERCLOS [8]; pupil diameter [6,7,9] and gaze position [8, 10, 11]).

1.4.1 EEG-based Lapse Detection

The electrophysiological correlates most reliable for lapse state estimation performance and which could provide an accurate online detection of fluctuations on attentional levels are based, mainly, on frequency domain measurements. Research into EEG-based lapse detection has been encouraged by studies showing that lapses are correlated with changes in EEG spectra, namely spectral amplitude and phase-locking measures.

1.4.1.1 Prestimulus Alpha Amplitude

The functional role of alpha activity has been brought about by high-density EEG and MEG recordings. Thereby, there is an increasing evidence towards alpha amplitude could predict visual performance [29]. Alpha waves are most evident in a resting condition

in comparison when a certain sensory stimuli is presented. Alpha amplitudes are also characterized to show a significant amount of variation, indicating that fluctuations in alpha amplitude point to different relevant brain states [29]. In line with this assumption, recent studies have explored if prestimulus alpha amplitudes could indeed predict whether or not a stimulus will be perceived. In fact, it has been suggested that the presence of alpha oscillations exerts an overall inhibitory effect in cortical processing, leading to an impairment in task performance and fluctuations on attentional levels.

Van Dijk et al. [2] have studied the influence of prestimulus alpha activity on visual perception. Stimuli at detection threshold were presented to investigate how discrimination ability is modulated by prestimulus amplitude in the alpha frequency band. They reported that alpha activity around the parieto-occipital sulcus modulated negatively the visual discrimination ability, impairing the detection of relevant stimuli (figure 1.9). These findings provide evidence that lapses in visual attention could be associated with brain states characterized by high amplitude of posterior alpha oscillations.

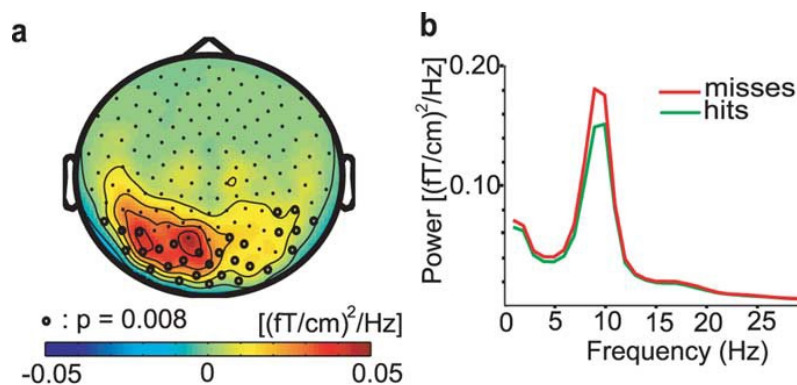


Figure 1.9: Results obtained by Van Dijk et al. [2] about prestimulus alpha amplitude between hit and missed trials - trials in which subjects did and did not perceive the stimulus, respectively. **(a)** Topography of the 8-12 Hz spectral amplitude of the difference between misses and hits (planar gradient) averaged over subjects. Electrodes showing significantly stronger alpha amplitude for misses than hits are highlighted with dots (p -value < 0.008; corrected for multiple comparisons). **(b)** Grand average of the spectra calculated for the prestimulus time window (-1000 to 0 ms), over the sensors that showed a significant difference between misses and hits in the alpha band (8-12 Hz).

Similarly, Ergenoglu et al. [69], using also a visual detection task, have reported a negative correlation between alpha amplitude and perception performance. Their results revealed that high levels of prestimulus alpha amplitude predicted a miss, whereas low levels of alpha amplitude predicted a hit.

Hanslmayr et al. [35] have also investigated the electrophysiological correlates of perceiving shortly presented visual stimuli, by analysing both amplitude and phase-coupling

of prestimulus oscillations. It was already reported in previous studies that the single observers differ in whether they correctly perceive a certain visual stimulus flashed shortly into their eyes, or not. Moreover, the same person may perceive the same stimulus in some situations but not in others. This variability was then explored by these authors, by searching for the prestimulus brain mechanisms which mediate this phenomenon and, therefore, could differentiate between perceiving and non-perceiving observers and perceived and unperceived trials within subjects. Similar to the above studies, interestingly, the negative relationship between alpha amplitude and perception performance was enhanced by the findings reported, emphasizing again that alpha oscillations represent an active filter mechanism indicating that the brain is inhibited when alpha oscillations are high in amplitude. It is assumed that failures to detect visual targets are related to lapses of attention, thus linking alpha oscillations to attention modulation.

Thereby, it seems that high alpha amplitudes indicate internally oriented brain states, which make it hard to perceive a shortly presented stimulus, whereas low alpha amplitudes are associated with externally oriented brain states, which bias the system toward processing information from the sensory sources. Based on the evidence that ongoing oscillatory activity prior to an event has a strong impact on subsequent processing, it was proposed that parieto-occipital alpha amplitude reflects the excitatory/inhibitory state of visual processing brain regions, enhancing or diminishing the likelihood of stimulus perception, respectively [29].

1.4.1.2 Alpha Phase at Stimulus Onset

The neural and perceptual responses to a stimuli are also modulated by the alpha phase at which stimulation occurs. Indeed, it was recently shown that sensory processing and awareness vary with respect to the phase of ongoing EEG alpha oscillations [29]. Globally, the studies about this issue have reported an improvement in the visual discrimination ability when the stimulus was presented at the positive peak of an alpha cycle [29]. Interestingly, despite not recording EEG signals, the study of Mathewson et al. [70] had an important impact on the understanding of this mechanism, because they showed that perception performance was best if a main stimulus was presented 82 ms after a prestimulus flicker, by varying the interstimulus period between the latter and the former, which exactly matches the period length of 12 Hz. Their study provided evidence that the detection of a visual stimulus can be optimized by manipulating alpha phase at stimulus onset via steady state visual evoked potentials. Concluding, it seems that positive phases of EEG alpha oscillations at stimulus onset are correlated with an improvement on visual attention levels.

1.4.1.3 Phase-Coupling in Alpha Frequency And Higher Frequency Bands

Whereas several works have studied how prestimulus alpha amplitude influences the discrimination ability of a visual stimulus, far fewer studies have investigated the role of the prestimulus phase-coupling phenomenon on task performance [29]. One reason for this may be the computational cost associated with the algorithm required for calculating phase-coupling, due to the many possible pairs of EEG sensors. The studies of Hanslmayr et al. [35] and Kranczioch et al. [71] are two examples in which the influence of the prestimulus phase-coupling on visual discrimination ability is explored.

Regarding the study of Hanslmayr et al. [35], contrasting trials in which the stimulus was correctly perceived (perceived trials), with trials in which the stimulus was not perceived (unperceived trials), they found a significant difference in prestimulus alpha phase-coupling, by applying the method of PLV calculation. In fact, perceived trials exhibited significantly lower levels of phase-coupling between frontal and parietal electrode locations than unperceived trials. They reported that subject's mean perception rate increases in a linear manner with decreasing alpha phase-coupling. Moreover, single trial analyses also indicate that perception performance can be predicted by the phase-coupling phenomenon not only in the alpha but also in beta and gamma frequency ranges. Beta and gamma PLV analyses revealed that perception performance decreases monotonically with decreasing phase-coupling in those frequency bands (figure 1.10). These results showed that changes in synchronization in the alpha, beta and gamma frequency ranges reflect changes in the attentional demands of the task and are directly related to behavioural performance.

Interestingly, Kranczioch et al. [71] have obtained similar results to Hanslmayr et al. [35]. Using an attentional blink paradigm, they compared the difference between trials in which the second trial was correctly perceived and in which the second target was missed, in terms of the phase-coupling phenomenon. Their findings have also revealed that periods of low alpha prestimulus phase-coupling predicted correct perception of the second target stimulus.

Concluding, the above cited findings reveal that whereas phase-coupling in the alpha frequency band inhibited visual perception, phase-coupling in high frequency bands such beta and gamma band supported perception performance. Thus, high levels of phase-coupling in the alpha frequency range probably indicate internally oriented brain states, whereas low levels of alpha phase-coupling indicate externally oriented brain states.

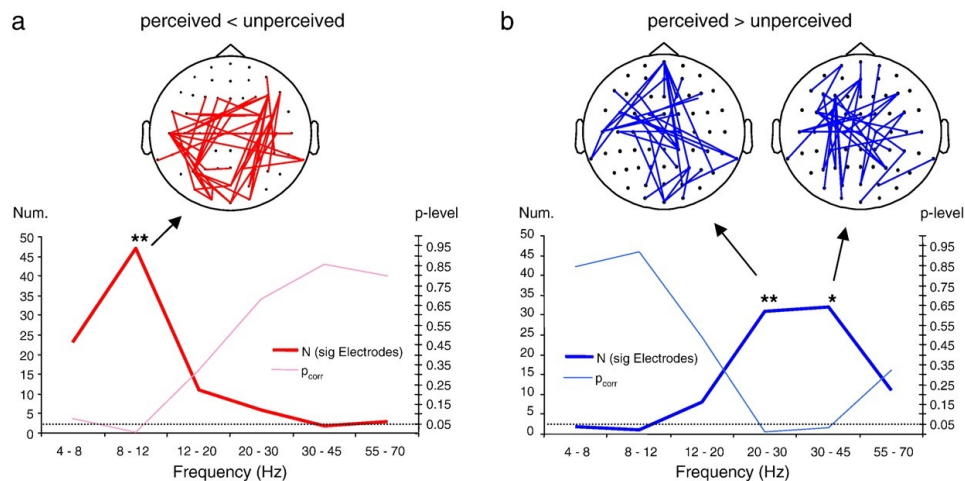


Figure 1.10: Results obtained by Hanslmayr et al. [35] about phase-locking in the alpha, beta and gamma frequency bands, for within-subjects analysis between perceived and unperceived trials. Note that for this analysis only data from Perceivers - subjects that correctly had perceived the stimulus - were considered. **(a)** Perceived trials showed decreased prestimulus (-500 to 0 ms) phase-coupling in the alpha frequency band (8-12 Hz), contrasting with unperceived trials. **(b)** Regarding higher frequency bands, perceived trials showed increased phase-coupling in the beta (20-30 Hz) and gamma range (30-45 Hz). The topography distribution of the electrodes pairs where phase-coupling was significantly decreased (red lines) and where phase-coupling was significantly increased (blue lines) for perceived trials is plotted on the left and on the right, respectively. To account for multiple testing, a two-stage randomization procedure was carried out to investigate which electrode pairs showed a significant difference between the two conditions: at first, Wilcoxon-tests were calculated for each electrode pair, and then a randomization test based on 5000 permutations was carried out. The thick red **(a)** and blue **(b)** lines (scaled on the left Y-axis) show the number of electrode pairs revealing significant difference between perceived and unperceived trials ($p\text{-value} < 0,005$, Wilcoxon-test). The light red **(a)** and blue **(b)** lines show the $p\text{-level}$ of the randomization test (scaled on the right Y-axis).

1.4.2 fMRI Lapse Detection

Recent functional neuroimaging studies have also shown that evoked response variability is correlated with ongoing activity fluctuations and that this variability transpires into perceptual variability. As a function of the paradigm, the effects of ongoing activity on perceptual performance have been observed both locally in accordingly specialized brain areas and in distributed spatial patterns that resemble resting-state or intrinsic connectivity networks [72]. Momentary lapses in attention can be predicted by patterns of brain activation in specific cerebral regions, using fMRI [3, 73, 74], although much more studies using EEG or MEG techniques have focused in this field, by identifying the electrophysiological signatures preceding lapses in attention [2, 35, 69, 71]. Relatively few studies so far have explored the prestimulus haemodynamic activity in brain regions and how it can influence attention levels, using fMRI, mainly because its poor temporal res-

olution. This limitation highly compromises the accurate definition of the actual timing and modulation of the underlying precursor signals of the haemodynamic response function associated with perturbations on attention state. Nevertheless, the study of Weissman et al. [3] is an example of a fMRI study which revealed prestimulus brain activity patterns which precede attention lapses. They reported that brain patterns in specific cerebral regions, as for example reduced prestimulus activity in anterior cingulate cortex and right prefrontal regions, less deactivation of the DMN, reduced stimulus-evoked sensory activity, and increased activity in widespread regions of frontal and parietal cortex, could predict the occurrence of lapses in attention.

Using fMRI, Eichele et al. [73] studied brain activity on a trial-by-trial basis using a visual task requiring rapid responses, finding a set of brain regions in which the temporal evolution of activation predicted performance errors. Their findings revealed that a relevant proportion of errors stemmed from both a decrease in task-related brain activity associated with engagement in the task and a simultaneous relative increase in DMN activity. Additionally, the study of Ress et al. [74] also using event-related fMRI showed that the BOLD response in early visual areas was correlated positively with performance in a visual pattern detection task. They reported that the increase in BOLD signal correlating with the detection ability reflects an attention-related increase in the baseline firing rates of a large population of neurons in the visual cortex.

Taking together, the above findings provide insights into the brain network dynamics related to human performance fluctuations using fMRI modality. Globally, it seems that perturbations on subject's attention state are associated with an inefficient DMN deactivation in combination with a low brain activation in task-positive regions.

1.4.3 Eye Parameters Predicting Attentional Fluctuations

As was mentioned before, visual perception highly influences task performance, mainly when the maintenance of a stable goal-directed behaviour (as driving) is required. Attention improves visual perception. In this line of research, several studies explored whether eye movements or parameters could predict perturbations on subject's attention levels. For example, some of those studies investigated the relationship between eye movements and driving performance, by measuring eye movement patterns of drivers, and assessing their drowsiness levels, concluding that gaze position and pupil diameter are reliable predictors of fluctuations in attention [7, 10, 75]. Other studies have examined subject's performance during extreme circumstances such as sleep deprivation, concluding that oculomotor parameters such as large changes in visual scanning may be indeed affected by fatigue effects, reflecting lower states of attention [76–78]. Additionally, by recording eye movements during a tracking task, Van Orden et al. [6] have found oculomotor

parameters strongly correlated with task performance, including eye blink frequency and duration, re-fixation frequency, size and pupil diameter, which could be combined in a multi-factorial index to detect attention decline conditions. According with those findings, changes in eye movements and/or pupil measures are correlated to changes in both levels of fatigue and attention. Currently, the main challenge is to determine whether oculomotor metrics can be generalized across tasks and different levels of task difficulty. These oculomotor patterns could be used to produce reliable workload indicators that predict poor performance in real time [7]. However, it is important to emphasize that it is currently unknown if transient fluctuations in those indirect measures of cognitive function correspond to changes in activity of brain networks related to attention [9].

1.4.3.1 Pupil Diameter Indicates Attentional Fluctuations

The pupil is defined as the opening through which light enters into the eye, being responsible for the onset of the visual perception's process. The diameter of this opening is determined by the relative contraction of two opposing sets of muscles, within the iris, the sphincter and dilator pupillae, being determined primarily by light and accommodation reflexes [79]. Additionally to the reflexive control of pupillary size, there are fluctuations in pupillary diameter, which are usually less than 0,5 mm in extent independent of luminance fluctuations. This miniature pupillary movements appear to be reflections of changes related with brain activation events which underlie human sensory procession and cognition [79]. Large-scale changes in pupillary diameter are defined as being apparent to a trained observer or recording apparatus and are often associated with peripheral or central nervous systems lesions. In contrast, small-scale pupillary movements are rapid fluctuations in pupillary diameter difficult to detect by unaided observation.

Pupillary dilation, the light reflex, and spontaneous fluctuations in pupil size have been used as dependent variables in several psychological investigations. There is increasing evidence for the effectiveness of the pupil as an index of autonomic activity in psychophysiological research. The degree of pupil dilation has been shown to be a reliable measure of cognitive load and vigilance state [80]. However, few studies have focused on the possibility that pupillometric parameters as the pupil diameter can predict lapses in attention, by inspecting changes in those measures considering prestimulus time windows. The majority of the research on this issue examined whether certain measures of pupillary changes could be used to detect phasic lapses in alertness, but only examining pre-response time windows, time segments defined after the stimulus onset and before the subject's response and, thus studying the pupillary reflex to the stimulus. It is important here to emphasize the study of Kristjansson et al. [81]. They reported a significant difference for the sample mean prestimulus baseline pupil diameter between long response

RTs (indicating lower alertness state) and “normal” response RTs (associated with an alert state) conditions, considering a 102 ms prestimulus time window. Indeed, on average, the baseline pupil diameter prior to longer RTs was 0,27 millimetres smaller compared to the baseline pupil diameter prior to “normal” RTs. According with these results, it seems that the prestimulus baseline pupil diameter could predict subject’s alertness levels.

Taking into account the above findings, it appears that pupil diameter could be a reliable indicator of the subject’s attention state, being probably correlated with fluctuations in task performance.

1.4.3.2 Gaze Position Dynamics as a Measure of Attention Levels

Some studies have also investigated how gaze position dynamics is correlated with mind wandering states associated with decreased alertness levels, when subjects are performing goal-directed tasks such as driving. By recruiting subjects to perform a car-following task in a low-traffic simulated driving environment, He et al. [11] reported that mind wandering states were associated with a reduced standard deviation of horizontal eye position, concluding that mind-wandering caused horizontal narrowing of drivers’ visual scanning. Similarly, Recarte et al. [10] investigated the consequences of performing verbal and spatial-imagery tasks on visual search when driving, reporting that visual functional-field size decreased horizontally and vertically, in particular for spatial-imagery tasks.

1.5 Management Systems for Predicting Vigilance Decline States

Recently, several computational algorithms and devices for attention management and monitoring were developed, which have been successful in predicting perturbations in subject’s attention levels. Some examples are described in the subsections below.

1.5.1 EEG/Eye Parameters-Based Machine Learning Algorithms For Predicting Lapses in Attention

Several algorithms based on machine learning techniques have been developed for lapse detection, based only on features extracted from EEG signals and on both EEG and eye activity measurements. Over the years, several attempts have been made to develop algorithms capable of predicting the subject’s task performance, mainly in the field of driving behaviour. As the variation of EEG rhythms has been linked with the occurrence of driving errors or drowsiness events, algorithms based on EEG-based features have been

widely explored in this field [82]. As an example, Fu et al. [83] have developed an algorithm based on EEG features which were extracted by applying a probabilistic model to the raw EEG data filtered in six different frequency bands - alpha (8-12 Hz), lower alpha (8-10 Hz), upper alpha (10-12 Hz), beta (19-26 Hz), gamma (38-42 Hz) and broad band (8-30 Hz). Their model was capable of distinguishing between fully awake and sleeping states in drivers, obtaining accuracy scores above 98% for all the subjects. They also tried to develop an algorithm which could predict three types of driver's alertness state: sleep, drowsy (associated with low attention levels) and awake. Recognition accuracies decreased for the three-state classification approach, as it was expected, because distinguishing between awake and sleeping states was much less demanding, although a mean accuracy value across subjects of 90% was obtained. However, it is important to emphasize here that it is much more difficult to predict fluctuations in attention as it was intended in this study, when compared with distinguishing between two completely different states as fully awake or sleeping.

Additionally, Lawhern et al. [84] have developed an algorithm which accurately captured changes in the statistical properties of the alpha frequency band. These statistical changes are highly correlated with short (0,5-2 seconds time length) bursts of high frequency alpha activity, called *alpha spindles* by some authors [85–87], and form a reliable measure for detecting those patterns in EEG, mainly in the parietal/occipital brain areas, which are statistically related to lapses in attention, as was mentioned in 1.4.1.1. They achieved approximately 95% accuracy in detecting *alpha spindles*, with timing precision to within approximately 150 ms.

The majority of the algorithms which have been developed in this field were based on the “offline” detection of different alertness states. However, the future research will address issues such as the online detection of the subject's drowsiness state during goal-directed tasks, such as driving [82].

1.5.2 Attention Management Devices

Three recently developed alertness management systems, based on EEG measurements and eye and head movements, are described below.

1.5.2.1 Classification of Subjects Attention Levels using Portable EEG Systems

Recently, driver fatigue detecting systems have gained increasing attentions in the area of driving safety. Several studies have been successful in applying EEG signals to accurately detect individuals fatigue/attention states in goal-directed tasks. However, these studies were performed using tethered, ponderous EEG equipment, which are not feasible to develop a fatigue detecting system appropriate to real life scenarios. To get

past this limitation, Wali et al. [88] have developed a system which classifies the driver drowsiness in four levels of distraction (neutral, low, medium and high), based on wireless EEG signals. The system developed acquires the EEG signals over the complete scalp using 14 electrodes. They tested a classification algorithm based on machine learning techniques, and have extracted two statistical features from the EEG data acquired when subjects performed a simulated driving task in a virtual reality based environment. Those features were obtained from the amplitude spectrum of the EEG signals considering four frequency bands (delta, alpha, beta and gamma), using a hybrid scheme based on different types of *wavelet* transforms functions and *Fast Fourier Transform* (FFT). The proposed system was tested in 50 subjects and provided a maximum classification accuracy of 79,21%.

Additionally, the NeuroSky[©] [89] has also developed a system capable to measure subject's attention and meditation levels, by indicate the user's level of mental focus, namely NeuroSky's eSense[™]. Their system comprises the NeuroSky MindSet, which consists in a portable bluetooth headset with a couple of sensors added that measure EEG signals, which is commercially available. By recruiting 14 subjects they tested their system by classifying the state of consciousness of each subject (in meditation, or "neutral" state; or in a more focused state, achieved by fixating their gaze on a dot on a screen). They achieved a classification accuracy of 86% for differentiating between these two type of mind workload.

1.5.2.2 Fatigue Detection using Smartphones

Recently, He et al. [90] have developed a driver fatigue detection system which uses a smartphone. Contrasting with other alternative fatigue detection systems, which use devoted in-vehicle cameras and EEG sensors, a smartphone-based fatigue detection technology would be more portable and affordable. In the proposed system, the front camera of a smartphone captures images of the driver, and then feeds the images to the processor of the smartphone for image processing, using computer vision algorithms for face and eye detection. For capturing images for data processing, the smartphone must be mounted on the dashboard of a vehicle, placed horizontally with the front camera aimed towards the driver's face. The system is based on fatigue detection algorithms which are carried in five steps: image preprocessing, face detection, eye detection and blink detection, and, lastly, fatigue judgement. In this latter stage, three criteria based on the frequency of head nods, frequency of head rotations and PERCLOS were used to assess the state of driver's fatigue. A simulated driving study using their system has demonstrated that drowsy drivers differed significantly in the frequency of head nod, head rotation and eye blinks, compared to when they were attentive. However, smartphone-based fatigue de-

tection systems have also disadvantages. One of the limitations associated with this type of systems is that eye detection is difficult for drivers wearing glasses. Although, this type of technologies have important applications in reducing traffic accidents related with drowsiness states and improving driving safety on the road.

Concluding, it is possible to distinguish between different states of alertness using EEG signals and eye measurements. Nevertheless, future refinement of these systems is necessary for them to be useful in a real life scenario.

Chapter 2

Materials and Methods

2.1 Visual Stimuli Paradigm and Behavioural Task

The visual task adopted in this study was designed to be monotonous and to be sensitive to lapses in attention. The scheme of the sequence of events was adapted from the studies of Yordanova et al. [1], Weissman et al. [3] and Bonnelle et al. [50]. The sequence file was developed in Matlab[®] (R2011a, The MathWorks, USA) using the Psychophysics Toolbox for display [91].

The task chosen was a simple choice reaction time task, designed to study the neural correlates of sustained attention using EEG. The task was simple enough to be performed accurately by all the subjects, but demanding enough for participants to show fluctuations in performance, measured as differences in the response RT, as the task progressed. Subjects were instructed to respond as quickly and as accurately as possible to one of two possible stimuli, having two response possibilities. Similar speeded reaction time tasks have been used in several studies to investigate sustained attention in humans [50].

The stimuli were generated with Matlab[®] (R2011a, The MathWorks, USA). They were designed to be clearly visible, in a way that all subjects should be able to perform the task in a satisfactory way. However, the stimuli selected were subtle enough to induce incorrect or missed responses by the subjects during attention lapses.

The task consisted in three runs of ~ 12 minutes each. Each run was divided in three blocks of trials. In the beginning of each block, subjects sitted comfortably at a distance of 55 centimetres from the screen were asked to focus in a light grey fixation dot ([230 230], RGB) which appeared in the centre of the screen for 15 seconds. Then, the grating square of the figure 2.1(c) appeared for 3 seconds, as a cue indicating the beginning of a sequence of trials. Each side of the square measured 2,91 degrees of visual angle. The square was filled by a vertical black and white sinewave grating consisting of ~ 18 cycles within the square. On top of the square, one of two targets chosen randomly were

displayed: an arrowhead pointing to the left - figure 2.1(a) - or an arrowhead pointing to the right - figure 2.1(b). The vertical sinewave grating forming the arrowheads was phase shifted by $\frac{\pi}{2}$ radians relatively to the background square (see figure 2.1).

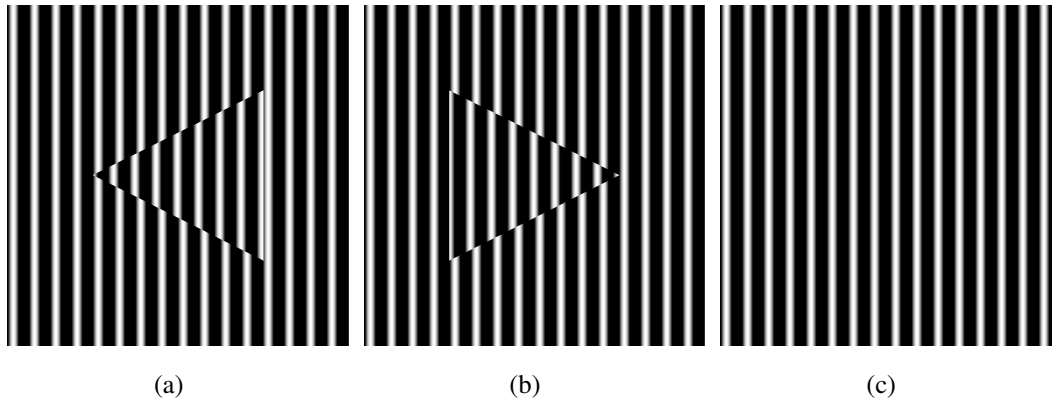


Figure 2.1: Stimuli used in the task and their background. The stimuli consisted in two different types of targets: **(a)** an arrowhead pointing to the left on top of a square both filled with a sinewave grating pattern; **(b)** the same stimulus, but with the arrowhead directed to the right. **(c)** The grating square only (without an arrowhead) remained in the centre of the screen, between the appearance of each stimulus along the task.

The interstimuli interval (ISI) jittered between 3 and 10 seconds to avoid expectancy effects. Targets were shown for 200 milliseconds at random intervals. After each stimulus, the background square - figure 2.1(c) - remained in the centre of the screen along the ISI. Subjects were asked to continue fixating the gaze in the centre of the screen until a new stimulus was presented. The number of trials in each block was determined by the trade-off between two parameters: the cumulative sum of the ISI values along each block of trials and its fixed duration, which was 240 seconds (see figure 2.2 for a schematic representation about the task). Participants were asked to press the key '1' on a keyboard for the target with the arrow pointing to the left - figure 2.1(a) - whereas was expected that subjects pressed the key '3' in response to the stimulus with the arrow directed to the right - figure 2.1(b). Accordingly, responses were produced with the left and the right index fingers. Subjects were also asked to maintain their index fingers in the same position along the whole task: the index finger of the left hand over the key '1' and the index finger of the right hand over the key '3', without pressing it. Additionally, it was requested that subjects responded as quickly as possible to each stimulus. Obviously, this behavioural task aimed at maintaining the subjects' attention on the visual stimuli during the EEG recording session.

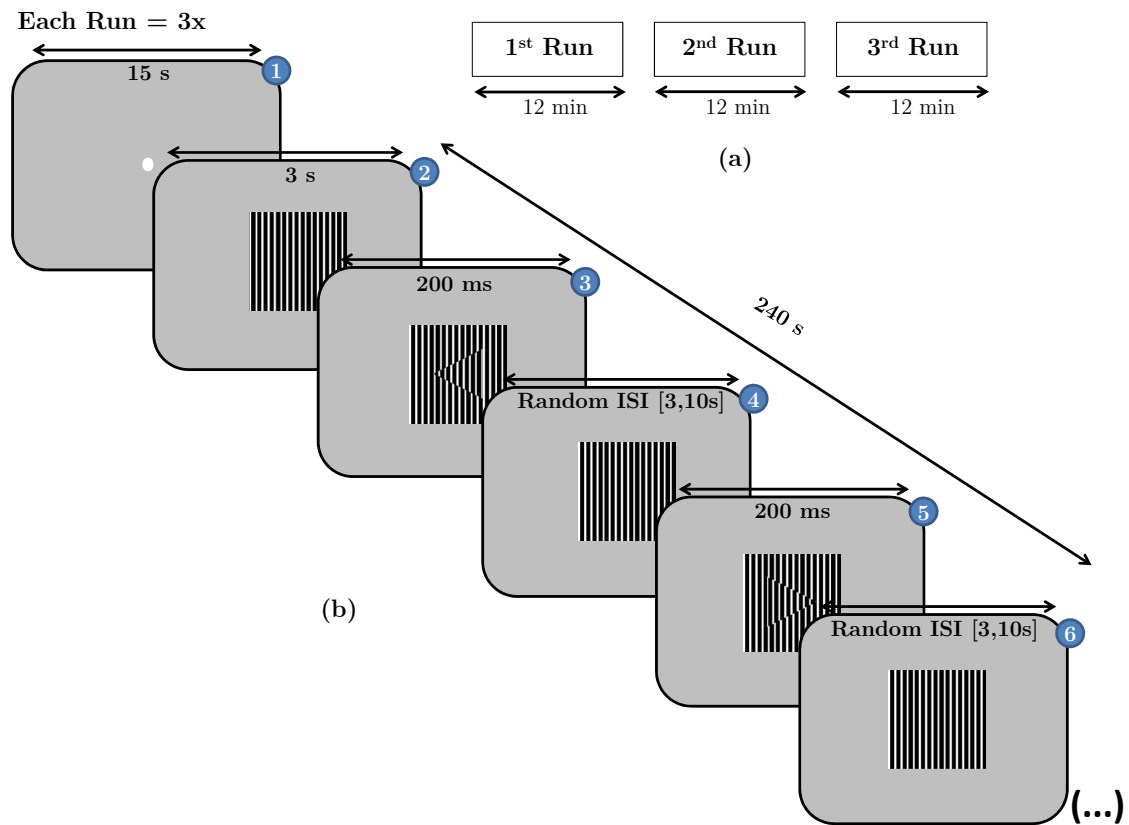


Figure 2.2: Scheme illustrating the simple choice reaction time performed by subjects. (a) The task consisted in three runs of approximately 12 minutes each. (b) Each run was divided in three blocks of trials of approximately 4 minutes each. (1) In the beginning of each run, subjects were asked to focus in a light grey fixation dot which appeared in the centre of the screen for 15 seconds. (2) Then, a grating square appeared for 3 seconds as a cue indicating the beginning of a sequence of trials. (3) and (5) Thereafter, one of the two possible stimuli was randomly chosen and presented, with an ISI jittered between 3 and 10 seconds to avoid expectancy effects. Targets were shown for 200 milliseconds at random intervals. (4) and (6) After each stimulus, the background square remained in the centre of the screen along the ISI. Subjects were asked to continue fixating the gaze in the centre of the screen until a new stimulus was presented.

For this purpose, a white noise¹ sound who contained every frequency within the band range of audible sound frequencies - between 20 Hz to 20 kHz - was played while subjects were performing the task, to block outside noises that might disturb their attention levels. The task was conducted in a slightly dimmed room and subjects sat in a comfortable chair. All participants completed the three runs and were given a rest break between each run to avoid eye strain and tiredness due to long visual stimulation. Subjects practiced the task for a few minutes before the beginning of recordings. In the figure 2.3 is presented an illustration of the behavioural task performed by subjects.

¹**White noise sound** - A white noise sound is described by a random signal with a flat (constant) power spectral density. In other words, it is an audio signal that contains equal power within any frequency band with a fixed width [92].

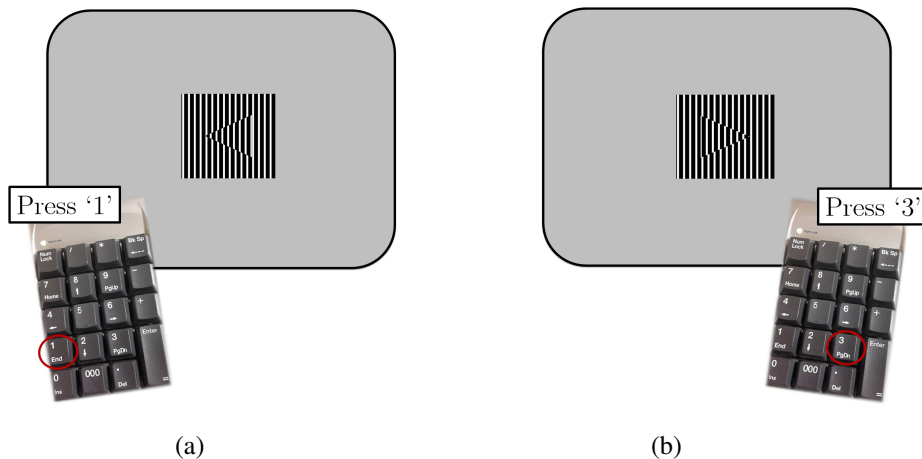


Figure 2.3: Behavioural Task. Subjects had to press response buttons with the index finger of their hand corresponding to the direction indicated by the target: **(a)** ‘1’ for the arrowhead on top of the grating square pointing to the left; **(b)** and ‘3’ for the stimulus with the arrowhead directed to the right. Responses must be produced with the left and right hand, respectively.

The stimuli were presented in the centre of a Dell monitor (Sensomotoric Instruments) with a resolution of 1680×1050 pixels and a monitor area of 47×30 cm, over a grey background ([80 80 80], RGB). The computer screen had a refresh rate of 60 Hz and was under computer control (3 GHz Intel Core 2 Duo), using a NVIDIA video board.

2.2 Participants

Participants’ characterization is in the table 2.1. Subjects signed an informed consent document (appendix A.1) before the beginning of the experiment. They were also asked to answer some surveys before the beginning of the task (see section 2.3). The participants agreed to participation in psychophysical, electrophysiological and eye measurements after a full description of the aims and methods implemented on the study. The study was approved by the Ethics Committee of the Faculty of Medicine of Coimbra; all procedures complied with relevant laws and institutional guidelines.

2.3 Surveys Performed

At the moment of recruiting or when subjects arrived at the laboratory for testing, they were inquired about personal socio-demographic and clinical aspects (appendix A.2). Subjects reported to have normal or corrected-to-normal vision and no neurological and/or psychiatric diseases. None of the participants inquired reported to have had problems with addictive substances consumption in the past and with illicit drugs ingestion at the present. Only one subject has reported to ingest frequently refrigerants which contain

Table 2.1: Participants characterization in terms of age, gender, academic degree, occupation and handedness (Age=mean \pm standard deviation).

Number of Participants	20	
Age (years)	22,900 \pm 1,714	
Sex	Male	9 (45%)
	Female	11 (55%)
Academic Degree	High School	1 (5%)
	Undergraduate Degree	11 (55%)
	Master (MSc)	8 (40%)
Occupation	Student	14 (70%)
	Employed	5 (25%)
	Unemployed	1 (5%)
Handedness	Right-handed	17 (85%)
	Left-handed	3 (15%)

caffeine (such as Coca-Cola[®], Pepsi[®], Ice-Tea[®], etc). Participants characterization in terms of daily habits such as drinking coffee, alcohol or smoking is in the figure 2.4.

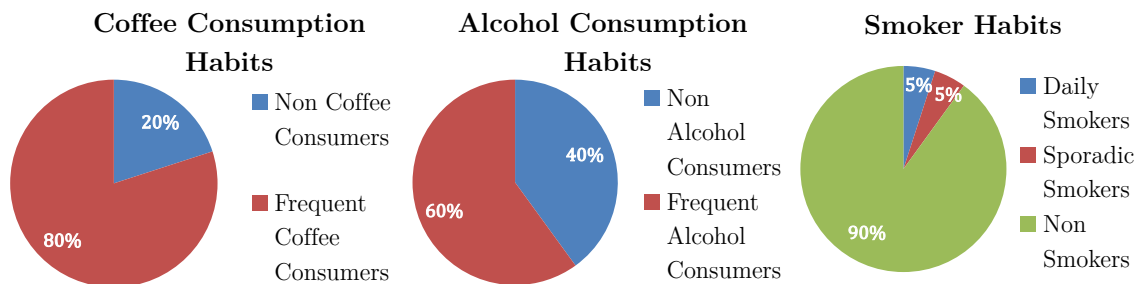


Figure 2.4: Participants characterization regarding daily habits in terms of drinking coffee, alcohol and smoking.

Because sleep deprivation/restriction influences attention levels and, consequently, task performance, as was mentioned in chapter 1, participants were also asked to response to the Pittsburgh Sleep Quality Index (PSQI) inventory, to assess their sleep habits regarding the month before testing (appendix A.3). For monitoring sleep patterns over the five days prior to testing, subjects were also asked about their sleep quality and duration, every day in that period of time preceding the test (see point 2.3.1.2). For each day, responses must be in accordance with what happened in the night and day before.

It was also conducted the Edinburgh Handedness Inventory (appendix A.4) to provide a quantitative assessment of handedness for each subject [93]. The results obtained for this survey are also in the table 2.1.

2.3.1 Sleep and Caffeine/Alcohol/Nicotine Consumption

2.3.1.1 Pittsburgh Sleep Quality Index

The PSQI is a self-rate questionnaire which assesses sleep quality and disturbances over a one-month time interval, distinguishing between “good” and “poor” sleepers [94]. This inventory quantifies sleep quality taking into account quantitative aspects of sleep such as sleep duration, sleep latency or number of arousals, as well as more purely subjective aspects, such as “depth” or “restfulness” of sleep. The PSQI provides a clinically and useful assessment of a variety of sleep disturbances, distinguishing between “good” and “poor” sleepers.

The PSQI inventory consists of 19 self-rated and 5 questions rated by the bedpartner or roommate (if one is available). The latter five questions are not tabulated in the scoring of the PSQI, being used for clinical information only. The PSQI is then calculated taking into account the 19-self rated questions, which are grouped into seven component scores, each weighted equally on a 0-3 scale. In all cases, a score of “0” indicates no difficulty, while a score of “3” indicates severe difficulty. The seven component scores are therefore summed to yield a global PSQI score, which has a range of 0-21. Those seven components are divided in subjective sleep quality, sleep latency, sleep duration, habitual sleep efficiency, sleep disturbances, use of sleeping medications, and daytime dysfunction. Higher PSQI scores indicate worse sleep quality. A global PSQI score of “0” indicates no sleep difficulties whereas a PSQI of “21” suggests severe difficulties in all components evaluated. It was established a threshold for the PSQI global score of 5 to determine good/poor sleep quality (PSQI \leq 5 associated with good sleep quality; PSQI $>$ 5 associated with poor sleep quality). The results for the PSQI inventory for the participants of this study are in the table 2.2.

2.3.1.2 Sleep Patterns and Caffeine/Alcohol/Nicotine Ingestion During the Five Days Prior to Testing

Subjects have then asked to report the time at which they went to bed and waked up, the number of sleep hours and the time in minutes which took to fall asleep, by answering to a survey every day along the five days prior to the test day. Each survey was supposed to be answered taking into account the day and night before. They were also inquired about the part of the day in which they felt more tired or drowsy and if they took a break for sleeping along the day before. Additionally, participants were asked about their sleep quality and if they felt tired in the morning. The first four forms were responded online (appendix A.5) and the last one (appendix A.6), which corresponded to the day and night before of the test day, was answered in the lab before the beginning of the experiment.

This last survey had additional questions about caffeine derivatives, alcohol, nicotine and psychoactive/illicit drugs ingestion on the day before and on the test day. Subjects were also inquired if they took any medication. Participants characterization in terms of all these factors is also in the table 2.2. None of the subjects inquired has reported to have smoked, or ingested medication both on the test day as on the day before.

Table 2.2: Participants characterization in terms of sleep patterns during the five days prior to testing and sleep quality and disturbances regarding the month before testing (PSQI index); and caffeine and alcohol ingestion on the day before and on the test day. *Mean \pm Standard Deviation. **[Minimum; Maximum]. ***33 ml bottles of refrigerants containing caffeine, such as Coca-Cola[®], Pepsi[®], Ice-Tea[®], etc.

Sleep Patterns during 5 days prior to testing	Number of sleep hours (5 days)	7,591 \pm 0,721*
		[5,626;9,000]**
	Minutes to fall asleep (5 days)	21,790 \pm 15,024
		[2,800;50,800]
	% of restful sleep nights (5 days)	80,000 \pm 19,467
		[40;100]
Sleep Habits regarding the month before testing	PSQI	3,952 \pm 2,334
		[1;9]
	Number of “poor” sleepers	3 (15%)
Caffeine Ingestion	Number of coffees on the day before	1,700 \pm 1,302
		[0;4]
	Number of coffees on the test day	0,700 \pm 0,733
		[0;3]
	Number of caffeine derivatives bottles*** on the day before	0,450 \pm 0,686
		[0;2]
Number of caffeine derivatives bottles*** on the test day	0,100 \pm 0,308	
	[0;1]	
Alcohol Ingestion	Number of subjects which consumed alcohol on the day before	3 (15%)
	Number of subjects which consumed alcohol on the test day	1 (5%)

As it can be concluded by observing the table 2.2, the participant’s sample used in this study was globally well-rested, excluding three subjects which revealed a PSQI score above the threshold considering for distinguish “good” from “poor” sleepers (subjects 5, 8 and 20).

2.4 EEG and Eye-Tracking Procedures

In the two subsections below (2.4.1 and 2.4.2) are described the EEG and eye-tracking recording procedures conducted in this study, respectively.

2.4.1 High-density EEG

EEG measurements employ a recording system consisting of electrodes with conductive media, amplifiers, an A/D converter and a recording device. Electrodes are required to record the signal from the head surface and amplifiers bring the microvolt signals into the range where they can be digitalized accurately. The role of the converter is to change from analogue to digital form [25].

An electrode cap - Quick CapTM from Compumedics Neuroscan - with 64 electrodes installed on its surface, which consist of Ag-AgCl disks was used in this study. This type of electrodes can record accurately changes in brain signals potential [25]. Successful recording of EEG depends on a good conductive path between the recording electrode and the scalp of the subject. There are several crucial steps that should be taken to ensure a good contact between the electrode and the subject's scalp. These steps are listed on 2.4.1.3.1.

Subjects were also routinely inquired about their comfort during preparation and also during EEG recordings.

2.4.1.1 Materials

In figure 2.5 are presented all materials which were necessary for the preparation of EEG recordings.

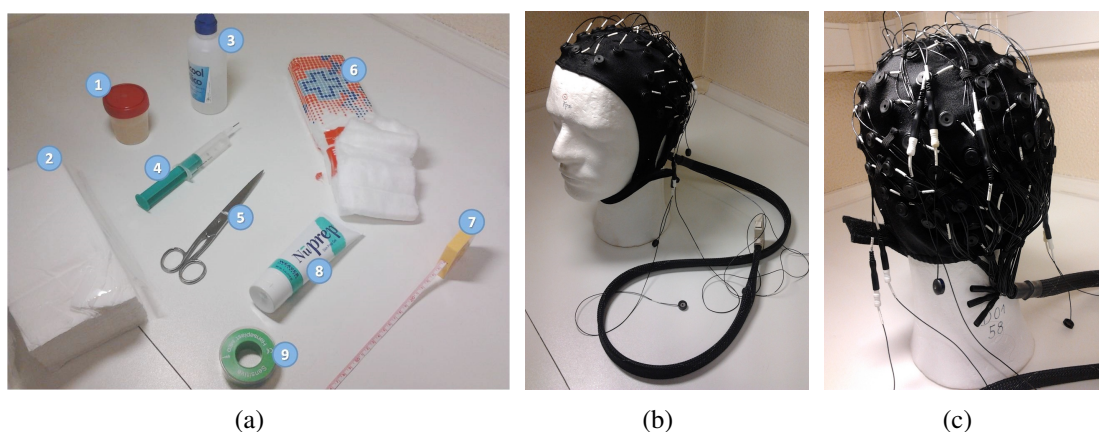


Figure 2.5: All materials required in the preparation phase were prepared in advance. (a) 1. Electro-gel, Quik Gel; 2. Cleaning wipes; 3. Alcohol; 4. Syringe with bult tip needle; 5. Scissor; 6. Cotton; 7. Tape measure; 8. Abrasive exfoliating gel; 9. Tape. (b) and (c) High-density 64 Channel Quick-Cap.

2.4.1.2 Devices

Several electronic devices were used to acquire EEG signals and eye measurements. For EEG data acquisition, software and hardware from NeuroScan (Compumedics NeuroScan, USA) were used. Behavioural task responses were recorded by the stimulation computer, which also run the stimuli presentation program script, using the Psychtoolbox available for Matlab[®] [91]. The EEG acquisition system from Neuroscan was under control of another computer.

2.4.1.3 EEG Recording Procedure

2.4.1.3.1 Subject Scalp Preparation and Positioning of the Cap

At first, subject's scalp surface was exfoliated using an abrasive gel (Nuprep) - figure 2.5(a). Secondly, it was important that skin areas were cleaned to ensure low impedances between the electrodes and the subject's scalp and skin surface. Therefore, these areas were cleaned with an alcohol swab.

After exfoliating the scalp and cleaning skin areas, the cap was positioned on the head of the participant. The cap was pulled onto the subject's head in a slowly and carefully manner, ensuring that midline row of electrodes was properly aligned on the head. For a precise positioning of the cap it is necessary mark the vertex on the subject's scalp. For that, it was used a tape measure to find the distance between the nasion and inion on the participant. The point half-way between these two points was the vertex. After identifying the CZ electrode on the EEG cap (see figure 2.6), it was adjusted to positioning the CZ electrode on the head's vertex. Then, it was checked if the CZ electrode was positioned halfway between the ears, considering the left and right pre-auricular points (see figure 2.7 for information about the location of nasion, inion and pre-auricular points). Finally, it was ensured that the lowest occipital electrode was approximately two fingers above inion, and FPZ approximately two fingers above the nasion.

All scalp electrodes were loaded with electrode gel beginning with the ground and reference electrodes, using a syringe with a blunt tip needle. The function of the electrode gel is to build a column of conductive medium between the scalp and the surface of the electrode. The first electrodes loaded were the ground and reference electrodes. The ground electrode is needed for getting differential voltage by subtracting the same voltages showing at active and reference points [25].

of the Neuroscan system permits visualization of electrodes impedance without interrupting data acquisition, based on a grating colour system (figure 2.8).

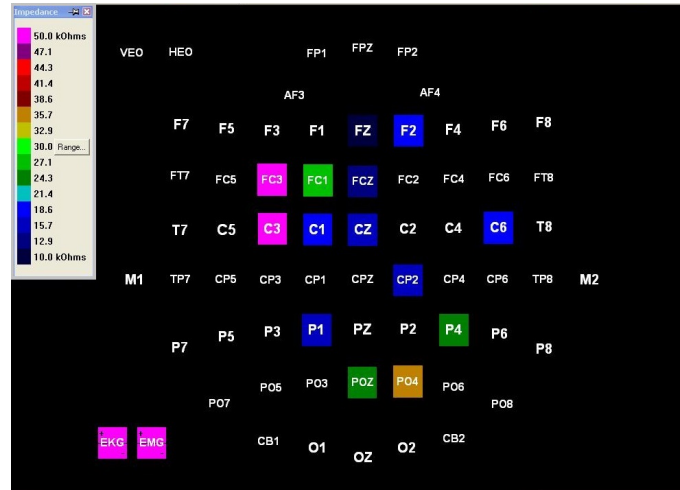


Figure 2.8: The simple visual display with impedance values for each electrode provided by the Acquire Data Acquisition software of the Neuroscan system used. Visual display is based on a grating colour system. Impedance testing is available without interrupting data acquisition. Performing impedances tests while applying the electro-gel is a good principle to obtain the best results. Electrodes with the highest impedance are represented in pink (>50 kOhm) and electrodes having the lowest impedance values are represented in black (<10 kOhm).

If most electrodes had impedances that were sufficiently low (<10 kOhm), no further preparation was required. However, it was frequently observed high impedances even after all electrodes were loaded with electro-gel. Abrading was often necessary, always began with the ground and reference electrodes. In this process, it was usually sufficient to make sure that the needle had contact with the scalp, and then simply rotate the needle in a circular manner (in a arc). Placing light pressure down the electrode holder with one hand while abrading with the other hand, ensured that the electrode gel remained confined to the reservoir of the electrode holder. As soon as the impedance for an electrode began to decrease, abrading was stopped and the preparation needle was removed from the electrode. Usually, it was also necessary inject a little more gel into the electrode holder after verifying that there were not air bubbles. In the figure 2.9 is presented a participant being prepared for EEG acquisition.

2.4.1.3.3 Data Acquisition

Before starting the recordings, participants were informed about the problems of bio-electric artifacts (as talking, blinking or body movements) and were requested to minimize them without too heavy attentional burden.

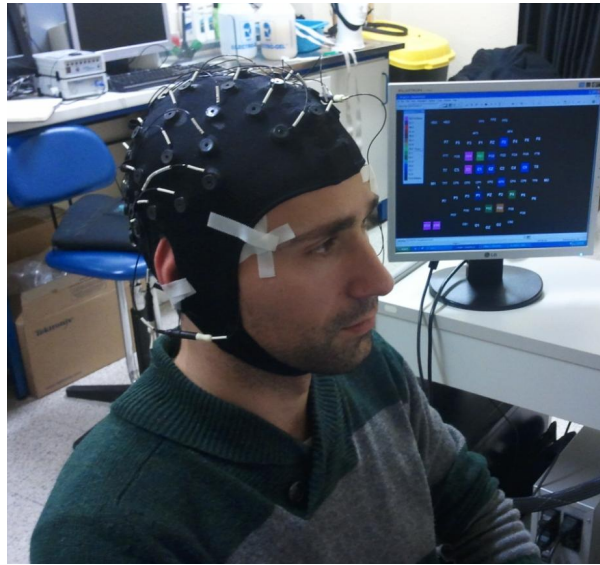


Figure 2.9: Example of a participant being prepared for EEG acquisition.

EEG signals were acquired from the scalp at a sampling rate of 1000 Hz. During recordings, the amplifier fed the signal through the Acquire Data Acquisition Software allowing the online visualization of the signals being recorded (figure 2.10).

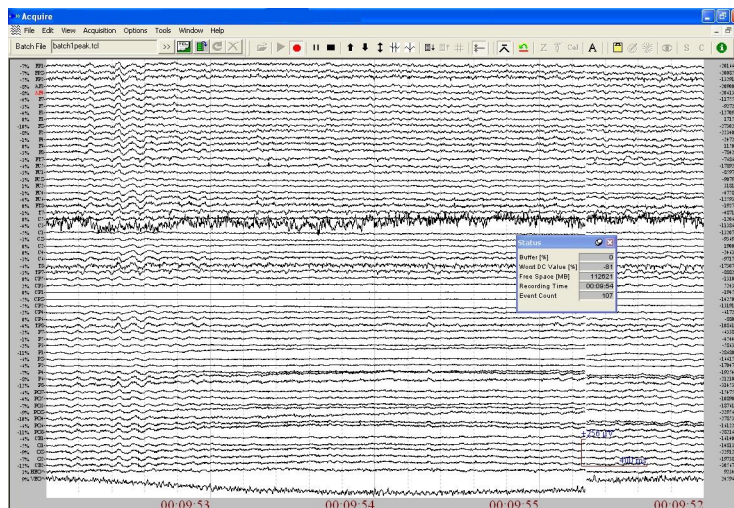


Figure 2.10: Acquire Data Acquisition software layout (Compumedics NeuroScan, USA).

Different trigger pulses were generated at the onset of each block of trials, for every instant a target was presented, and when subjects pressed a button in response to a target. The trigger pulses were sent for the EEG software acquisition, to allow further preprocessing procedures.

During recordings, some electrodes were marked as bad and skipped from analysis by having high impedances, interference and too much noise or no reliable acquisition.

The digitized EEG signals were saved and processed offline.

2.4.2 Eye-Tracking Method

A Dark Pupil Eye Tracking System was used in this study to monitor subject's gaze position and pupil measures, which requires a calibration step before each experimental run. In this type of systems, the eye is illuminated by an infrared light at an angle from an infrared sensitive camera. The eye and face reflect this illumination but the pupil absorbs most infrared light and appears as a high contrast dark ellipse. The centre of the pupil is then located and mapped to gaze position via an eye-tracking algorithm [95].

2.4.2.1 Devices

Hardware and software from iView XTM (SensoMotoric Instruments - SMI) were used for eye monitor measurements. Two computers controlled the eye-tracking device, one controlling it remotely - the stimulation computer - and other controlling all camera equipment and which run the iView XTM software, the iView XTM workstation. This latter also processes all eye signals from the experiment.

2.4.2.2 Eye-Tracking Recording Procedure

2.4.2.2.1 Preparing Stimulation Computer and Eye-Tracking Device

After the subject was prepared for EEG data acquisition, the iView XTM Software was initialized and software settings were checked for starting the automatic calibration procedure, in order to proceed for the eye tracking measurements.

2.4.2.2.2 Test Person Placement

The person's head was positioned in front of the stimulation computer on a chin rest to maximize head stability. In order to test if person's eyes were correctly tracked by the eye-tracking device, the participant's position was adjusted at the beginning of each run. The participant must be located in front of and centred with the stimulation monitor, and two white dots - figure 2.11(a) - must be visible in the RED Tracking Monitor (a monitor that helps to place the subject in front of the eyetracker and which is part of the eye-tracking software), indicating that the subject was correctly positioned. If the subject was not centrally placed relatively to the eyetracker, arrows indicated the direction of the adjusted position - figure 2.11(b). In the figure 2.12 is presented a participant correctly positioned and prepared to starting the task.

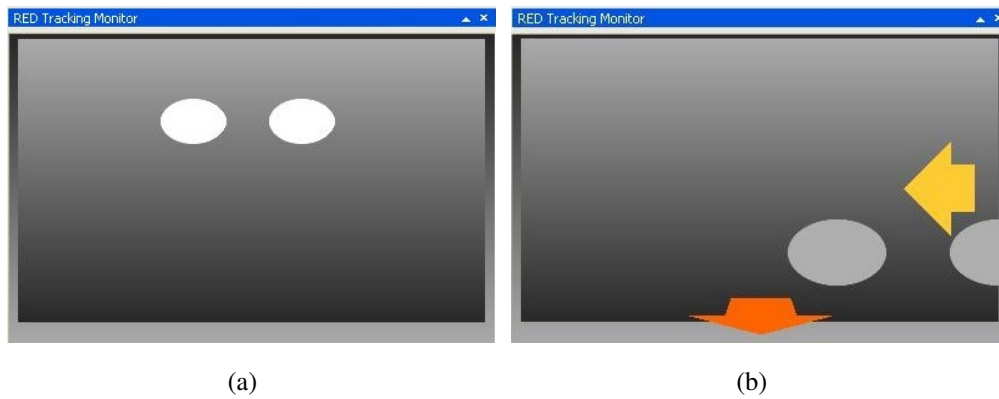


Figure 2.11: RED Tracking Monitor from iView XTM Software. **(a)** RED Tracking Monitor gives a representation of the tracked eyes and the test subject's placement. If no test person is sitting in front of the RED camera system, the control only shows a blank page. **(b)** If the test person was seated inadequately an arrow appeared on the RED Tracking Monitor, indicating the direction of the adjusted position.



Figure 2.12: Example of a participant prepared for EEG acquisition correctly positioned for the eye-tracker monitoring his eyes.

2.4.2.2.3 Calibrating Eye-tracking Device

All systems that map gaze position require a calibration set before recording in order to relate orbital position to a point in the test person's view [95].

Calibration of the iView XTM eye-tracking system involved instructing the participant to look at specific points while the system observed the pupil position at these points. The system could then develop the necessary algorithm to translate pupil position to gaze position to all points in the area defined by the calibration. It uses the point targets as reference points and creates a mapping function that relates all eye positions to points in

the calibration area, which is defined by the area on which the eyetracker is calibrated (in this specific case, it was considered all the screen area).

The calibration procedure adopted in this study was programmed to run automatically. By starting this procedure, one calibration point was displayed for each time for the participant and the system automatically accepted each calibration target and proceeded to the next point. It was adopted a 5-points calibration method and it was ensured that the test person complied with the calibration and did not look away from points too early.

2.4.2.2.4 Data Acquisition

Before starting the recordings, participants were asked to minimize the amount of upper body movements along the recordings, for a correct monitoring of their eyes for the eye-tracking system.

Eye-tracking data was controlled remotely by the stimulation computer. The stimulus presentation program script had the remote commands necessary for sending the trigger pulses for iView XTM workstation, starting eye measures recording and saving the recorded data. Trigger pulses generated online corresponding to each event of the experiment (the onset of a new block of trials, the presentation of a stimulus, a response given by the subject) were send by the stimulation computer for the eye-tracking system, to allow further preprocessing procedures. The result of each measurement run was stored by the software to a binary *.idf* file. For analysis, IDF (iView Data File) data were imported offline into the IDF Converter program (SensoMotoric Instruments, Germany) and converted to a text file which could be loaded and read using Matlab[®]. Gaze position, based on the point of regard, for horizontal and vertical directions, and pupil diameter measurements, for both right and left eyes were recording with a sampling rate of 500 Hz.

2.5 Data Analysis

All the behavioural, EEG and eye-tracking data analysis performed were conducted using Matlab[®] scripts. EEG data from two subjects were not considered for analysis due to excessive external noise and bioelectric artifacts.

2.5.1 Analysis of Behavioural Responses

The Matlab[®] script wrote to run the task in the stimulation computer and for displaying it on the monitor also recorded each key pressed by the participant along the experiment, and the time instant at which the subject pressed it. It also recorded the sequence of stimuli and ISI values generated online. The struct containing task parameters and behavioural measures was automatically stored after each experiment in the stimulation computer. Another Matlab script was also built to analyse performance measures

from the behavioural data stored for each subject. With this script, it was possible to obtain the indexes of correct, wrong and no responses (or missed trials). Only the first key pressed after stimulus' appearance was taken into account for responses analysis. Correct responses were considered when the subject pressed the correct button. If the first key pressed by the subject after target's appearance was not the correct one, it was assigned as an incorrect response. A missed trial was reported when the subject did not press any button between two consecutive events (see figure 2.13 for a schematic representation of the motor responses classification procedure).

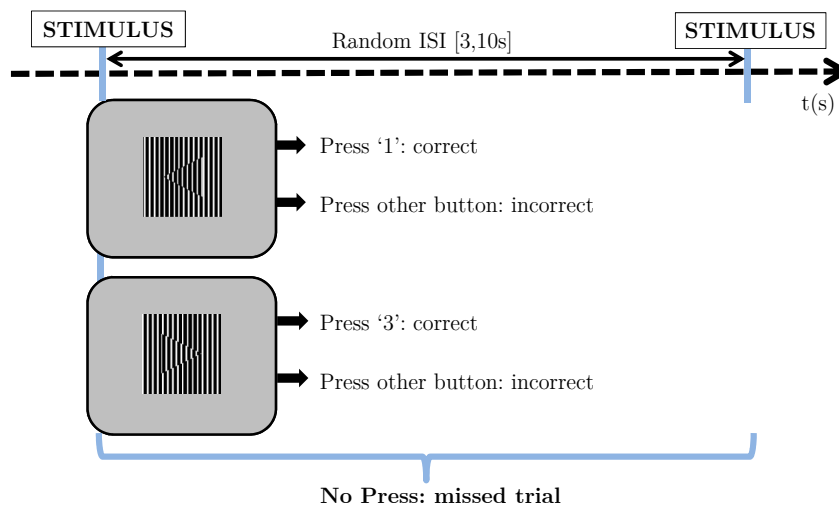


Figure 2.13: Conceptual diagram explaining the criteria to characterize and count the behavioural responses. Only the first button pressed after the stimulus' appearance was taken into account for motor responses classification. Correct responses were considered when the subject pressed the correct button. If the first key pressed by the subject was not the correct one it was assigned as an incorrect response. A missed trial was reported when the subject did not press any button between two consecutive events. Response RT values are defined as the elapsed time between stimulus onset and the instant of the first button press.

The mean and median values for the response RT, defined as the elapsed time between stimulus onset and the instant of the first button press, were computed for each hand separately considering only the correct responses. The percentage of errors and missed trials were also computed.

2.5.2 Criteria to Select Conditions for EEG and Eye-Tracking Data Analysis

RT measurements were used to characterize and compare subjects' attention levels. It was assumed that increases on response RT reflected reductions of attention to the relevant stimulus. Therefore, in order to select the conditions based on RT measures to be compared regarding the EEG and eye-tracking data analysis, the following procedure was

performed. For the definition of conditions, the analysis of RT was conducted separately for each hand. RT values for each hand were divided into quartiles. The corresponding trials for each quartile were joined for both hands. The overall number of trials was then organized in four groups, according with response time measurements, as systematized below (figure 2.14).

The trial's indexes of each group were used to split EEG and eye-tracking data according with four different conditions - RT_{Q1} , RT_{Q2} , RT_{Q3} and RT_{Q4} - ranging from fast trials (RT_{Q1}) to slow trials (RT_{Q4}). Group and individual analysis of spectral amplitude, phase coherence and eye-tracking measures were conducted considering all the conditions (RT_{Q1} , RT_{Q2} , RT_{Q3} and RT_{Q4}). For individual phase coherence analysis on a single trial basis, RTs were converted in *z-score* values, considering each hand separately.

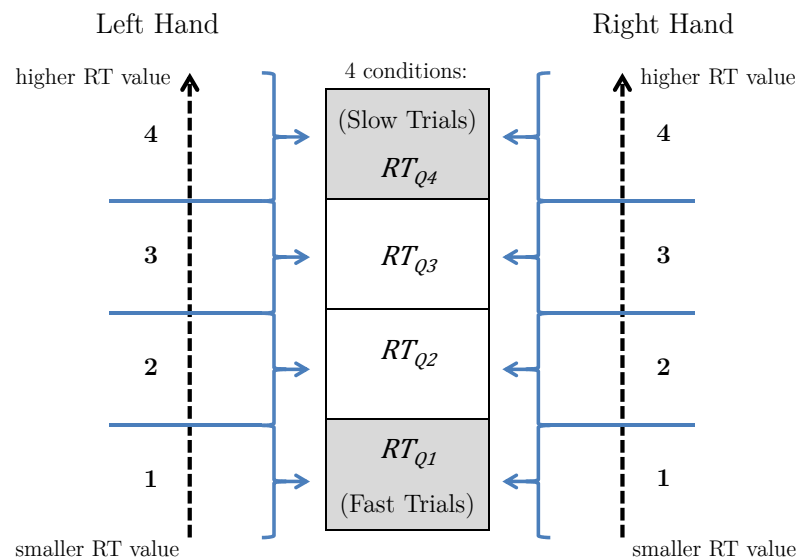


Figure 2.14: Scheme illustrating how trials were divided in four bins (conditions) based on corresponding RT values. At first, trials were distributed in quartiles (1, 2, 3 or 4), according with corresponding RT values, for each hand separately. Then, the trials which corresponded at the same quartile (1, 2, 3 or 4) were joined for both hands, being the overall number of trials divided in four different conditions: RT_{Q1} , RT_{Q2} , RT_{Q3} and RT_{Q4} , ranging from fast - RT_{Q1} - to slow trials - RT_{Q4} .

2.5.3 EEG Data

2.5.3.1 EEG Data Analysis

The pre- and processing steps applied to EEG data are schematized in the figure 2.15.

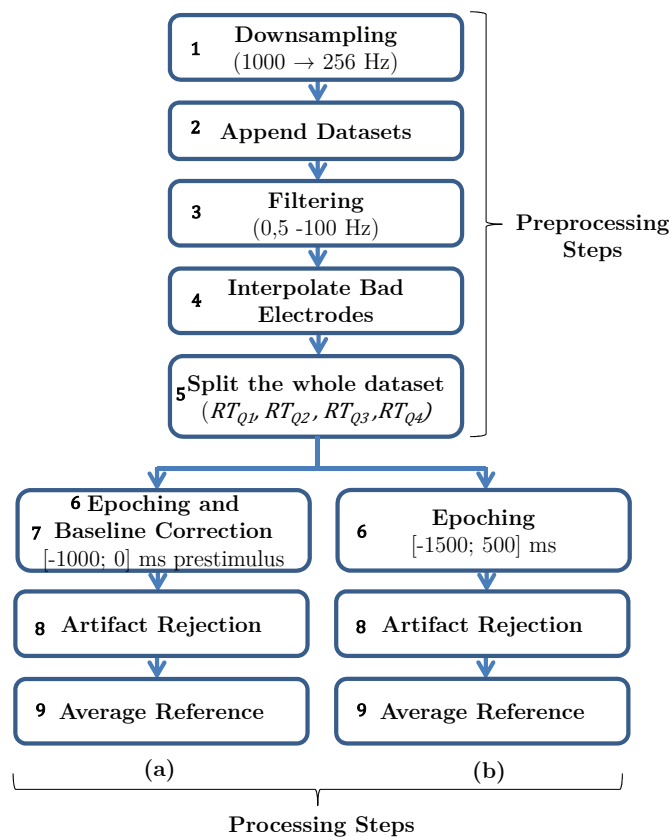


Figure 2.15: Pre- and processing steps applied to EEG data for (a) amplitude spectral and (b) phase coherence analysis. **(Preprocessing Steps)** **1.** At first, sampling rate of EEG data was changed to 256 Hz, because data were acquired at 1000 Hz. The purpose of reducing the sampling rate is to save memory and disk storage. **2.** Then, the three data sets of EEG data representing each run of the experiment were appended in a single data set. **3.** Next, the data was filtered using a linear finite impulse response (FIR) filter, implementing a routine which applies the filter forward and then again backward, to ensure that phase delays introduced by the filter are nullified. Due to memory issues, in order to obtain a band-pass signal, first a high-pass filter with a cutoff frequency of 0,5 Hz was applied to the data, and then data was low-passed, using a filter with a cutoff frequency of 100 Hz. **4.** After filtering, bad electrodes (showing external noise) were removed and interpolated using a spherical method. **5.** Thereafter, the whole data set was split in four different files by selecting the specific trials' indexes corresponding to each condition defined by the procedure explained in the figure 2.14, based on RT values. Each one of the data sets generated corresponded to a different condition. **(Processing Steps)** **(a)** **6.** Then, for alpha amplitude analysis, each file was divided into epochs defined by a prestimulus interval of 1000 ms (from -1000 ms to the onset of the stimulus, 0 s). **7.** Baseline correction was performed along each time segment. **8.** The artifact rejections were run automatically on the basis of deflections with amplitude higher than $100 \mu\text{V}$, considering a 1000 ms prestimulus time window. **9.** EEG recordings were also re-referenced to a common average reference, excluding the electrooculogram and earlobe electrodes. **(b)** For phase coherence analysis a similar EEG processing procedure was conducted, excluding for the steps **6.** and **7.** For this analysis, epochs from -1500 ms to 500 ms poststimulus were defined (step **6.**), and none baseline correction was applied (step **7.**).

After EEG data were processed, statistical comparisons were conducted for assessing if there were significant differences between the number of trials retained for analysis, for each condition (see subsection 2.5.5 for information about the statistical methods applied in each analysis).

2.5.3.2 Frequency Domain Analyses of EEG data

EEG data can be represented in the frequency domain using *Fourier* transforms or *wavelets*, as was mentioned in chapter 1. In this study, the FFT method was implemented for amplitude spectral analysis and Morlet *wavelets* for phase coherence analysis. First, it was determined at the group level if there were significant differences between trials associated with different RTs. Second, it was investigated which individuals present significant differences.

2.5.3.2.1 Spectral Analysis

For computing the frequency spectrum, it was used the FFT, an efficient and fast algorithm that computes the *Discrete Fourier Transform* or DFT. The FFT assumes that the number of data points in the data intervals is a power of two. In order to be applied to data intervals of arbitrary length, those intervals are frequently padded with zeros. Therefore, to avoid interpolation of FFT data at a given frequency, the original sampling rate of 1000 Hz was reduced for 256 Hz (a power of two) in the preprocessing phase.

Before applying the FFT, EEG data processed were windowed (figure 2.16). Since the FFT method assumes that the segment repeats itself in a periodically manner, artifacts can occur in high frequency ranges due to discontinuities at the segment boundaries. These artifacts can be reduced, by applying a window function to the data prior to performing a FFT. Therefore, a Hamming window was applied to the data and the FFT was computed from the resultant signal. It was specified a percentage value of 10% for the fraction of the signal segment which would be affected by the windowing ($P = 0,10$). The window function $w(t)$ which was applied to each segment data is mathematically expressed by the formula:

$$w(t) = \begin{cases} \alpha - \beta \cos\left(\frac{2\pi}{P} \frac{t}{SL}\right), & \text{when } 0 \leq t \leq t_1 \\ 1, & \text{when } t_1 < t < t_2 \\ \alpha - \beta \cos\left(\frac{2\pi}{P} \left(1 - \frac{t}{SL}\right)\right), & \text{when } t_2 \leq t \leq SL \end{cases} \quad (2.1)$$

where : $\alpha = 0,54$; $\beta = 0,46$; $P = 0,10$; and $t_1 = SL \frac{P}{2}$; $t_2 = SL - t_1 = SL \left(1 - \frac{P}{2}\right)$.

The time point t lies within the data segment of length SL . In the figure 2.16 is presented the Hamming window defined by the equation 2.1.

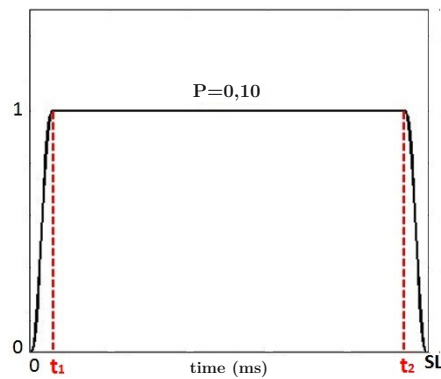


Figure 2.16: Graphic illustrating the Hamming window applied to a data segment of length SL . The P value specifies the range in which the window function is used as a percentage. Note that when P approaches 0 refers to the rectangular window where no values in the whole segment are damped by the data window. Taking $P = 1$ corresponds to the original definition of Hamming. The lower is this specified percentage, the smaller the range affected by the window function.

The *Fourier* method for analysing a finite time series of a certain T length (in seconds) is built around a sinewave of frequency $1/T$ - in Hz - and its harmonics. The output of the FFT is then taken for such frequency bins. The maximum resolution in the frequency domain is determined by the ratio between the sampling rate of the signal and the extended segment length in data points being analysed.

Computing Prestimulus Alpha Amplitude

Spectral amplitude in the alpha frequency range was computed for parietal, parieto-occipital and occipital electrodes (P7, P5, P3, P1, PZ, P2, P4, P6, P8, PO7, PO5, PO3, POZ, PO4, PO6, PO8, O1, OZ, O2), using the windowing method explained above and the FFT, and taking into account both prestimulus windows of 500 and 1000 ms length. Considering that the segment epochs used for this analysis had 128 (for the 500 ms prestimulus window) and 256 time points (for the 1000 ms prestimulus window); and the signal had a sampling rate of 256 Hz, FFT was computed in defined frequency bins of 2 Hz, for the 500 ms prestimulus window; and in frequency bins of 1 Hz for the 1000 ms prestimulus window. For calculating alpha amplitude, alpha peak frequency (α_{peak}) was first determined for each subject within the range of 8-13 Hz, taking the mean spectra for selected electrodes and all trials. Thereafter, the area under the curve (AUC) was computed in the window defined by $\alpha_{peak} \pm 2$ Hz, for each single trial and for those electrodes, for both 500 ms and 1000 ms prestimulus windows. Alpha amplitude was then compared between the four conditions defined in subsection 2.5.2 - RT_{Q1} , RT_{Q2} , RT_{Q3} and RT_{Q4} .

Both group and individual analysis were performed for each prestimulus window. Statistical comparisons were conducted considering the pooled values across all electrodes and for each electrode separately for both the group and individual analysis. For group analysis, single trial alpha amplitude values were converted to z -scores, by subtracting each value to the mean of all conditions considered, divided for their standard deviation, for each subject separately. Then, the mean alpha amplitude (AUC) for all trials and for each electrode was computed. Statistical analyses were run on the mean z -score across all electrodes and on individual electrodes. Regarding the individual analysis, single trial alpha amplitude values were used for comparisons between the four conditions and also the two conditions more extreme (RT_{Q1} and RT_{Q4}).

2.5.3.2.2 Analysis of Synchronization Between Electrodes

For calculation of synchronization between oscillating signals, cross channel phase coherence analysis was employed, using EEGLAB functions for group analysis; and single trial phase deviation (a measure of phase coherence on a single trial basis), adapted from the study of Hanslmayr et al. [35], for individual analysis. All possible pairs of channels were considered in both analyses, excluding the electrooculogram and earlobe electrodes, which gives a total of 1891 possible pairs (all possible combinations between 62 channels).

Group Phase Coherence Analysis

For group analysis of synchronization between electrodes, it was used the EEGLAB function *newcrossf*, which implements the method developed by Delorme et al. [34], defined above in chapter 1 (1.2.2.1.1), by the equation 1.5. For time frequency decomposition of EEG segments Morlet *wavelets* were used. This type of *wavelet* is a Gaussian-windowed sinusoidal wave segment comprising several cycles, a family of *wavelets* comprising compressed and stretched versions of the “mother wavelet” to fit each frequency to be extracted from the EEG. For this reason it is traditionally constrained to contain the same number of cycles across frequencies [96]. This illustrates an important property of *wavelet* analysis: at low frequencies, frequency resolution is good but time resolution is poor whereas at high frequencies time resolution is good but frequency resolution is poor. To avoid this phenomenon, the number of *wavelet* cycles can be increased slowly with frequency, leading therefore to a better frequency resolution at higher frequencies than the conventional *wavelet* approach that uses constant cycle length [34]. This method of suiting the number of *wavelet* cycles according with the frequency band specified is implemented on EEGLAB functions which require time frequency decomposition using

wavelets. More specifically, one of those functions - *newcrossf* - which was used here, computes the phase coherence between two signals from two different channels in sets of trials, an index which represents relative constancy of the phase differences (Δ phase) between those signals along the considered trials, varying between 1 (for perfect phase-locking) and 0 (for random phase-locking) - equation 1.5, chapter 1. EEGLAB function *newcrossf* parameters were defined in terms of the number of *wavelet* cycles, frequency range, time window and number of output frequencies. It was determined a number of cycles ranging from 4, considering the lowest frequency of 7 Hz, until 20, for the highest frequency of 70 Hz. Although it was desired to obtain phase coherence values only in a time range defined from -500 to 0 ms relatively to the stimulus onset, it was calculated for a time window from -1500 to 500 ms, to account for edge artifacts associated with time-frequency analysis. The number of output frequencies was adjusted for obtaining output values for frequency bin centres spaced from 1 Hz. This phase coherence index was then computed for each condition (RT_{Q1} , RT_{Q2} , RT_{Q3} and RT_{Q4}) and each pair of channels among all possible combinations. Therefore, a vector with 1891 values was obtained for each condition, each frequency value within the range specified (7-70 Hz) and each subject, averaged across all time points in a time window defined from -500 to 0 ms prestimulus. The resulting phase coherence indexes were collapsed across three frequency bands - alpha (8-12 Hz), beta (20-30 Hz) and gamma (30-45 Hz) - for each electrode pair. Comparisons between the four conditions (RT_{Q1} , RT_{Q2} , RT_{Q3} and RT_{Q4}) were made using a two-stage statistical procedure adapted from the method described by Hanslmayr et al. [35], in order to correct statistical results for multiple comparisons, which is described in subsection 2.5.5.

Individual Phase Deviation Analysis

To determine the phase coherence on a single trial basis for individual analysis, a procedure based on the method developed by Hanslmayr et al. [35] was applied. After computing the phase difference (Δ phase) as described above, the following procedure was carried out. First, the circular mean of phase differences (Δ phase) was calculated across all single trials. The circular mean can be interpreted in this case (mean Δ phase) as the direction of the resultant vector obtained by representing each single trial Δ phase by a unit-length vector in the complex plane - see the scheme (a) of the figure 2.17. Then, the deviation from the mean Δ phase was computed for each single trial, frequency value in the range specified (7-70 Hz), and time point. Deviation from mean Δ phase was calculated using the circular variance procedure, described by Fisher [97]. The circular variance can be then computed by subtracting the length of the resultant vector, defined

by \bar{R} , obtained by representing the circular mean across all trials (mean Δ phase) and the Δ phase for each specific trial by unit-length vectors - see figure 2.17(b) - in the complex plane, to the unit (which is equivalent to taking $1-\bar{R}$). Therefore, this yields a value from 0 to 1, where values close to 0 indicate low deviation, and values close to 1 indicate high deviation from the mean Δ phase. Both circular mean and circular variance values were computed using the Circular Statistic Toolbox for Matlab[®] [98].

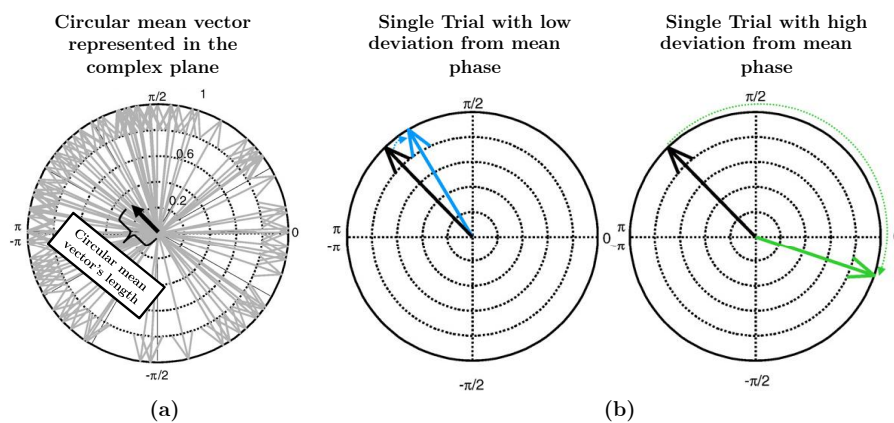


Figure 2.17: Graphic representation of the procedure adopted for computing individual phase deviation, a measure for phase coherence on a single trial basis (scheme adapted from [35]). **(a)** The circular mean (mean Δ phase) is the direction of the resultant vector (plotted as the black arrow) obtained by representing phase differences (Δ phase) by unit-length vectors in the complex plane, which has a certain length. **(b)** The deviation from the mean Δ phase (being this latter represented as a black arrow) is plotted for two examples of single trials. The example in the left depicts a single trial with low deviation (light blue vector) and the example in the right corresponds to a single trial with high deviation from mean Δ phase (light green vector).

After collapsing phase deviation values over the prestimulus interval defined from -500 to 0 ms, for each electrode pair and subject, those values were also averaged within the three frequency bins defined for the group analysis - alpha (8-12 Hz), beta (20-30 Hz) and gamma (30-45 Hz).

Thereafter, the single trial values were sorted and grouped into 10 bins (from lowest deviation to highest deviation). It was intended to obtain the electrode pairs which showed a significant correlation between the 10 phase deviation bins and the corresponding averaged RT values for each bin (converted in *z-scores* for each hand separately) - figure 2.18. Thus, a two-stage statistical procedure was carried out, similarly with group analysis (see section 2.5.5 for a detailed description).

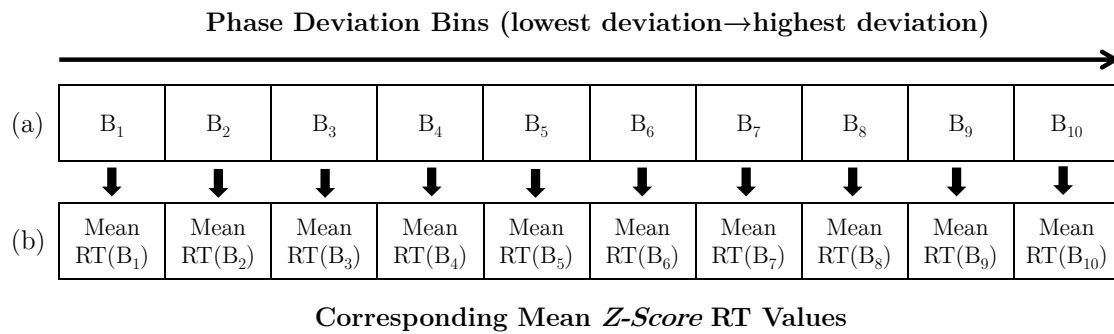


Figure 2.18: Scheme illustrating how the two vectors (a) and (b) used for statistical correlation analysis between RT values and single trial phase deviation were generated. At first, single trial phase deviation values were sorted from lowest to highest value and grouped into 10 bins, ranging from B_1 to B_{10} - vector (a). The corresponding *z-score* RT values were averaged for each one of the 10 bins - vector (b). Those two resulting vectors were used for correlation analysis.

2.5.4 Eye-Tracking Data

Gaze position and pupil diameter data were analysed taking into account the criteria referred above, based on response RT measurements. The generated text file contained right eye pupil diameter and left eye pupil diameter values in millimetres; and gaze position (point of regard) measurements in pixels for both horizontal (X) and vertical (Y) directions, relatively to the overall screen area. Pupil diameter and gaze position data were then analysed taking into account the trial's indexes which corresponded to the conditions defined in subsection 2.5.2 - RT_{Q1} , RT_{Q2} , RT_{Q3} and RT_{Q4} . However, due to artifacts associated with eye blinks and head movements, eye tracking data were first preprocessed, using the procedure described below (2.5.4.1).

2.5.4.1 Preprocessing of Eye Tracking Data

The whole data set of eye-tracking data including horizontal gaze position, vertical gaze position and pupil diameter values was split in prestimulus windows of 500 and 1000 ms length and labelled with the condition of the corresponding trial (RT_{Q1} , RT_{Q2} , RT_{Q3} and RT_{Q4}), based on RT values. Then, the data points corresponding to time intervals at which the eyetracker lost track of the subject's eyes were rejected, due to eye blinks or head movements. In similarity with the procedure adopted by Alnæs et al. [99], trials with less than 50% of the data remaining after removal of the null points were excluded of further analysis. The remaining trials were kept with accordingly reduced data points. A statistical comparison between the number of trials per condition - RT_{Q1} , RT_{Q2} , RT_{Q3} and RT_{Q4} - for all subjects was made for each measure to ensure that there were not significant differences (see subsection 2.5.5). If any one of the parameters tested showed

a significant difference between the number of trials retained per condition, the lowest value among all the conditions was considered for each subject, being this number of trials randomly selected for the remaining conditions. Additionally, to ensure that there were not statistically significant differences between the number of time points removed for each one of the trials retained for further analysis, comparisons were also made between the four conditions, for the mean number of points removed across trials (see subsection 2.5.5).

After data were cleaned, gaze position values for both horizontal and vertical directions were subtracted to screen centre coordinates obtaining, therefore, values which represented deviation of gaze from screen centre in the horizontal and vertical directions. Thereafter, data vectors of 500 ms and 1000 ms time length corresponding to each trial were averaged in time, for both pupil diameter and gaze position - defined as *RPD*, *LPD*, for right eye pupil diameter and left eye pupil diameter; and *Gaze Pos_X* and *Gaze Pos_Y*, for gaze position in X and Y direction, respectively. Standard deviation values were also computed - *Std RPD* and *Std LPD*, for pupil diameter; and *Std Gaze Pos_X* and *Std Gaze Pos_Y*, for gaze position. Thus, for each condition and each prestimulus window, it was generated a vector containing only one value for each one of those parameters. Standard deviation values were obtained for studying the variability of each measure across time. For both pupil diameter and gaze position, both group and individual analysis were conducted, in similarity with EEG measurements.

2.5.4.2 Pupil Diameter and Gaze Position Analysis

For group analysis, at first, pupil diameter values for both right and left eyes - *RPD*, *Std RPD*; and *LPD*, *Std LPD*, respectively - were converted in *z-score* values, for each subject individually, using the same procedure applied in spectral amplitude analysis (see 2.5.3.2.1). Then, single trial values were averaged for both right and left eyes, being defined as *PD* and *Std PD*. After removing outliers ($|z\text{-score}| > 3$), data vectors were averaged across trials for each condition, in order to obtain one single value for each subject. Thereafter, statistical comparisons were made between the conditions *RT_{Q1}*, *RT_{Q2}*, *RT_{Q3}* and *RT_{Q4}* (see 2.5.5 for further information about the statistical methods applied). For individual analysis, the same trials regarding the group analysis were used. After removing the outliers' indexes determined in group analysis, single trial values not converted in *z-scores* were averaged only for both eyes. Then, single trials values were used to compare *PD* and *Std PD* measures between the four conditions, for each subject individually, using the statistical hypothesis tests described in 2.5.5.

For analysing gaze position deviations relatively to the screen centre, a similar procedure was carried out. However, both group and individual analysis were carried out

separately for gaze position, relatively to the horizontal and vertical directions.

All the steps adopted for eye parameters analysis are schematized in the figure 2.19.

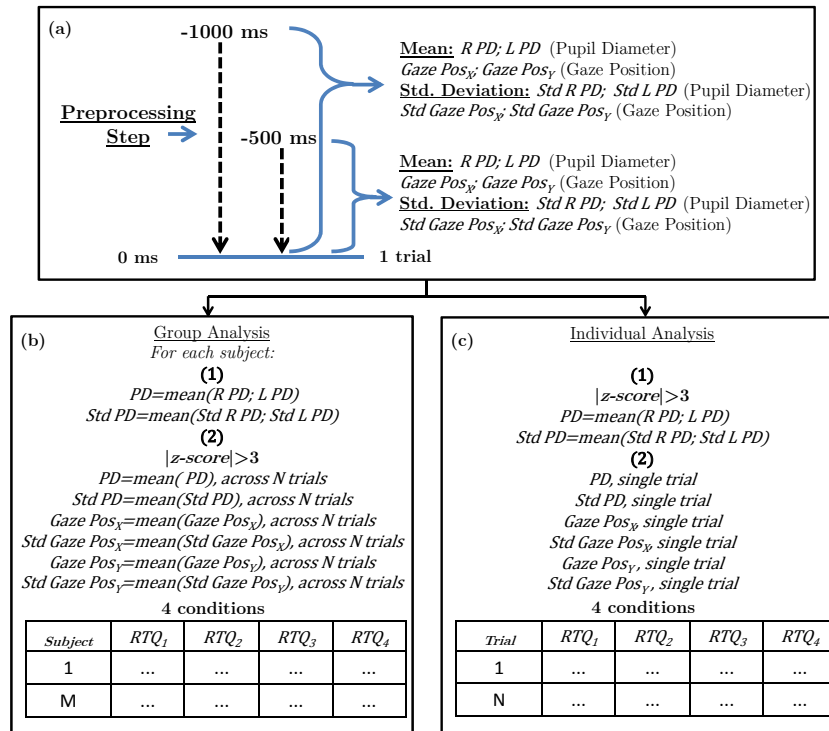


Figure 2.19: Scheme explaining how both group and individual analysis were conducted. (a) After preprocessing, both pupil diameter parameters values for right and left eyes and gaze position for the X and Y direction relatively to the screen centre were averaged across time (for prestimulus windows of 500 and 1000 ms time length). (b) **1.** For group analysis, at first, all measures were converted in *z-scores*. Then, pupil diameter measures were averaged for both right and left eyes for each trial and subject. **2.** After removing the outliers for each condition, eye parameters values were collapsed over *N* trials for each subject individually, and those values were used for group comparisons, considering *M* subjects. (c) **1.** For individual analysis, after removing the outliers' indexes determined in group analysis, pupil diameter parameters values were averaged for both right and left eyes. **2.** Thereafter, single trial values for all eye parameters were used for individual comparisons. Std. Deviation: standard deviation.

2.5.5 Statistical Analysis

In general, statistical tests were conducted for group analysis using repeated measures analysis. Note that for this type of analysis it was considered the mean value across trials for each subject and condition, which gives an equal number of instances per condition. On the contrary, for individual analysis, unpaired statistical tests were carried out. More detailed descriptions about the statistical procedures implemented for each analysis are presented in the paragraphs below.

Statistical Procedures implemented on Group Analysis

For group analysis of prestimulus alpha amplitude (see 2.5.3.2.1), the mean *z-score* values across trials and all parietal/parieto-occipital/occipital channels were compared between the four conditions using Repeated Measures ANOVA. For the comparisons made taking into account each electrode separately, the Repeated Measures ANOVA was applied at first, and only if there were electrodes showing significant differences between conditions ($p\text{-value} < 0,05$; two-tailed), a correction for multiple comparisons was applied using the False Discovery Rate (FDR) method [100], with the *fdr* function provided by EEGLAB. A parametric test was implemented, because variables were normally distributed, according with the Shapiro–Wilk Normality test ($p\text{-value} > 0,05$; two-tailed).

Regarding the group analysis of prestimulus phase coherence between electrodes (see 2.5.3.2.2), as was mentioned before, a two-stage statistical procedure adapted from the study of Hanslmayr et al. [35] was carried out to account for multiple testing, as phase coherence was calculated and compared between conditions for 1891 electrode pairs. At first, Friedman tests were calculated for each electrode pair to investigate which electrode pairs showed a significant difference between the four conditions (RT_{Q1} , RT_{Q2} , RT_{Q3} and RT_{Q4} , ranging from fast to slow trials), according with the criterion $p\text{-value} < 0,005$ (two-tailed). Then, those pairs were submitted to a nonparametric permutation-based Repeated Measures ANOVA, provided by the function *statcond* available on EEGLAB [34], in which phase coherence values for each pair was permuted across conditions, for 5000 runs. Then, the FDR method was applied for correcting for multiple comparisons. Non-parametric tests were used in this analysis because some variables failed to be normally distributed and also to avoid influences from outliers.

For prestimulus eye parameters (see 2.5.4.2), comparisons between the four conditions were also made. As pupil diameter measures were not normally distributed (according to the Shapiro–Wilk Normality test), non parametric tests were used for these comparisons (Friedman tests). All the other parameters (*Std PD*, *Gaze Pos_X*, *Gaze Pos_Y*, *Std Gaze Pos_X* and *Std Gaze Pos_Y*) were normally distributed and parametric Repeated Measures ANOVA tests were used.

As was referred before, for each type of the analyses performed (alpha amplitude, phase coherence and eye parameters), it was assessed if there were significant differences between the number of trials used for each condition. The results of those statistical tests are presented below (tables 2.3 and 2.4). As all the samples did not follow a normal distribution, according with the Shapiro–Wilk Normality test outputs obtained ($p\text{-value} < 0,05$; two-tailed), non parametric tests were used.

Table 2.3: Number of trials per condition for group analysis of EEG data.

Number of Subjects	Type of Measure	Number of Trials per Condition				<i>p</i> -value Friedman Test
		RT_{Q1}	RT_{Q2}	RT_{Q3}	RT_{Q4}	
18	Alpha Amplitude	52,000 ± 2,910	51,556 ± 3,399	51,056 ± 3,096	50,778 ± 3,318	0,127
	Phase Coherence	51,722 ± 3,102	51,389 ± 3,744	50,833 ± 3,434	50,778 ± 3,457	0,124

Table 2.4: Number of trials per condition used for analysis of eye parameters (pupil diameter and gaze position relatively to the screen centre). * indicate the eye parameters for which there were significant differences between the number of trials for each condition; having been thereafter determined the lowest value among the conditions considered, and selected randomly an equal number of trials for all the conditions. This procedure was applied for all subjects. In the table are presented the original number of trials.

Number of Subjects	Type of Measure	Number of Trials per Condition				<i>p</i> -value Friedman Test
		RT_{Q1}	RT_{Q2}	RT_{Q3}	RT_{Q4}	
20	<i>PD</i> 500 ms	48,800 ± 8,433	48,000 ± 9,695	48,950 ± 7,515	47,750 ± 9,267	0,308
	<i>Std PD</i> 500 ms	48,650 ± 8,546	47,340 ± 9,439	48,700 ± 7,435	46,950 ± 9,185	-*
	<i>PD</i> 1000 ms	48,850 ± 8,248	48,150 ± 9,109	49,000 ± 7,441	47,950 ± 9,102	0,567
	<i>Std PD</i> 1000 ms	48,550 ± 8,344	47,800 ± 9,024	48,700 ± 7,533	47,450 ± 8,852	0,428
	<i>Gaze Pos_X</i> 500 ms	48,750 ± 8,571	47,950 ± 9,671	48,800 ± 7,770	47,250 ± 9,014	0,174
	<i>Std Gaze Pos_X</i> 500 ms	48,250 ± 8,175	47,150 ± 9,241	48,450 ± 7,817	47,250 ± 9,113	0,654
	<i>Gaze Pos_X</i> 1000 ms	48,900 ± 8,404	48,150 ± 9,092	48,900 ± 7,546	47,500 ± 8,823	0,141
	<i>Std Gaze Pos_X</i> 1000 ms	48,500 ± 8,075	47,350 ± 8,707	48,100 ± 7,490	47,450 ± 8,929	0,627
	<i>Gaze Pos_Y</i> 500 ms	48,800 ± 8,569	48,050 ± 9,605	48,800 ± 7,445	47,200 ± 9,030	-*
	<i>Std Gaze Pos_Y</i> 500 ms	48,450 ± 8,538	47,300 ± 9,537	48,550 ± 7,708	47,250 ± 9,153	0,581
	<i>Gaze Pos_Y</i> 1000 ms	48,850 ± 8,267	48,300 ± 9,068	48,800 ± 7,424	47,450 ± 9,058	0,091
	<i>Std Gaze Pos_Y</i> 1000 ms	48,550 ± 8,192	47,600 ± 8,882	48,550 ± 7,323	47,150 ± 9,005	0,471

The results for the statistical comparisons made between conditions for the mean number of data points removed across trials which were used for pupil diameter and gaze position analysis are also showed, regarding the preprocessing step of eye-tracking measures (table 2.5). As all the samples did not follow a normal distribution (according with the Shapiro–Wilk Normality test), non parametric tests were also used.

Statistical Procedures implemented on Individual Analysis

For individual analysis of spectral amplitude in the alpha frequency band, at first, Kruskal Wallis tests were conducted considering the alpha amplitude values pooled over the parietal/parieto-occipital/occipital electrodes, for comparisons between the four condition; and the Mann Whitney Test for comparisons between fast and slow trials. No subject showed statistically significant differences. Next, alpha amplitude was compared

Table 2.5: Percentage of data points removed from time segments after eye tracking data (pupil diameter and gaze position) were preprocessed. Mean \pm standard deviation values across all subjects are presented below. Statistical comparisons were made between all the four conditions, considering the mean value across trials for each subject.

Number of Subjects	Type of Measure	% number of points removed in each time segment across subjects				<i>p</i> -value Friedman Test
		RT_{Q1}	RT_{Q2}	RT_{Q3}	RT_{Q4}	
20	<i>PD</i> 500 ms	2,428 \pm 2,982	2,954 \pm 3,257	3,027 \pm 3,628	2,691 \pm 3,380	0,278
	<i>Std PD</i> 500 ms	2,481 \pm 3,039	2,809 \pm 3,140	2,962 \pm 3,590	2,531 \pm 3,124	0,460
	<i>PD</i> 1000 ms	2,973 \pm 3,503	3,308 \pm 4,019	3,406 \pm 4,111	3,267 \pm 3,817	0,754
	<i>Std PD</i> 1000 ms	3,008 \pm 3,439	3,283 \pm 4,009	3,315 \pm 4,014	3,221 \pm 3,769	0,861
	<i>Gaze Pos_X</i> 500 ms	2,454 \pm 2,971	2,862 \pm 3,237	2,909 \pm 3,604	2,700 \pm 3,399	0,781
	<i>Std Gaze Pos_X</i> 500 ms	2,316 \pm 2,962	2,690 \pm 3,225	2,827 \pm 3,642	2,582 \pm 3,310	0,672
	<i>Gaze Pos_X</i> 1000 ms	2,987 \pm 3,500	3,223 \pm 4,053	3,342 \pm 4,123	3,279 \pm 3,831	0,895
	<i>Std Gaze Pos_X</i> 1000 ms	2,916 \pm 3,500	3,141 \pm 4,052	3,123 \pm 4,077	3,122 \pm 3,760	0,984
	<i>Gaze Pos_Y</i> 500 ms	2,346 \pm 2,898	3,084 \pm 3,468	3,013 \pm 3,574	2,687 \pm 3,477	0,220
	<i>Std Gaze Pos_Y</i> 500 ms	2,330 \pm 2,908	2,831 \pm 3,298	2,954 \pm 3,591	2,590 \pm 3,369	0,715
	<i>Gaze Pos_Y</i> 1000 ms	3,011 \pm 3,482	3,271 \pm 4,035	3,357 \pm 4,030	3,205 \pm 3,828	0,754
	<i>Std Gaze Pos_Y</i> 1000 ms	2,902 \pm 3,548	3,258 \pm 4,033	3,274 \pm 3,972	3,178 \pm 3,870	0,776

between conditions for each electrode separately. Therefore, a nonparametric, unpaired and permutation-based testing procedure was implemented in which alpha amplitude values were permuted across conditions for each electrode, using 5000 runs, by applying the *statcond* function for EEGLAB, and using the one-way ANOVA test, for comparisons between four conditions. Thereafter, correction for multiple comparisons was applied to the results obtained using the FDR criterion [100]. In addition, comparisons between the two conditions more extreme - RT_{Q1} and RT_{Q4} , which represent fast and slow trials, respectively - were also conducted, adopting the same procedure, but using the t-test instead of the one-way ANOVA.

For individual analysis of phase deviation (a measure of phase coherence on a single trial basis), also a two-stage statistical method was carried out. In order to investigate which electrode pairs showed a significant correlation between the phase deviation bins grouped from lowest phase deviation (1st bin) to highest phase deviation (10th bin) and the corresponding averaged RT values, the Spearman's rank correlation coefficient (Spearman's *rho*) and the corresponding *p*-value were computed, for each electrode pair. Only the electrodes whose corresponding *p*-value was less than 0,005 for the correlation were retained for the second stage of the procedure. Thereafter, a permutation test based also on Spearman's *rho* was conducted for those electrode pairs, using the function *mult_comp_perm_corr* provided by David Groppe [101], which adjusts the *p*-values of each variable for multiple comparisons. Only the electrode pairs which showed a *p*-value < 0,05 after this stage were selected for further analysis.

Regarding the eye measures (pupil diameter and gaze position relatively to screen centre coordinates), the non-parametric Kruskal Wallis test was used for comparisons between all the four conditions.

The Kruskal Wallis and Friedman tests were performed using Matlab[®] functions from Statistics Toolbox[™] [102]. The functions *swtest* and *anova_rm*, available in Matlab[®] Central, were used for the Shapiro Wilk Normality Test and Repeated Measures ANOVA, respectively.

2.5.6 Machine Learning Algorithms for Attentional Lapses Detection

Machine learning techniques have been widely employed in automatic classification of several physiological signals, including those related with subject's attention levels, as was mentioned in chapter 1. Generally speaking, a classifier is a computational algorithm which is trained to distinguish if a certain instance or object belongs to one or another class of a given set, taking into account its features. The core objective of a classifier is then to generalize from its experience; being able to classify accurately new, "unseen" examples after having experienced a learning data set. In this study, supervised learning algorithms were used, which are trained on labelled examples (instances whose class they belong is known) [103]. These type of algorithms attempt to generalise a function or mapping for inputs to outputs which can then be used to generate an output for previously "unseen" inputs.

Frequently, in biomedical data classification projects, the classification algorithm which is applied may not be suitable for the given data set [104]. Therefore, three algorithms based on supervised learning theory - two types derived from *support vector machine* (SVM) algorithm and *k-nearest neighbours* (KNN) - were explored to maximize the chances of achieving good classification performance. SVM and KNN classification algorithms have been widely used in EEG-based classification platforms [104]. Three main types of unimodal classifiers (or simple classifiers) - based on the three type of measures analysed in this study: eye parameters, alpha amplitude and EEG phase deviation - were developed taking into account the three classification algorithms referred above, with the aim to predict the occurrence of an attentional lapse. Four additional classifiers - hybrid classifiers - were also developed, which take into account a combination of the classification outputs given by the three main unimodal classifiers [105]. It was intended to develop a set of classifiers specific for each subject and select the one which ensured the highest classification rate for each subject. The mean value across subjects indicated which type of classifier gave the best results considering all subjects. Each trial was classified into two different classes: "Non Lapse" and "Lapse". The four groups (RT_{Q1} , RT_{Q2} , RT_{Q3} and

RT_{Q4}) used in the statistical analyses were therefore aggregated into two groups, according with the scheme presented in the figure 2.20.

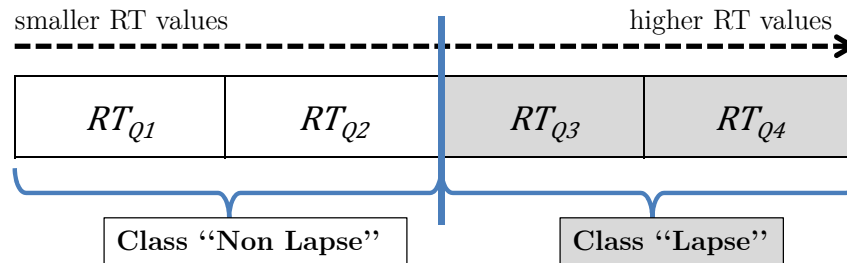


Figure 2.20: Scheme illustrating how the four groups - RT_{Q1} , RT_{Q2} , RT_{Q3} and RT_{Q4} - used in the statistical analysis approach were aggregated into two classes - “Non lapse” and “Lapse” - for the classification task. For each subject, it was assigned one of two possible labels to each trial (or instance) - “Lapse” or “Non Lapse”. The classifiers were developed to distinguish between these two type of classes.

To develop a classification platform the following sequence tasks was performed: data preprocessing, features creation, features preprocessing, features extraction and training of the classifier (figure 2.21).

As was referred above, the binary classifiers were developed using features derived from EEG and eye-tracking data. Some of them were addressed on the statistical analysis approach. However, there were some modifications, specifically related with the pre-processing procedure of eye parameters and with the measure used for single trial EEG phase coherence between electrode sites, which are detailed in 2.5.6.1. In the following subsections, the features chosen for training the classifiers will be described as well as the performance metrics applied to select the one that ensured the best classification performance.

2.5.6.1 Features Creation and Extraction of the Most Relevant Features

The choice of the most relevant features is a task of considerable importance in the development of classification platforms. The features chosen for the development of each classifier were based on the existing literature and on the patterns previously identified as the most adequate for predicting lapses in attention for both EEG data and eye measurements. Note that some parameters which were used for statistical comparisons between conditions were submitted to some modifications and others were replaced for more adequate measures for the classification task. Those changes are described in the following paragraph. For the features derived from the patterns already studied in the statistical approach, only the values regarding the single trial analysis were used. The outliers from each distribution were not removed in order to use all trials in the classification.

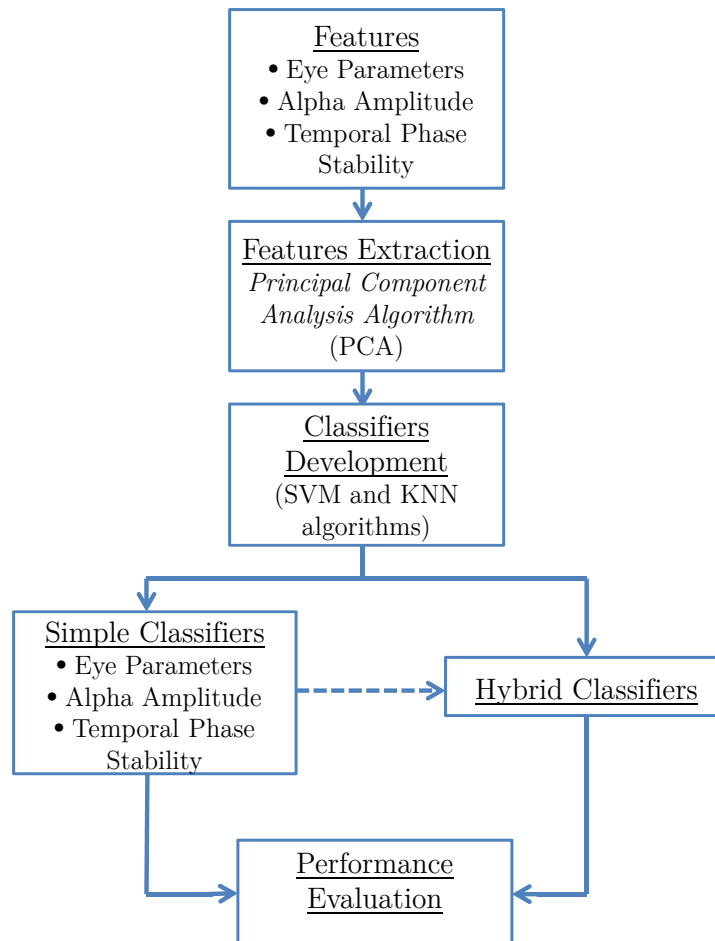


Figure 2.21: Scheme illustrating the procedure adopted to develop a set of classifiers for predicting lapses in attention for each subject of the study. The measures used in the statistical approach addressed above were taking into account for the classification task developed, excluding for EEG phase coherence between electrode sites. In this specific case, other measure different from the single trial phase deviation was used, which is well characterized in 2.5.6.1 - the temporal phase stability. Because possibly they were highly correlated, the most adequate features with relevant differences between them were extracted, using the *Principal Component Analysis* algorithm (PCA) - which is described with more detail afterwards. Then, using three main types of classification algorithms - two based on *Support Vector Machine* (SVM) algorithm and *K-Nearest Neighbours* (KNN) - were developed simple classifiers based on eye parameters, alpha amplitude and temporal phase stability values. Hybrid classifiers were also built by fusing the recognition results at the decision-level based on the outputs obtained with the simple classifiers. The final step of the classification procedure adopted in this study was the evaluation of the performance of each classifier developed (for both simple and hybrid classifiers), considering specific metrics which are described in 2.5.6.3.

For eye parameters, the preprocessing step adopted in the generation of the features for training the classifiers was much simpler than the one which was adopted for statistical analysis (described at 2.5.4.1). After epoching in time segments of 500 and 1000 ms prestimulus time length and removing the points at which the eyetracker did not monitored the subject's eyes, only the completely null trials (without any time point) were discarded in order to maximize the number of trials used. By simplifying the preprocessing steps, the computational cost in terms of complexity and time consumption was reduced; and, in this specific case, it is intended to develop a classifier which could be trained as quickly as possible every time the system is submitted to a new subject. Additionally, and for the same reasons, instead of using phase deviation as a measure of single trial phase coherence in the classification platform developed here, it was computed other measure, based on the phase stability between two signals from two different electrode sites along time, which does not take into account the mean Δ phase across trials. If the phase deviation was used for training the classifiers chosen for this study, a considerable number of trials would be necessary for calculating a reasonable value for the mean Δ phase. Therefore, and based on the study of Wang et al. [106], a measure which reflects the temporal phase stability for a specific trial was computed in this context. This measure takes into account the length of the resultant vector in the complex plane when each phase difference (Δ phase) for each time point is represented by a unit-length vector in the complex plane (figure 2.22).

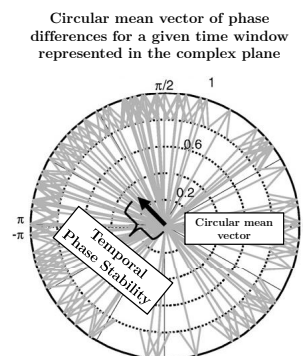


Figure 2.22: Scheme illustrating how the temporal phase stability was obtained, a type of feature used in the classification platform developed here instead of the single trial phase deviation, used in the statistical approach (scheme adapted from [35]). The temporal phase stability is the length of the resultant vector (black arrow) obtained by computing the circular mean of a set of unit-length vectors, where each one represents the phase difference for each time point (grey arrows) within a time window (in this specific case, 500 ms prestimulus), in the complex plane. Each grey arrow represents the phase difference between two signals from two different electrode sites, for a given frequency value and time point.

This representation of the procedure adopted in the complex plane is equivalent to the equation used for Wang et al. [106]: $|\langle e^{j\Delta\phi(t)} \rangle_t|$, where $\Delta\phi(t)$ is the difference of instantaneous phases between two signals for each time point, and $\langle \cdot \rangle_t$ is the operator

of averaging over time. In the case of complete phase difference stability across time, $\Delta\phi(t)$ is constant over time and this measure yields a value of 1. In the case of maximum phase difference instability, then $\Delta\phi(t)$ follows a uniform distribution and the result of the equation above is 0. For the calculation of the difference of instantaneous phases, Morlet *wavelets* were used with the same parameters values for time-frequency decomposition (number of cycles, frequency range, time window - 500 ms prestimulus - and number of output frequencies) as in the statistical analysis of phase coherence for both group and individual analysis. After obtaining the temporal phase stability for each trial and for each frequency value, this measure was averaged within the beta frequency range (20-30 Hz). In the table 2.6 are presented the features used to develop each type of unimodal classifier.

Thereafter, features vectors were normalized by subtracting to each feature's instance value the mean across all the instances and dividing by the corresponding standard deviation. This features preprocessing step has a strong impact on classification algorithms, because, due to the great difference in the characteristics of the feature components, they should be normalized to make their scale similar.

Extracting the Most Significant Features: *Principal Component Analysis* Algorithm

As the selected features could be highly correlated among them, it was necessary to discard those whose contribution is redundant for the classification procedure. In fact, a low-dimensional representation reduces the risk of overfitting [103] and the computational complexity, improving the classifier's generalization ability. By determining a subset of available features that guarantees the building of a good model for the classification process, the dimensionality reduction problem is solved. Several procedures can be implemented to choose adequate features with relevant differences between them. The *Principal Component Analysis* (PCA) algorithm was implemented here, which is a features extraction's method that generates new features from the existing ones, retaining the most meaningful attributes. PCA algorithm performs an orthonormal transformation to the original data for retaining only significant eigenvectors. Each eigenvector is associated with a variance represented by the corresponding eigenvalue. A principal component of the data is defined by each eigenvector, which corresponds to an eigenvalue representative of a significant variance of the whole data set. Based on the definition of PCA algorithm, the most important decision is the determination of how many eigenvectors must be retained [103]. For this purpose, the cumulative percent variance criterion was used to discard the less meaningful features from the new set generated after the PCA algorithm.

Table 2.6: Features used to develop the simple/unimodal classifiers. *Note that one classifier was developed for each prestimulus window separately, and for each type of measure, which gives a total of six classifiers, derived from three main unimodal classifiers.

Type of Classifier	Prestimulus window*	Number of features	Features	Description
Eye Parameters	500 ms or 1000 ms	10	Right Eye Pupil Diameter (<i>R PD</i>)	Mean value of right eye pupil diameter across specified prestimulus window for each trial in millimeters.
			Right Eye Standard Deviation of Pupil Diameter (<i>Std R PD</i>)	Standard deviation value of right eye pupil diameter across defined prestimulus window for each trial in millimeters.
			Left Eye Pupil Diameter (<i>L PD</i>)	Mean value of left eye pupil diameter across specified prestimulus window for each trial in millimeters.
			Left Eye Standard Deviation of Pupil Diameter (<i>Std L PD</i>)	Standard deviation value of left eye pupil diameter across defined prestimulus window for each trial in millimeters.
			Right/Left Eye Pupil Diameter (<i>PD</i>)	Mean value between right and left eyes for pupil diameter across specified prestimulus window for each trial in millimeters.
			Right/Left Eye Standard Deviation of Pupil Diameter (<i>Std PD</i>)	Mean value between right and left eyes for standard deviation of pupil diameter across defined prestimulus window for each trial in millimeters.
			Gaze Position X (<i>Gaze Pos_x</i>)	Mean value of gaze position in the horizontal direction across specified prestimulus window for each trial in pixels. Gaze position was defined in terms of deviation from screen centre.
			Standard Deviation of Gaze Position X (<i>Std Gaze Pos_x</i>)	Standard deviation value of gaze position in the horizontal direction (relatively to screen centre coordinates) across defined prestimulus window for each trial in pixels.
			Gaze Position Y (<i>Gaze Pos_y</i>)	Mean value of gaze position in the vertical direction (in relation to screen centre coordinates) across defined prestimulus window for each trial in pixels.
			Standard Deviation of Gaze Position Y (<i>Std Gaze Pos_y</i>)	Standard deviation value of gaze position in the vertical direction (relatively to screen centre coordinates) across specified prestimulus window for each trial in pixels.
Alpha Amplitude	500 ms or 1000 ms	19	Alpha Amplitude (parietal, parieto-occipital and occipital electrodes)	Alpha amplitude within the frequency range specified for each subject, in the prestimulus window defined, for each trial and each electrode among the specified set.
Temporal Phase Stability	500 ms	946	Single Trial Temporal Phase Stability, for beta frequency range (electrode pairs among all possible combinations between frontal and parietal/parieto-occipital/occipital areas, CB1 and CB2 electrodes)	Length of the resultant vector in the complex plane when the phase differences between each electrode pair for all time points within the prestimulus window defined are represented by unit-length vectors in the complex plane, for each single trial.

The cumulative percent variance is a measure of the percent variance captured by the first l principal components generated after PCA [107]. In this study, the first l principal components were selected, which accounted just under 95% of the input variance, for each data set analysed, excluding for the case of the temporal phase stability classifier, because of the curse-of-dimensionality problem. Indeed, the amount of data needed to properly describe the different classes increases exponentially with the dimensionality of the features vectors. If the number of training data is small relatively to the size of the features vectors, the classifier could give poorer results. Therefore, it is recommended to use, at least, five to ten times as many training samples per class as the dimensionality [104]. The amount of original features (946) used in the temporal phase stability classifier was reduced to a mean value across subjects of $115,500 \pm 25,852$ after the PCA, considering the first l principal components which accounted just under 95% of the input variance. However, this number notably exceeds the mean number of training samples across subjects for each class (91,167 and 92,667; for the classes “Lapse” and “Non Lapse”, respectively). In addition, a trade-off between the amount of relevant information discarded and the number of features extracted to avoid the curse-of-dimensionality reduction problem, was taken into account for the number of principal components extracted after the PCA algorithm, in specific for this classifier. Instead of considering the criterion for a maximal amount of extracted features corresponding to 20% of the number of training samples per class, a number of features corresponding to 20% of the total number of samples per class (including both the instances for training and testing) was chosen, to avoid the loss of more significant features. Therefore, the mean value across subjects for the cumulative variance of the features extracted after the PCA using this criterion was about 68%.

Using these conditions, for the classifiers regarding the eye parameters and alpha amplitude, considering all the subjects, the original number of features was reduced to approximately 4/5 features (table 2.7). For the classifiers based on temporal phase stability features, approximately 20 features for the classification task were used (table 2.7).

Table 2.7: Mean number of principal components/features chosen after applying the PCA algorithm across subjects for each unimodal classifier developed. Std. Deviation: standard deviation.

Classifier	Time window	Mean \pm Std. Deviation
Eye Parameters	500 ms	4,550 \pm 0,826
	1000 ms	4,450 \pm 0,826
Alpha Amplitude	500 ms	5,511 \pm 2,055
	1000 ms	4,778 \pm 2,016
Temporal Phase Stability	500 ms	20,444 \pm 1,381

2.5.6.2 Classifiers

2.5.6.2.1 Classification Algorithms used to Develop the Unimodal Classifiers

The two main classification algorithms (*Support Vector Machine* and *K-Nearest Neighbours*) used to develop the simple/unimodal classifiers considered in this classification platform (see table 2.8) are described in the two paragraphs below.

Support Vector Machine *Support Vector Machine* (SVM) is a classification algorithm that can be linear or nonlinear. It can distinguish between two different types of objects by finding a separating hyperplane with the maximal margin between two classes, when applied to data [104]. Two general attributes define the SVM algorithm: C , a hyper-parameter which controls the trade-off between margin maximization and error minimization; and kernel, a function that map training data into high-dimensional features spaces [108]. The kernel function is used to train SVMs classifiers. The type of kernel function used is a key factor on the performance of SVM classification algorithm. The types which are more commonly used are the linear (Linear SVM) and the gaussian (Radial Basis Function, RBF) - RBF SVM [108]. In this study, both methods were adopted. By using SVM algorithm considering the radial mapping function a third parameter must be optimized: σ , the width of the gaussian function. It is always necessary to define the best combination of the two hyper-parameters C and σ that defines the kernel RBF model, in order to determine the one which ensured the best performance. For Linear SVM, different values for the constraint parameter C were explored: $C \in \{0,001;0,01;0,1;1;10;50;100\}$. For RBF SVM, different combinations of the cost parameter C and kernel σ were tested: $C \in \{0,001;0,01;0,1;1;10;50;100\}$ and $\sigma \in \{0,001;0,01;0,1;1;10;50;100\}$. The code used for implementing SVM algorithms was from *Statistics Toolbox* (Matlab[®]) [102].

SVMs are being widely applied to medical data, being very efficient for discovering informative features or attributes both in feature selection methods and classification processes. In general, the performance of SVM classification algorithm is better than KNN. However, a comparing study between them was made in order to determine the best classification's architecture for each subject in specific.

K-Nearest Neighbours KNN is a non-parametric algorithm used for objects classification based on closest training examples in the problem space [103]. It is considered the simplest classification algorithm of all machine learning techniques [109], and should be one of the first choices for a classification study when there is little or no prior knowledge about the distribution of the data. For the classification of a given object, this algorithm takes into account the majority vote of its neighbours. Therefore, the object is assigned

Table 2.8: Simple classifiers developed.

Type of features	Time window	Classification Algorithms
Eye parameters	500 ms	Linear SVM RBF SVM KNN
	1000 ms	Linear SVM RBF SVM KNN
Alpha Amplitude	500 ms	Linear SVM RBF SVM KNN
	1000 ms	Linear SVM RBF SVM KNN
Temporal Phase Stability	500 ms	Linear SVM RBF SVM KNN
	1000 ms	Linear SVM RBF SVM KNN

to the class more common amongst its k nearest neighbours. In order to attain the best results in the classification task, the value of parameter k can be changed. For example, if $k = 1$ the object is simply classified as an instance of the class of its nearest neighbour. Therefore, a specific distance metric is applied to define the nearest neighbour of each object being classified. In order to minimize the computation time and the complexity of the algorithm, the Euclidean distance was applied here, which is the metric more frequently used [103]. The KNN classification algorithm was tested for 1 to 30 nearest neighbours - $k \in \{1 : 30\}$. Functions from the *Statistical Pattern Recognition Toolbox* [110] (Matlab[®]) were used for the designing of KNN classification algorithms.

2.5.6.2.2 Hybrid Classifiers

Hybrid classifiers can be developed using several approaches. A commonly used method is simply to fuse the recognition results at the decision-level based on the outputs of separate unimodal classifiers (decision-level fusion technique). This is an approach which has shown great potential to increase classification accuracy beyond the level reached by individual classifiers [105], and for this reason, it was also implemented on this study. The scheme of the figure 2.23 explains how to obtain the output of a decision-level fusion approach taking into account the labels assigned to each instance by each unimodal classifier selected for the classification task employed in this study, as an

example. The combinations of unimodal classifiers considered for this approach are also enumerated in the table 2.9.

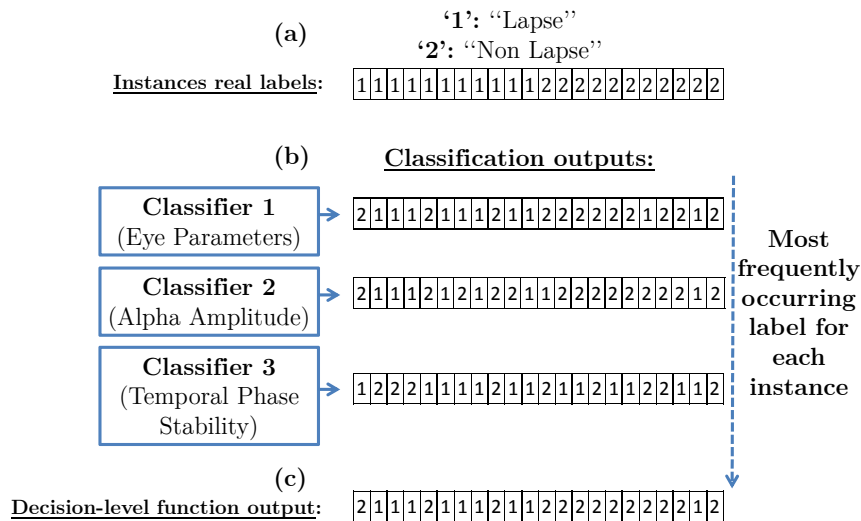


Figure 2.23: Scheme explaining how to obtain the output of the decision-level fusion approach adopted in this study, which takes into account the labels assigned to each instance by each unimodal classifier implemented. (a) Real labels for a given set of instances. (b) After considering the output for each instance given by each one of the three classifiers considered (eye parameters, alpha amplitude and temporal phase stability), the final output vector (c) is obtained by taking the most frequently occurring label for each instance.

Table 2.9: The four hybrid classifiers developed taking into account all possible combinations between unimodal classifiers.

Hybrid Classifiers			
1.	Eye Parameters (500 ms)	Alpha Amplitude (500 ms)	Temporal Phase Stability (500 ms)
2.	Eye Parameters (500 ms)	Alpha Amplitude (1000 ms)	Temporal Phase Stability (500 ms)
3.	Eye Parameters (1000 ms)	Alpha Amplitude (500 ms)	Temporal Phase Stability (500 ms)
4.	Eye Parameters (1000 ms)	Alpha Amplitude (1000 ms)	Temporal Phase Stability (500 ms)

2.5.6.3 Performance Evaluation

In general, for assessing the performance of a classifier, some data from the original data set are selected randomly and the model built predicts its output values. The predicted values are therefore compared to the real ones, and the classifier's accuracy can be computed. This measure is obtained based on the following quantities: true positives (TP), true negatives (TN), false positives (FP) and false negatives (FN). In this specific situation, a "positive" denotes a "Lapse" in attention (previously predicted); and a "negative" denotes a "Non Lapse". Consequently, a TP is a trial which was correctly predicted

as a ‘‘Lapse’’, and a FP is a ‘‘Non Lapse’’ trial which was wrongly predicted as a ‘‘Lapse’’ event. Taking into account these definitions, the classifier’s accuracy (Acc) can be computed using the equation below:

$$Acc = \frac{TP + TN}{TP + TN + FP + FN} \quad (2.2)$$

In order to select a good classifier from a set of classifiers it is necessary to adopt an accuracy estimation method. This procedure is frequently called model selection. In this study, a three-stage procedure was carried out for evaluating the performance of the several classifiers developed. Only the accuracy measure (given by the equation 2.2) was taken into account for assessing the performance of each binary classifier and not other performance measures as the sensitivity or specificity, because the data set used was balanced for the two classes being classified.

At first and just after applying PCA algorithm to the whole data set, $\sim 10\%$ of the total number of trials were set aside, and the remaining 90% were used for assessing the classification algorithms’ parameters which ensured the highest classification rate: the constraint parameter C , for Linear SVM; the hyper-parameters C and σ , for RBF SVM; and the number of neighbours (k), for KNN classification algorithms. For this purpose, it was implemented the cross-validation method, one of the most commonly used methods for performance evaluation. In this method, the whole data set is randomly split into n different subsets (folds). Thereafter, the classifier is trained and tested n times. In each iteration, one subset is used as the validation set, and the classifier trained with the remaining $n-1$ subsets. In the next iteration, the subset assigned as the test set will be used in the training set. The overall estimated accuracy is the average among the n iterations and it depends on the number of subsets or folds (n) selected [111]. In this study, 5-folds cross-validation was used. After selecting the most adequate parameter values which ensured the highest classification rate in the cross-validation method, for each simple/unimodal classifier developed and corresponding algorithm (RBF SVM; Linear SVM; and KNN), the best combination among each classifier and algorithm was chosen for the third stage of the procedure. Those models were then tested with the $\sim 10\%$ of data set aside initially, a set of values completely ‘‘unseen’’ and ‘‘unknown’’ by the classifiers. Both the values obtained in the cross-validation method and in the test were taken into account for analysing the performance of each simple classifier (eye parameters, alpha amplitude, and temporal phase stability), considering each subject (see figure 2.24 for an explanation of the three-stage procedure adopted).

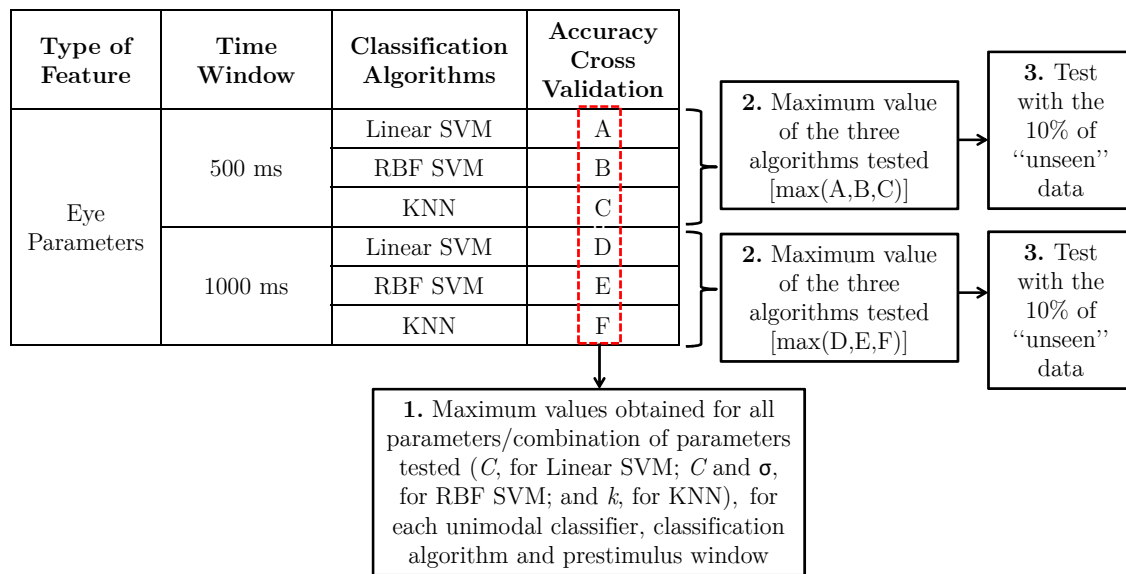


Figure 2.24: Graphic illustration for the three-stage procedure adopted for evaluating the unimodal classifiers developed, for each prestimulus window, using as an example the classifier which used eye parameters as features. **1.** At first, the parameter values/combination of parameters which ensured the highest classification rate in the cross-validation method were determined for each unimodal classifier, classification algorithm and prestimulus time window. **2.** Then, the best combination among each classifier and classification algorithm was chosen, taken into account the highest value obtained in the cross-validation method. **3.** Those models were then tested with the $\sim 10\%$ of data set aside initially, a set of values completely "unseen" and "unknown" by the classifiers.

The mean number across subjects of trials/samples for each class used for training and testing each unimodal classifier are presented in the table 2.10.

Table 2.10: Number of trials/samples across subjects per class used for training each simple classifier developed; and the corresponding number of trials set aside after PCA and used for assessing the accuracy of the classifier when it was submitted to "unseen" data ($\sim 10\%$ of the whole data set). Values are presented as mean \pm standard deviation.

Classifier	Number of subjects	Time window	Number of trials for training		Number of trials for testing	
			Class "Lapse"	Class "Non Lapse"	Class "Lapse"	Class "Non Lapse"
Eye Parameters	20	500 ms	91,600 \pm 8,888	92,000 \pm 9,498	10,700 \pm 0,733	10,700 \pm 0,733
		1000 ms	92,250 \pm 8,130	92,700 \pm 8,578		
Alpha Amplitude	18	500 ms	91,278 \pm 5,443	93,000 \pm 5,292	10,556 \pm 0,856	10,556 \pm 0,856
		1000 ms				
Temporal Phase Stability	18	500 ms	91,167 \pm 5,752	92,667 \pm 5,750	10,444 \pm 0,922	10,444 \pm 0,922
		1000 ms				

Regarding the hybrid classifiers, performance evaluation was conducted by, at first, retaining the most adequate parameter values/combination of parameters which ensured the highest classification rate in the cross-validation method for each unimodal classifier

and classification algorithm - Linear SVM; RBF SVM and KNN (step 1. of the figure 2.24). Then, the $\sim 10\%$ of data set aside initially were submitted for classification, taking into account each one of the options enumerated in the figure 2.25.

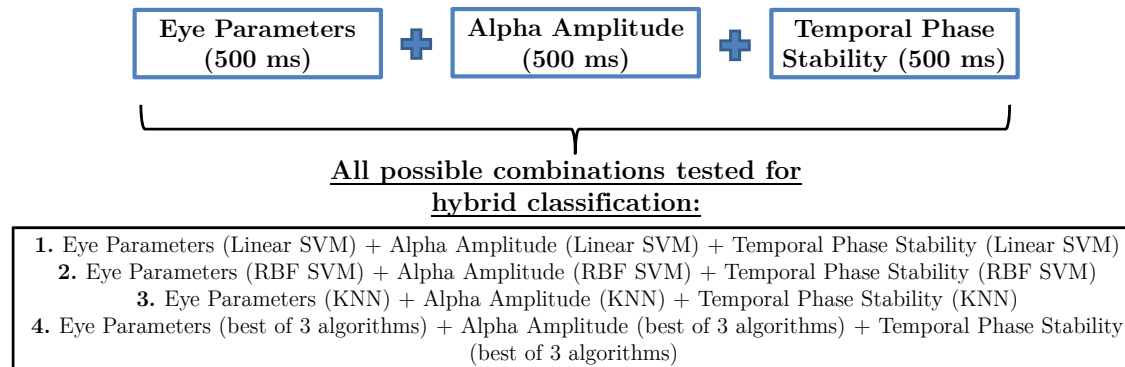


Figure 2.25: All possible combinations tested for the hybrid classification approach, considering the three unimodal classifiers and the three classification algorithms implemented in this study, taking as example the output labels fusion of the classifiers for eye parameters (500 ms), alpha amplitude (500 ms) and temporal phase stability (500 ms). For hybrid classification, four approaches were taken into account. Regarding the first three options, the output labels from the three separate classifiers were obtained by considering the same classification algorithm for all the classifiers - options **1**, **2** and **3**; taking into account the best parameter/combination of parameter values in the cross-validation method. In the last option (**4**), the classification algorithm among Linear SVM, RBF SVM and KNN which ensured the best classification performance in the cross-validation, specifically for each type of unimodal classifier, was selected. For all the options, the output labels given for each type of classifier (eye parameters, alpha amplitude and temporal phase stability) were considered for the hybrid classification of the $\sim 10\%$ of instances set aside initially and completely “unknown” for all the classifiers tested.

After combining the results at the decision-level based on the outputs of the three separate classifiers as it is explained in the figure 2.23, for the four options explored, the accuracy value for each hybrid classification was obtained by comparing the final output label vector with the real labels of the instances. At the end, the best option among the presented in the figure 2.25 was determined, for each combination of unimodal classifiers of the table 2.9, for each subject. The table 2.11 refers to the mean number of trials per class across subjects selected for training the unimodal classifiers used in the hybrid classification approach and for the testing stage with $\sim 10\%$ of the whole data set.

Table 2.11: Number of trials/samples per class across subjects in common between the simple classifiers used in combination for the hybrid classification approach, both for training and for testing ($\sim 10\%$ of the whole data set in the last case).

Classifier	Number of Subjects	Number of trials for training		Number of trials for testing	
		Class "Lapse"	Class "Non Lapse"	Class "Lapse"	Class "Non Lapse"
Eye Parameters (500 ms) + Alpha Amplitude (500 ms) + Temporal Phase Stability (500 ms)	18	89,056 \pm 9,985	90,667 \pm 9,159	10,333 \pm 1,188	10,333 \pm 1,188
Eye Parameters (500 ms) + Alpha Amplitude (1000 ms) + Temporal Phase Stability (500 ms)					
Eye Parameters (1000 ms) + Alpha Amplitude (500 ms) + Temporal Phase Stability (500 ms)		89,278 \pm 9,749	90,944 \pm 8,881	10,333 \pm 1,188	10,333 \pm 1,188
Eye Parameters (1000 ms) + Alpha Amplitude (1000 ms) + Temporal Phase Stability (500 ms)					

Chapter 3

Results

In section 3.1 are described the behavioural results. In section 3.2 and 3.3 are presented the results of the study of the neural and eye correlates of intra-individual RT variability, both at group and individual levels. Finally, the last section (section 3.4) contains the results obtained with the classification platform developed for predicting attention lapses for each one of the participants of the study.

3.1 Behavioural Results

Regarding the behavioural results (table 3.1), it can be observed that, globally, subjects have performed the task in a satisfactory way, taking into account both the correct responses' and missed trials' rate. All the subjects had a hit rate above 90% and only one subject missed more than 5% of the trials - subject 19. RT values are presented separately for each hand to avoid possible hand-effects, caused by different subject's handedness. Median RT values are also considered instead of mean values, because RTs are not normally distributed with a longer tail of slow compared with fast responses. Most subjects responded on average between ~ 400 and ~ 600 ms after stimulus onset, excluding subject number 6, who showed values for both hands considerably higher than the other subjects (~ 800 ms). Nevertheless, her performance was the best among all the participants, in terms of hit's rate and percent of missed trials. Note that for the interpretation of the following results (regarding EEG and eye measurements) the intra-individual variability of response RTs was considered to define different states of attention. Therefore, given that participants were instructed to respond as fast as possible, it was assumed, within a subject, that a better task performance was associated with faster responses, whereas slower responses were interpreted as an impairment on task performance, indicating the eventual occurrence of an attention lapse.

Table 3.1: Behavioural results for all the subjects in terms of median RT values for both left and right hands, percent of correct responses and missed trials. Std. Deviation: standard deviation.

Subject	Left Hand Median RT (ms)	Right Hand Median RT (ms)	Correct Responses (%)	Missed Trials (%)
1	480,094	462,293	99,083	1,357
2	445,367	427,094	98,643	0,000
3	433,937	452,032	99,083	0,000
4	550,318	478,953	99,095	0,450
5	479,109	468,083	96,833	0,450
6	800,689	755,411	100,000	0,000
7	444,634	398,157	98,190	0,000
8	457,145	430,797	95,946	0,000
9	414,483	414,419	98,190	0,000
10	446,683	403,671	91,284	0,457
11	547,183	512,336	98,182	0,000
12	515,479	530,574	97,222	0,917
13	499,586	473,611	99,061	3,620
14	487,245	489,717	98,630	0,000
15	441,194	433,373	94,444	0,461
16	597,460	504,291	97,696	1,810
17	460,910	502,516	99,543	0,455
18	489,884	466,666	100,000	0,909
19	483,770	514,495	94,924	9,633
20	616,351	537,140	97,653	1,389
Mean \pm Std. Deviation	504,576 \pm 87,894	482,781 \pm 76,304	97,685 \pm 2,147	1,095 \pm 2,196

3.2 EEG Measurements

3.2.1 Prestimulus Alpha Amplitude

In order to investigate if the alpha amplitude could predict fluctuations in subject's performance, the prestimulus alpha amplitude in posterior brain areas was compared between different attention states on a group and individual basis. All the analyses performed in this context were based on two time segments of 500 and 1000 ms time length defined prior to stimulus onset. Regarding the group analysis, and similarly to the procedure adopted by Hanslmayr et al. [35], comparisons between the four conditions defined in chapter 2, which represent different levels of subject's task performance, were made; taking into account the pooled values for the prestimulus alpha amplitude over 19 electrodes located in the posterior brain area. Additionally, and also regarding the group analysis, alpha amplitude was compared between conditions for each electrode separately for the two prestimulus periods referred above, similarly to the approach adopted in the study of Ergenoglu et al. [69]. In order to evaluate if at the individual level the prestimulus alpha

amplitude could predict fluctuations in performance, single trial values were compared between conditions for each participant independently.

3.2.1.1 Group Comparisons

Regarding the group comparisons between the four conditions - RT_{Q1} , RT_{Q2} , RT_{Q3} and RT_{Q4} , ranging from fast to slow trials - it was not found a statistically significant difference (p -value > 0,05, Repeated Measures ANOVA; two-tailed) for the mean alpha amplitude (AUC) across subjects, considering the pooled values over the electrode sites within the parietal, parieto-occipital and occipital area, for both the prestimulus time windows of 500 ms and 1000 ms - figure 3.1. However, graphically, there was a tendency for RT values increasing with increasing prestimulus alpha amplitude. Thus, the lack of statistical significance at the 0,05 level was possibly due to an insufficient number of trials.

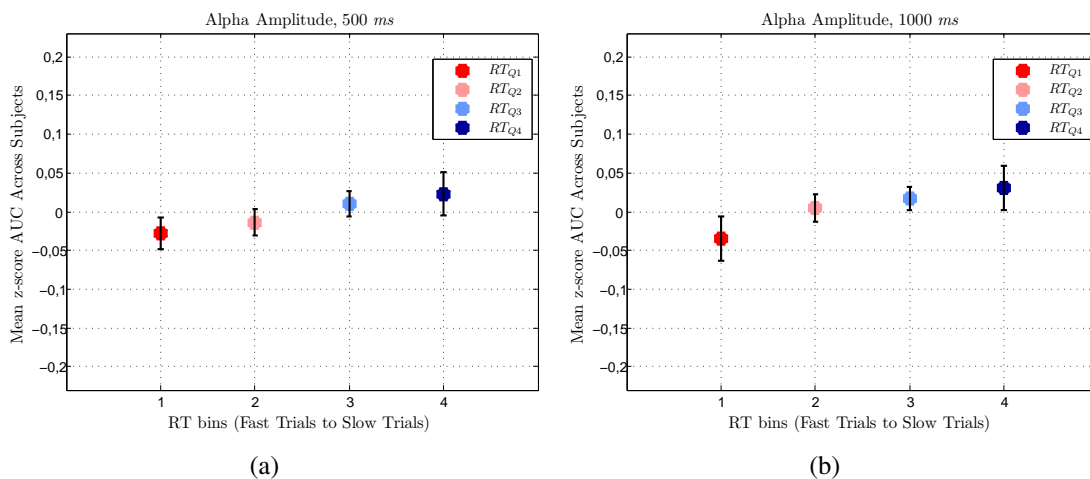


Figure 3.1: Mean z -score for alpha amplitude (AUC) values, pooled over the electrodes within the parietal/parieto-occipital/occipital area, across subjects for each one of the four conditions, considering (a) 500 ms (p -value, Repeated Measures ANOVA: 0,436) and (b) 1000 ms prestimulus time windows (p -value, Repeated Measures ANOVA: 0,348). Error bars represent standard errors.

The same comparisons (between conditions RT_{Q1} , RT_{Q2} , RT_{Q3} and RT_{Q4}) was conducted, but considering each electrode separately. However, no channel showed a significant difference between conditions after correction for multiple comparisons using the FDR procedure, for both prestimulus time windows.

3.2.1.2 Individual Comparisons

Individual comparisons were also conducted for all the measures analysed, because it was intended to study if EEG or eye parameters could predict the occurrence of an attention lapse before it happens, at the individual level. No significant differences were

found between all the conditions or the two conditions more extreme (fast and slow trials), by taking the pooled values over the posterior electrode sites considered above, for all the participants of the study. Considering statistical comparisons for each electrode separately, no subject showed a significant difference during both 500 ms and 1000 ms time windows prior to stimulus onset for comparisons between the four conditions, after correction for multiple comparisons. Next, only prestimulus alpha amplitude values regarding fast and slow trials were compared. In table 3.2 are presented the subjects and corresponding electrodes which showed a statistically significant difference between fast - RT_{Q1} - and slow trials - RT_{Q4} - for the two prestimulus time windows, after correction for multiple comparisons using the FDR method.

Table 3.2: Subjects and corresponding parietal/parieto-occipital/occipital channels which showed a statistically significant difference between the more extreme conditions (RT_{Q1} and RT_{Q4} , which corresponded to fast and slow trials, respectively) after correction for multiple comparisons.

Subject	Parietal/Parieto-Occipital/Occipital Channels	
	500 ms	1000 ms
2	P3; PO5; PO3; O2	PO5
5	P1; PZ; POZ; OZ	P1; PZ; P2; P4; P6; P8; POZ; OZ
9	P3; P1; PO3; PO4; PO6; PO8; OZ; O2	PO3; POZ
12	P1; PZ	P1; PZ; P2; P4; P6; P8; POZ; PO4; PO6; PO8; OZ; O2
13	P8; PO7	P4; PO4; PO6; PO8; OZ; O2
18	P1; PZ; PO5; PO3; POZ; O1	P5; P3; P1; PZ; PO5; PO3; POZ; O1

For all the electrodes of the table 3.2, the mean AUC was higher for slow than fast trials, which indicates that, for those subjects, a higher prestimulus alpha amplitude was associated with a slowing of the response RT and, therefore, with an impairment on task performance as predicted.

In the figure 3.2 are presented the results obtained for the subject number 18 as an example, in terms of the location of the electrodes showing a significant difference among fast and slow trials in the electrode cap, considering both time windows of 500 ms and 1000 ms prior to stimulus onset; the mean spectra across trials for an electrode in common with those two sets (PZ), for each condition and prestimulus time window; and the corresponding boxplot representing the variability of prestimulus alpha amplitude (AUC) values across trials. The AUC for this subject was computed within the range 9-13 Hz.

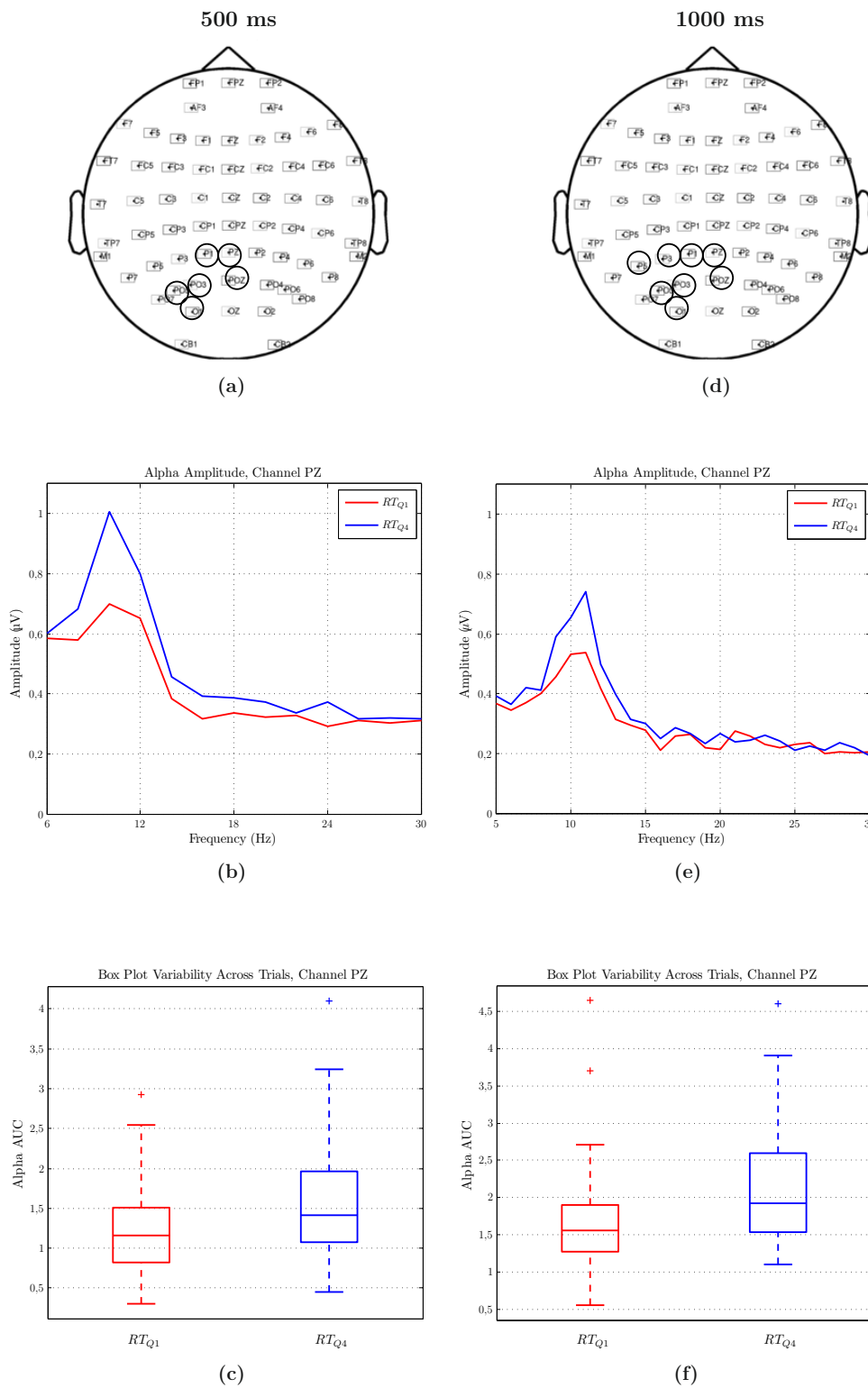


Figure 3.2: An example of a subject (number 18) showing significant differences between fast (RT_{Q1}) and slow trials (RT_{Q4}) for alpha amplitude for six electrodes within the parietal/parieto-occipital/occipital area, and for the prestimulus time window of 500 ms length (**left panel**); and for eight electrodes, considering the 1000 ms time window prior to stimulus onset (**right panel**). Spectral representations for one of those electrodes in common with the two sets (PZ) for each prestimulus window are also plotted - 500 ms (**left panel**) and 1000 ms (**right panel**). **(a) and (d)** Topographical representations of each electrode's set in the cap. **(b) and (e)** Mean spectra across all single trials for electrode PZ for both conditions. **(c) and (f)** Boxplot of prestimulus alpha amplitude (alpha AUC) of slow and fast trials for electrode PZ.

Note that the mean spectra across trials revealed an alpha peak visually higher for slow trials (RT_{Q4}) than fast trials (RT_{Q1}) condition. This result suggests that when parietal alpha oscillations are high in amplitude in the channels highlighted in the graphics (a) and (b) of the figure 3.2, depending on the prestimulus time window considered, this subject showed slower response RTs and, therefore, an impairment on task performance.

Possibly, statistical significant differences were not found between conditions for the group analysis, whereas some subjects revealed significant differences between fast and slow trials for some electrodes, because the number of trials or, eventually, subjects was not large enough to observe an effect of group. The inter-subjects variability could have also contributed to obtain inconclusive results regarding the whole group.

3.2.2 Synchronization Between Electrodes

3.2.2.1 Group Comparisons: EEG Phase Coherence

Similarly to the prestimulus alpha amplitude, it was intended also to investigate if the phase coherence measure was capable to predict attention lapses, in three defined frequency bands: alpha (8-12 Hz); beta (20-30 Hz) and gamma (30-45 Hz), by adopting a procedure based on the study of Hanslmayr et al. [35]. For the group analysis, it was taken into account the phase coherence index given by the equation developed by Delorme et al. [34] (see chapter 1, equation 1.5), which represents relative constancy of the phase differences (Δ phase) between two signals from two different electrodes along a defined set of trials. One single value was calculated for each subject and condition, and comparisons were made taking into account this specific value for each one of the different conditions. Only segments of 500 ms time length prior to stimulus appearance were taken into account for this analysis.

For group comparisons between conditions for prestimulus phase coherence values, and in accordance with what was already mentioned, a two-stage statistical procedure was adopted for selecting the electrode pairs which showed a statistically significant difference between conditions RT_{Q1} , RT_{Q2} , RT_{Q3} and RT_{Q4} (see chapter 2, point 2.5.2). In the figure 3.3 is presented a graphical illustration of the number of electrode pairs which remained after the last step of the statistical procedure implemented - the non-parametric permutation test followed by correction for multiple comparisons using the FDR criterion - for each frequency bin considered - alpha (8-12 Hz), beta (20-30 Hz) and gamma (30-45 Hz). The electrode pairs which showed statistically significant differences among the four conditions, were divided in the electrode pairs which revealed a higher value for the mean phase coherence across subjects for fast trials in comparison with slow trials ($RT_{Q1} > RT_{Q4}$); and those which revealed this tendency in the opposite direction

($RT_{Q1} < RT_{Q4}$) - see figure 3.3. According with previous studies, as it was mentioned before in chapter 1, in 1.2.2.1.1, it was expected that for alpha frequency range increased prestimulus phase coherence values were associated with increased RT values, and, therefore, with an impairment on task performance; whereas the opposite pattern should be observed, regarding the beta and gamma frequency ranges, for the electrode pairs showing significant differences between the conditions.

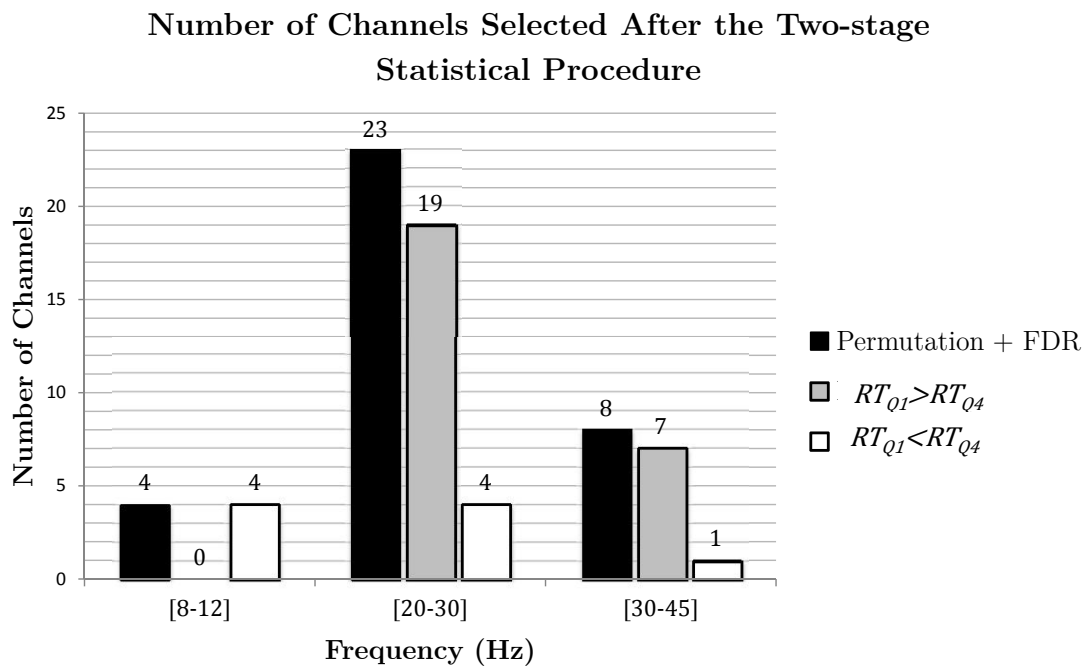


Figure 3.3: Number of electrode pairs retained after the last step of the two-stage statistical test implemented for selecting those which showed a significant difference between the four conditions, and which were associated with a higher or a smaller value for the mean phase coherence across subjects for fast trials in comparison with slow trials (conditions $RT_{Q1} > RT_{Q4}$ and $RT_{Q1} < RT_{Q4}$, respectively), for each frequency bin - alpha (8-12 Hz), beta (20-30 Hz) and gamma (30-45 Hz).

By analysing the graphic of the figure 3.3 it can be observed that, regarding the alpha frequency band, 4 electrode pairs remained after the non-parametric permutation test followed by correction for multiple comparisons using the FDR procedure, namely F5-C1; CPZ-TP8; FCZ-P4 and FCZ-OZ. All of these pairs revealed decreased phase coherence values for fast trials (condition RT_{Q1}) in comparison with slow trials (condition RT_{Q4}), as it was expected, taking into account the results obtained by Hanslmayr et al. [35].

For the beta frequency band, after the whole statistical procedure remained 23 electrode pairs, being the topography representation of the 19 pairs for which fast trials

revealed a higher phase coherence value averaged across subjects in comparison with slow trials and, therefore, increased prestimulus phase coherence was associated with the fastest responses, in the figure 3.4(a). The topographical representation of the remaining 4 channel pairs which revealed the opposite pattern - increased prestimulus phase coherence associated with the slowest responses - is also presented in the figure 3.4(c). Finally, taking into account the results for the gamma frequency range, 8 electrode pairs were obtained after the last stage of the statistical procedure. For this group, 7 pairs showed a higher value for prestimulus phase coherence for fast than slow trials, whose corresponding topographical representation on the electrode cap is in the figure 3.5(a); and only one electrode pair revealed this tendency in the contrary direction - figure 3.5(c).

The results obtained for beta and gamma frequency bands are plotted in the figures 3.4 and 3.5, respectively. For both these frequency ranges, the inspection of the topography of the electrode pairs which showed a significant difference among the four conditions and for which the fastest responses were associated with increased prestimulus phase coherence values, shows that mainly fronto-parietal electrode pairs contributed to this effect. In the figures 3.4(b) and 3.5(b) are also presented the mean phase coherence values for those electrode pairs across subjects, for beta and gamma frequency bands, respectively. Only 4 electrode pairs revealed this opposite pattern for the beta frequency band, and one single pair, for the gamma frequency range. In the figures 3.4(d) and 3.5(d), are also presented the mean phase coherence values for those electrode pairs across subjects, for beta and gamma frequency bands, accordingly.

Taking into account that the number of electrode pairs which showed an increased prestimulus phase coherence associated with the fastest responses is almost 83% and 88% of those which remained after the two-stage statistical procedure, for beta and gamma frequency bands, respectively, it can be concluded that, globally, with an increase on prestimulus phase coherence values, RT values decreased and, therefore, subject's performance improved. This result was in accordance with the pattern expected for those two frequency ranges.

These results lead to the conclusion that fluctuations in phase coherence regarding the beta and gamma frequency bands could, indeed, predict fluctuations in task performance.

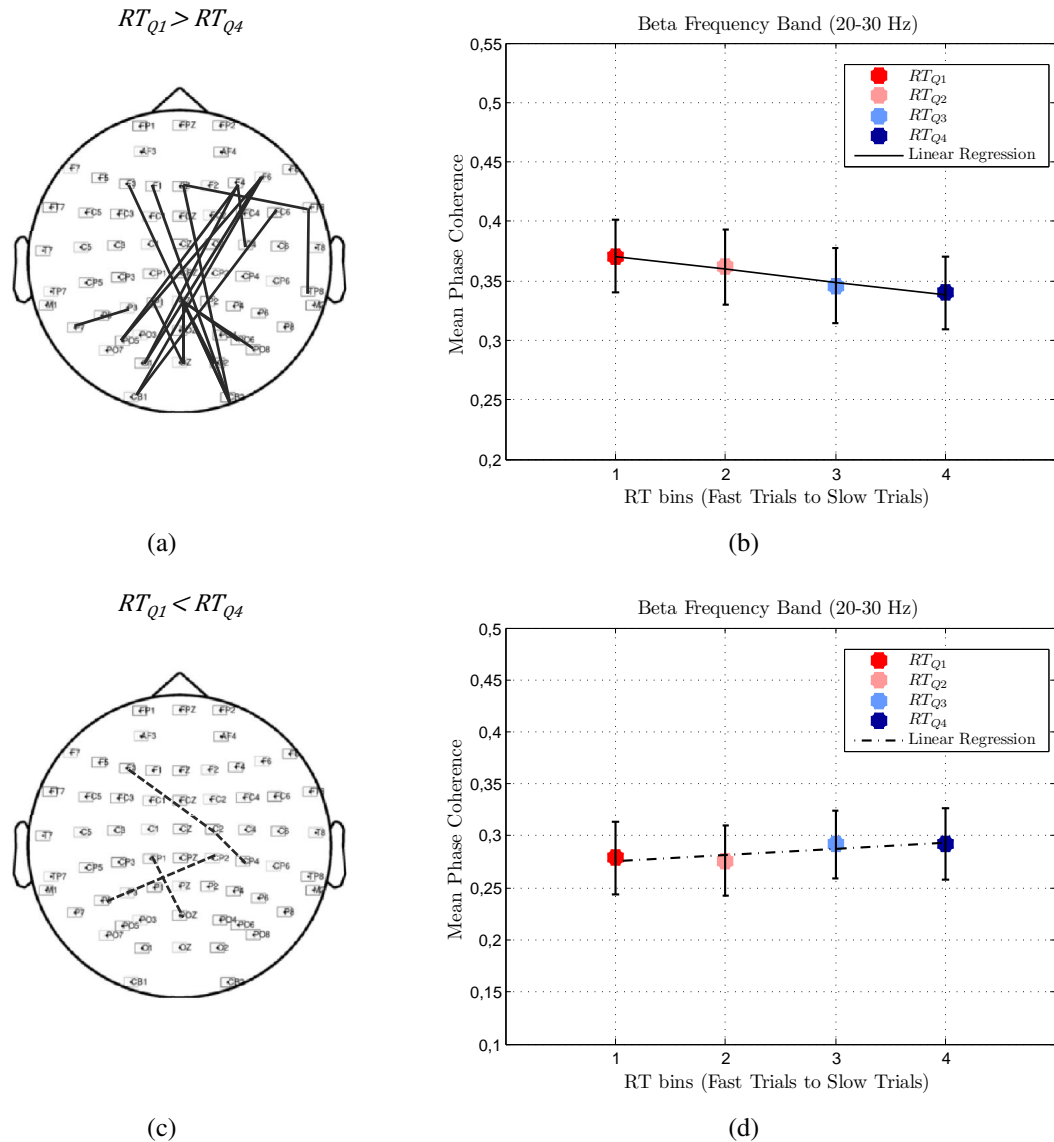


Figure 3.4: Results for group comparisons between the four conditions relative to phase coherence analysis for beta frequency range (20-30 Hz). **(a) and (c)** Scalp map displaying the electrode pairs which showed a statistically significant difference between the four conditions and a higher mean phase coherence value for fast trials - condition RT_{Q1} - than slow trials - condition RT_{Q4} ; and in the opposite direction, respectively. **(b) and (d)** Plots showing mean phase coherence values for those electrode pairs and corresponding linear regression line. Error bars represent standard errors.

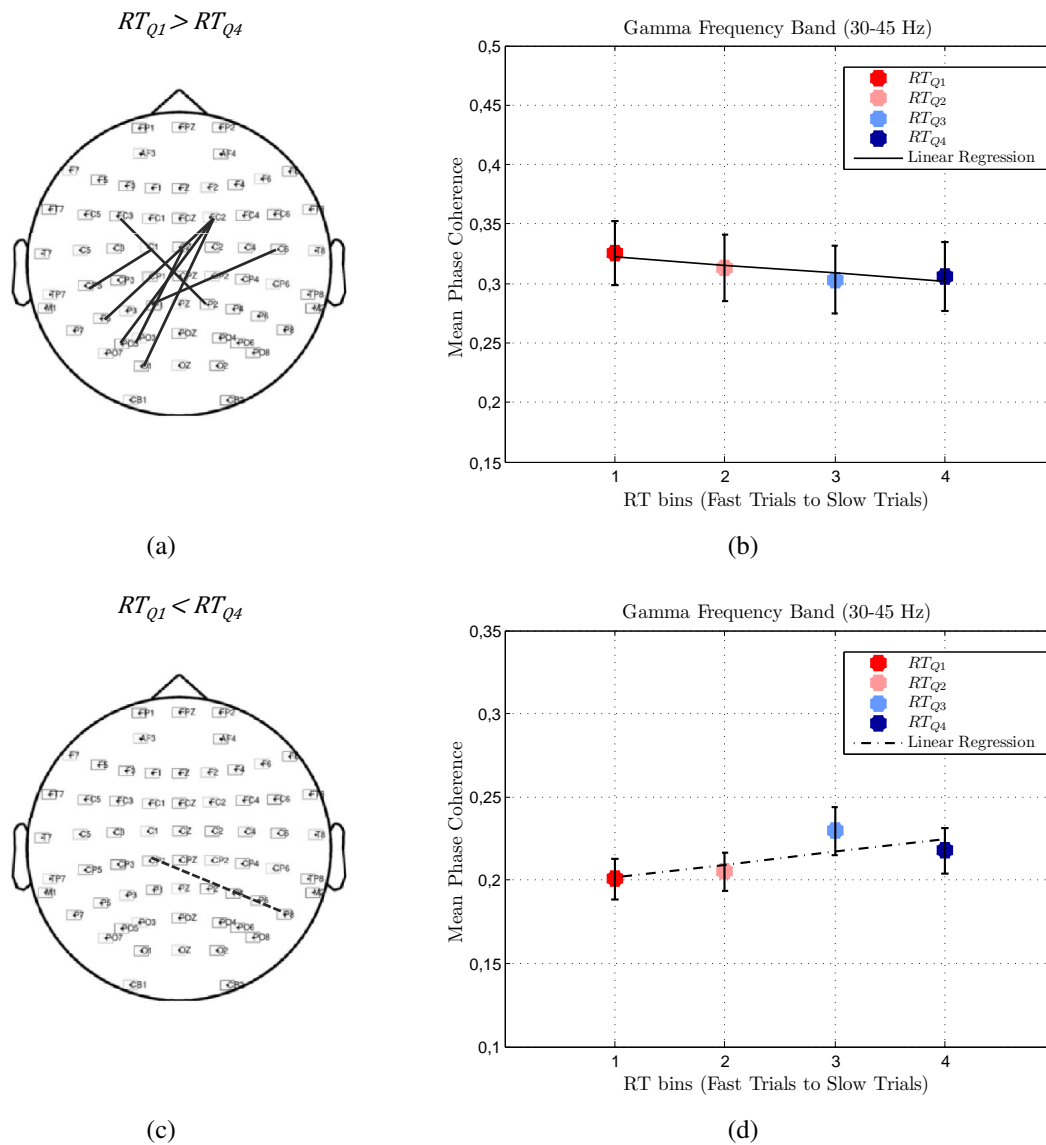


Figure 3.5: Graphical representations of the results obtained for group comparisons between the four conditions relatively to phase coherence analysis regarding the gamma frequency range (30-45 Hz). **(a) and (c)** Scalp map displaying the electrode pairs which showed a statistically significant difference between the four conditions and a higher mean phase coherence value for fast trials - condition RT_{Q1} - than slow trials - condition RT_{Q4} ; and in the opposite direction, respectively. **(b) and (d)** Plots showing mean phase coherence values for those electrode pairs and corresponding linear regression line. Error bars represent standard errors.

3.2.2.2 Individual Comparisons: EEG Phase Deviation

As it was also intended to investigate if phase coherence measures would be capable of predicting fluctuations in attention at the individual level, comparisons between conditions were also made within the same subjects. However, the equation developed by Delorme et al. [34] could not be used in this context, because the phase coherence index obtained with his method is calculated based on the circular mean of the phase differences (Δ phase) between two different signals across a given set of trials, giving, therefore, one single value for a set of trials. Because, in order to conduct individual comparisons it was necessary to use a measure which was capable to illustrate the phase synchrony between two electrode sites on a single trial manner, the phase deviation approach proposed by Hanslmayr et al. [35] and described on chapter 2, at the point 2.5.3.2.2, was adopted here. Phase deviation results must be interpreted on the contrary way relatively to phase coherence analysis. A high phase deviation value for a single trial indicate that the phase differences (Δ phase) between two signals from two different electrode sites for a given period of time highly deviate from the mean Δ phase across trials, being therefore associated with low phase synchrony between those two channels for the given trial. On the other hand, a low phase deviation value for a specific trial is associated with a high phase coherence between two electrode sites. Based on previous studies, single trial phase deviation analysis for the alpha frequency band should reveal that RT values decrease monotonically with increasing phase deviation values. In contrast, analysis for beta and gamma frequency bands should reveal the opposite pattern, in which RT values increase monotonically with increasing deviation from the mean Δ phase [35].

Single trial phase coherence analysis revealed highly variable results among subjects. The electrode pairs which showed a negative and linear correlation between 10 phase deviation bins and the corresponding mean *z-score* RT values, for the alpha frequency band, and those which revealed the opposite pattern for beta and gamma ranges, did not indicate a defined pattern for each frequency band for the location of the coupled electrode sites, from subject to subject. In the figures 3.6, 3.7 and 3.8 are plotted the results obtained in this analysis for two subjects as an example for alpha, beta and gamma frequency bands, respectively. Note that only the electrode pairs which showed a statistically significant correlation are plotted, according to the two-stage statistical procedure adopted and described in 2.5.5.

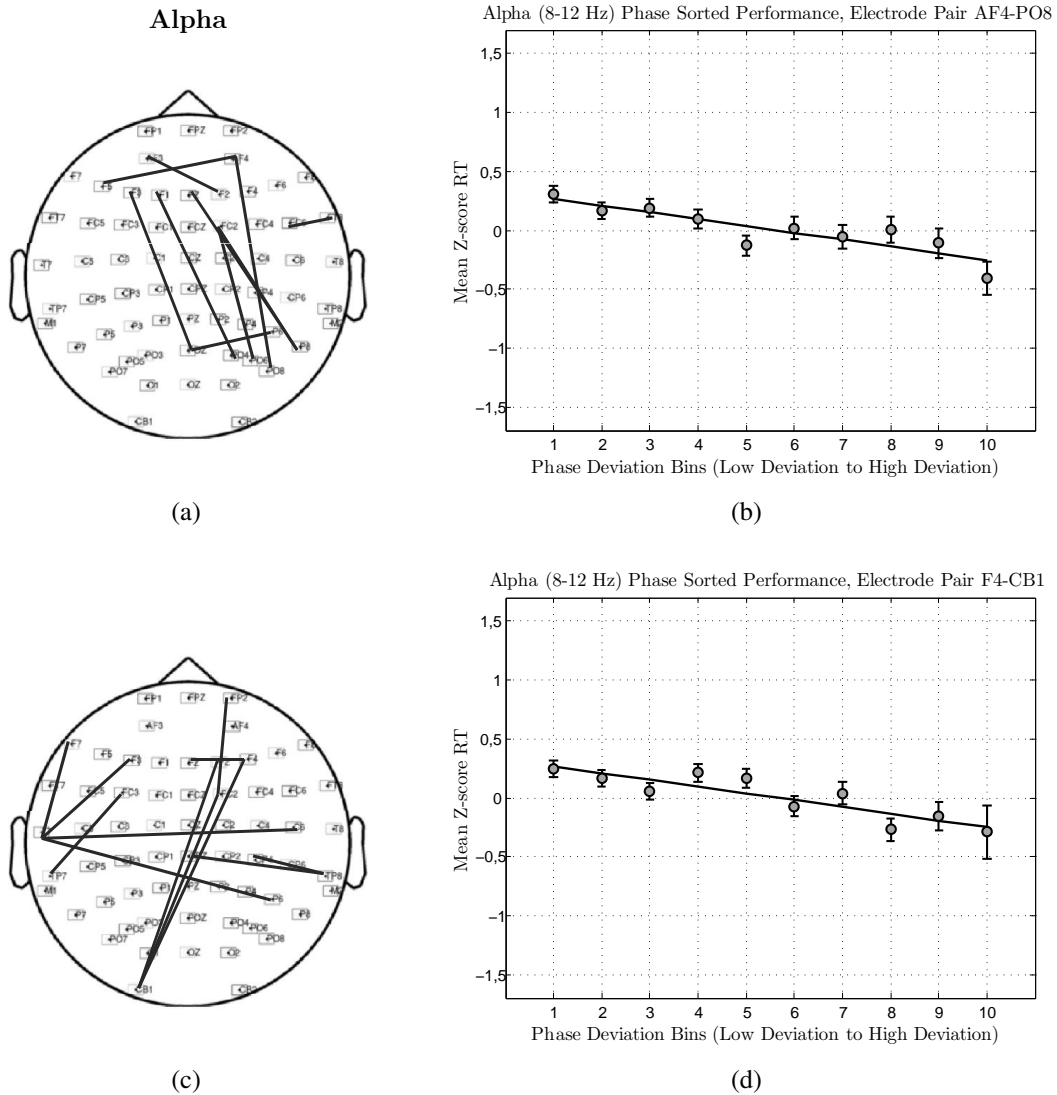


Figure 3.6: Single trial phase coherence analysis is plotted for subjects 15 and 16 and for alpha frequency range. **(a) and (c)** Scalp topography of the electrode pairs for which mean *z-score* RT (scaled on the Y-axis) decreases linearly with increasing prestimulus alpha phase deviation (X-axis). **(b) and (d)** Graphical representation of this correlation for one of those electrode pairs for each subject (AF4-PO8 and F4-CB1, respectively). Error bars represent standard errors.

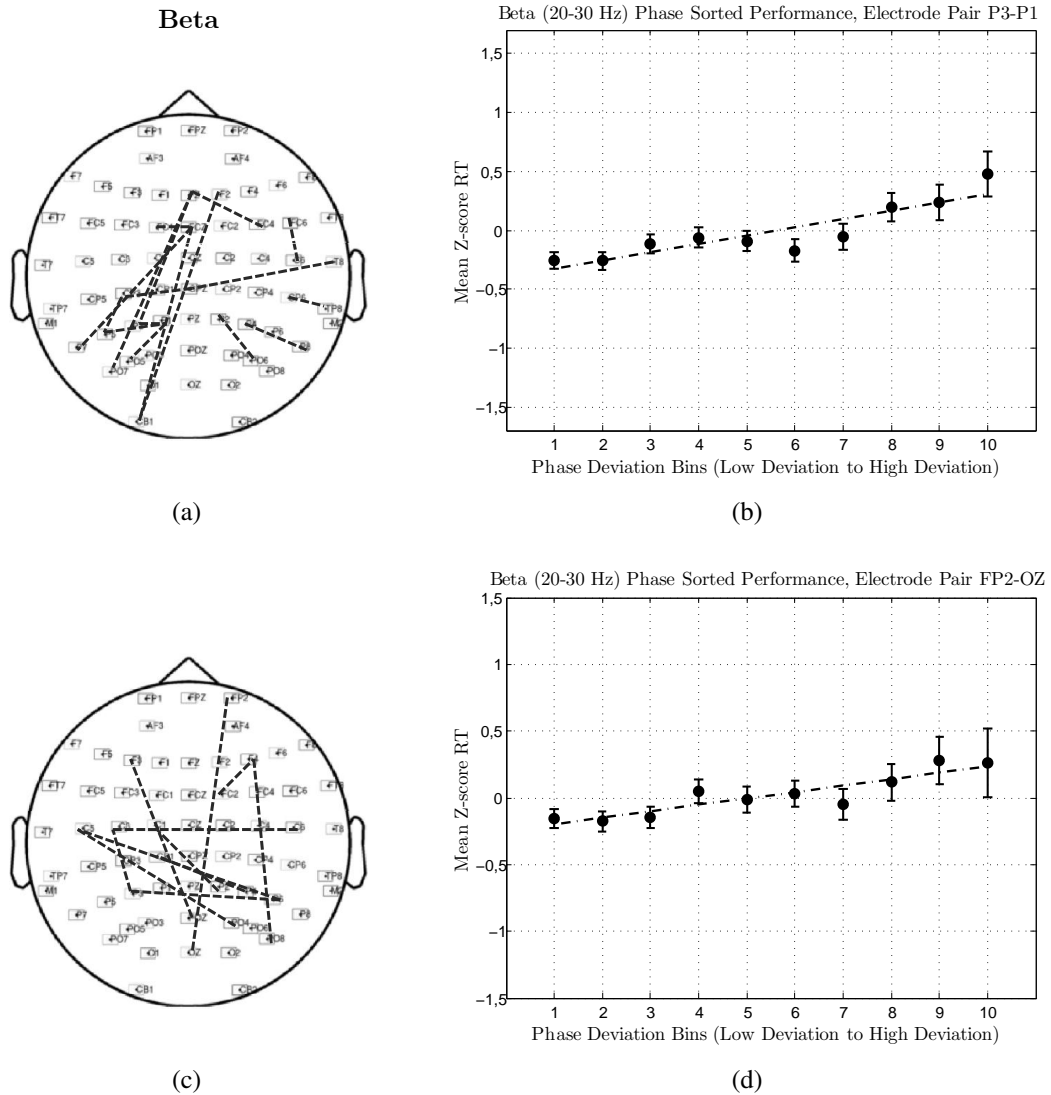


Figure 3.7: Results for single trial phase coherence analysis for subjects 15 and 16, regarding the beta frequency range. **(a) and (c)** Representation of the electrode pairs in the cap which showed a linear positive correlation between mean *z-score* RT and prestimulus phase deviation bins. **(b) and (d)** Representation of this correlation for one of those electrode pairs for each subject (P3-P1 and FP2-OZ, respectively). Error bars represent standard errors.

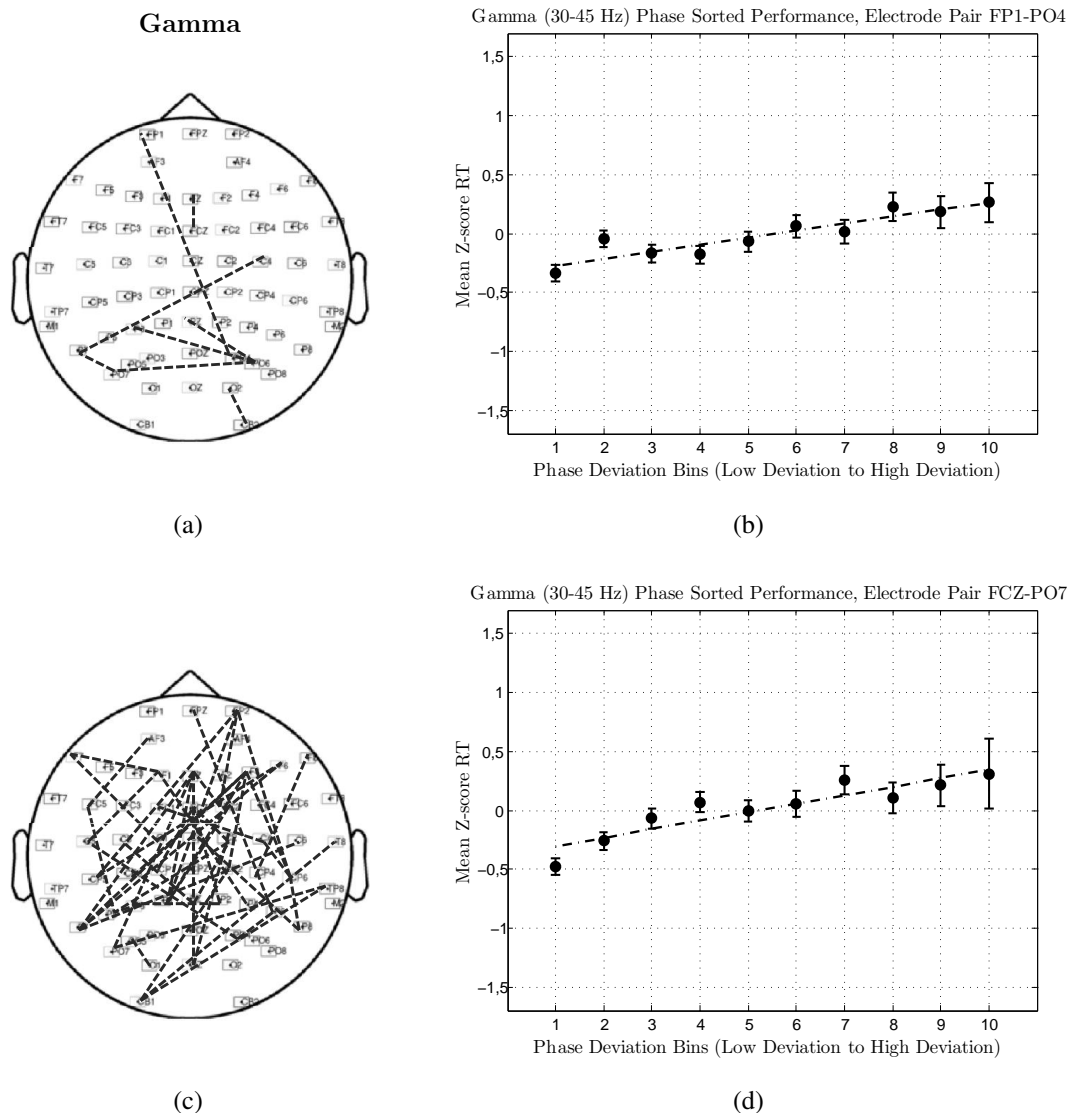


Figure 3.8: Plot regarding the single trial phase coherence analysis, for subjects 15 and 16 and for gamma frequency range. **(a) and (c)** Scalp topography for the electrode pairs for which mean z -score RT increases linearly with increasing phase deviation values. **(b) and (d)** Graphical representation of this correlation for one of those electrode pairs for each subject (FP1-PO4 and FCZ-PO7, respectively). Error bars represent standard errors.

Comparing the topographical representations of the electrode pairs which showed a linear correlation between RT values and phase deviation bins according with the direction expected for each frequency band (as it was explained before) for the two subjects, highly variable results were obtained. As it can be seen, different electrode pairs showed a linear and negative correlation between those two measures, for the alpha frequency band, for the two subjects. The same results were obtained regarding the beta and gamma frequency

bands. It is also important to emphasize the difference among the number of electrode pairs selected for the gamma frequency band between the two subjects. Subject number 16 revealed much more electrode pairs in accordance with the tendency expected for the RT values with phase deviation bins, in comparison with subject number 15. Similar results were obtained for the remaining participants.

Concluding, different results were obtained for the topographical representation of the electrode pairs which demonstrated significant differences among different states of attention, defined based on RT measurements, between the group and individual analysis. Probably anatomical differences among subjects have contributed to obtain different results between the different individuals. However, it is important to emphasize that, for the majority of the subjects, mainly couplings between frontal and frontal, parietal and parietal and frontal and parietal electrodes showed to be significantly correlated with RT measurements. This observation reinforces again the influence of the phase synchrony, mainly in frontal-parietal networks, on subject's task performance, which has been linked to the maintenance of sustained attention levels, during attentionally demanding tasks [3, 40].

3.3 Eye Measurements

3.3.1 Pupil Diameter

As other authors have concluded that pupillometric measures are correlated with the subject's task performance in goal-directed tasks [79–81], in this study it was also conducted an exploratory analysis taking into account two time segments of 500 and 1000 ms time length prior to stimulus presentation, in order to investigate if the mean and standard deviation of pupil diameter within the above defined time windows were capable of predicting fluctuations in subject's task performance. Mean and standard deviation values of pupil diameter were compared between different states of attention, both on a group and individual basis. Note that for individual comparisons, the single trial values, which represent the averaged values of each one of the two measures analysed across time windows of 500 or 1000 ms time length, were used. For the group analysis, single trial values were averaged across trials for each condition, for each subject.

3.3.1.1 Group Comparisons

Pupil diameter values 500 and 1000 ms prior to stimulus presentation were compared between conditions RT_{Q1} , RT_{Q2} , RT_{Q3} and RT_{Q4} , ranging from fast to slow trials. In table 3.3 are summarized the results obtained for these comparisons, considering the measures analysed for pupil diameter and the two prestimulus time windows. Only pupil

diameter revealed a significant difference between conditions (p -value $<0,05$, Friedman; two-tailed), for both 500 ms and 1000 ms time windows.

Table 3.3: Group analysis p -values for pupil diameter measures, considering 500 ms and 1000 ms prestimulus windows and comparisons between all conditions (RT_{Q1} , RT_{Q2} , RT_{Q3} and RT_{Q4}). The numbers in bold indicate statistically significant differences among conditions at the 0,05 level. PD : Mean pupil diameter across subjects. $Std PD$: Mean standard deviation of pupil diameter across subjects.

Type of Measure	p -value 4 conditions
PD 500 ms	0,005
PD 1000 ms	0,041
$Std PD$ 500 ms	0,946
$Std PD$ 1000 ms	0,393

In the figures 3.9 and 3.10 are presented the results regarding the mean pupil diameter (PD) and mean standard deviation of pupil diameter values ($Std PD$) across subjects for each one of the four conditions, respectively.

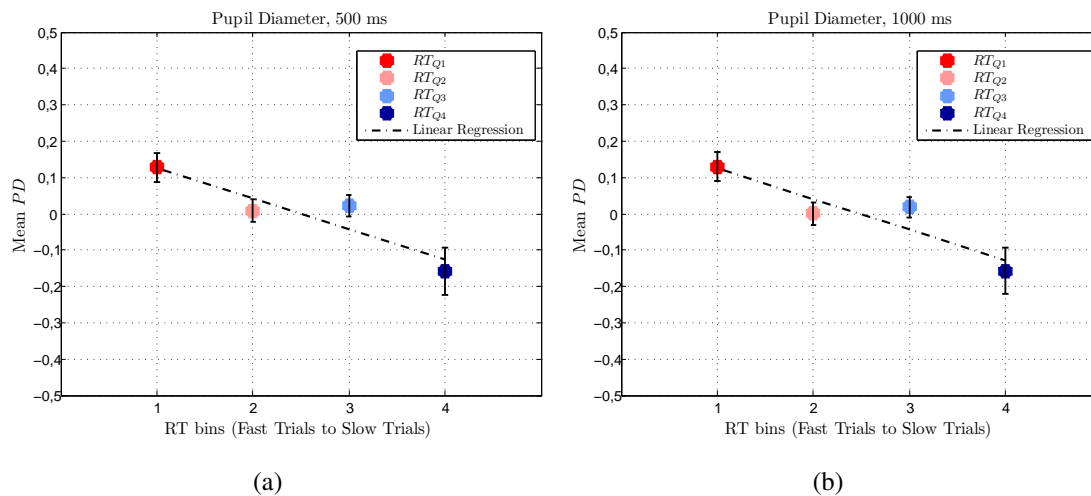


Figure 3.9: Graphical representation of the mean pupil diameter values across subjects - PD , in z -score values - for (a) 500 ms and (b) 1000 prestimulus windows, for each RT bin and corresponding linear regression line. Error bars represent standard errors.

It can be observed that, for both 500 ms and 1000 ms time windows prior to stimulus, pupil diameter is higher for fast trials (RT_{Q1}) than slow trials (RT_{Q4}) (figure 3.9). This result suggests a tendency for subjects responding faster with increasing prestimulus pupil diameter. On the other hand, for standard deviation of pupil diameter analysis it can be observed, graphically, that there is not a so obvious difference among the four

conditions (figure 3.10) in comparison with the pupil diameter measure, for both prestimulus time windows, as it can be confirmed by the results obtained in the statistical tests ($p\text{-value}>0,05$, Repeated Measures ANOVA; two-tailed).

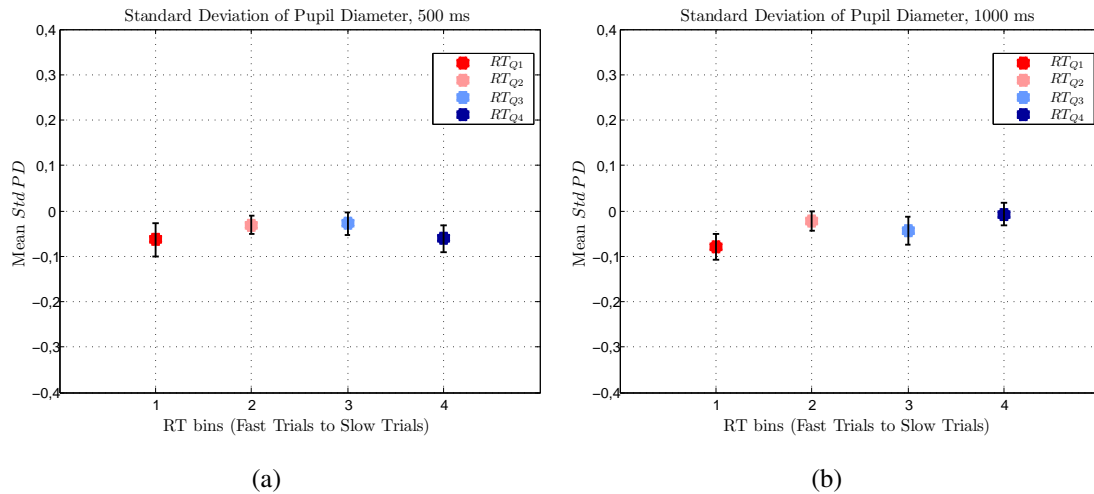


Figure 3.10: Graphical representation of mean values for standard deviation of pupil diameter - *Std PD*, represented in *z-score* units - across subjects, for each RT bin and (a) 500 ms and (b) 1000 ms prestimulus windows. Error bars represent standard errors.

3.3.1.2 Individual Comparisons

Similarly to the EEG measures, individual comparisons were performed also for pupil diameter and standard deviation of pupil diameter, in order to determine if both the pupilometric parameters could be used to predict an attention lapse, for each subject. The results for individual comparisons for the pupil diameter between the four conditions considered (RT_{Q1} , RT_{Q2} , RT_{Q3} and RT_{Q4}) are in table 3.4. Additionally, in table 3.5 are the results obtained for individual comparisons regarding the standard deviation of pupil diameter. In each table is presented the corresponding $p\text{-value}$ for the Kruskal Wallis test. In order to evaluate how RT values relate to pupil diameter measures for each subject, it is also presented the value corresponding to the subtraction between the mean values across trials for each one of the two more extreme conditions: RT_{Q1} and RT_{Q4} , which represent fast and slow trials, respectively. All the results presented below are about both prestimulus time windows: 500 ms and 1000 ms prior to stimulus presentation.

Regarding the individual comparisons for prestimulus pupil diameter values - table 3.4 - in the time window of 500 ms prior to stimulus onset, it can be observed that five subjects showed a statistically significant difference among the four conditions, which represent 25% of the whole sample. Taking into account the results obtained for the 1000 ms prestimulus time window, in addition to the subjects which showed significant differences

Table 3.4: Individual comparisons for pupil diameter values, considering 500 ms and 1000 ms time windows. Numbers in bold indicate values associated with statistically significant differences among the four conditions at the 0,05 level (two-tailed). *PD*: Mean pupil diameter across each prestimulus time window (500 ms or 1000 ms prior to stimulus onset).

Subject	Pupil Diameter, <i>PD</i>			
	500 ms		1000 ms	
	<i>p</i> -value Kruskal Wallis	$RT_{Q1} - RT_{Q4}$ (mm)	<i>p</i> -value Kruskal Wallis	$RT_{Q1} - RT_{Q4}$ (mm)
1	0,777	-0,054	0,540	-0,087
2	0,004	0,483	0,004	0,504
3	0,869	0,040	0,761	0,067
4	0,038	0,030	0,048	0,050
5	0,149	0,354	0,157	0,319
6	0,618	-0,020	0,389	-0,029
7	0,789	-0,262	0,809	-0,269
8	0,064	0,195	0,047	0,254
9	0,719	0,070	0,642	0,103
10	0,393	-0,013	0,402	-0,042
11	0,932	0,003	0,748	-0,016
12	0,000	0,819	0,000	0,826
13	0,000	0,919	0,000	0,888
14	0,533	0,039	0,521	0,092
15	0,188	0,004	0,192	-0,002
16	0,000	0,457	0,000	0,431
17	0,628	-0,093	0,655	-0,091
18	0,278	0,315	0,258	0,306
19	0,149	0,251	0,079	0,256
20	0,366	0,161	0,404	0,165

among the four conditions for 500 ms, only one more subject also demonstrated this difference, representing this sample 30% of the whole group. Additionally, regarding both prestimulus time windows, for the subjects which showed a significant difference among the four conditions, the mean tendency's direction of pupil diameter values with RT bins was consistent across subjects. Indeed, all of those subjects have showed a higher mean prestimulus pupil diameter value across fast trials (RT_{Q1}) in comparison with slow trials (RT_{Q4}), a result in accordance with which was obtained for the whole group.

By evaluating the results obtained for the comparisons regarding the standard deviation of pupil diameter - table 3.5 - only one subject showed a significant difference between the four conditions for the 500 ms prestimulus time window. Specifically for this subject, a higher mean prestimulus standard deviation value across trials was obtained for fast trials (RT_{Q1}) in comparison with slow trials (RT_{Q4}), which indicates that this subject has responded faster when pupil diameter has varied more during a time window of 500 ms length prior to stimulus appearance. For the comparisons between conditions but regarding the 1000 ms time window, also only two subjects showed a significant difference. Contrary to the subject which revealed a significant result for the 500 ms prestimulus

Table 3.5: Individual comparisons for standard deviation values of pupil diameter, considering 500 ms and 1000 ms time windows. Numbers in bold indicate values associated with statistically significant differences among the four conditions at the 0,05 level (two-tailed). *Std PD*: Standard deviation of pupil diameter across each prestimulus time window (500 ms or 1000 ms prior to stimulus onset).

Subject	Standard Deviation of Pupil Diameter, <i>Std PD</i>			
	500 ms		1000 ms	
	<i>p-value</i> Kruskal Wallis	$RT_{Q1} - RT_{Q4}$ (mm)	<i>p-value</i> Kruskal Wallis	$RT_{Q1} - RT_{Q4}$ (mm)
1	0,243	-0,022	0,474	-0,008
2	0,315	0,006	0,067	0,023
3	0,342	0,005	0,671	0,006
4	0,834	0,013	0,650	0,014
5	0,880	-0,010	0,904	0,001
6	0,309	-0,003	0,112	-0,010
7	0,177	-0,015	0,071	-0,021
8	0,356	0,016	0,161	0,003
9	0,637	0,000	0,487	0,004
10	0,529	0,014	0,723	0,004
11	0,752	-0,006	0,705	-0,006
12	0,047	0,017	0,833	0,003
13	0,814	-0,001	0,903	-0,024
14	0,833	0,001	0,934	0,003
15	0,515	-0,003	0,006	-0,013
16	0,257	-0,031	0,020	-0,045
17	0,522	0,004	0,252	0,000
18	0,531	-0,021	0,524	-0,026
19	0,357	-0,034	0,322	-0,007
20	0,660	-0,006	0,117	-0,037

window, these two participants showed a higher value for the mean standard deviation of pupil diameter for slow trials in comparison with fast trials. These results indicate that for those subjects, the fastest responses were obtained when the pupil diameter has varied less among the prestimulus time window of 1000 ms prior to stimulus onset, in comparison when they have responded slower. Taking into account the few number of subjects which revealed a significant difference between conditions for both prestimulus windows, these results are in accordance with those obtained for the group analysis. Indeed, the standard deviation of pupil diameter is not a reliable parameter for predicting fluctuations in subject's task performance, taking into account the results obtained for both the analyses.

Concluding, pupil diameter has proven to be a reliable predictor of fluctuations in attention levels for $\sim 30\%$ of the total number of participants of this study. All of those subjects have responded faster when their pupils were enlarged during both the prestimulus time periods of 500 and 1000 ms, a result in accordance with the group analysis. On the contrary, standard deviation of pupil diameter did not predict fluctuations in subject's attention levels, both on an individual and group basis.

3.3.2 Gaze Position

As the correlation between gaze position patterns and subject's task performance was also previously studied by other authors [10, 11], in this study, analyses were conducted in order to investigate if the gaze position in the horizontal and vertical directions and standard deviation of gaze position in both directions were associated with fluctuations in subject's task performance, considering also time segments defined from -500 or -1000 ms prior to stimulus presentation. Indeed, both the studies of Recarte et al. [10] and He et al. [11] have concluded that variations on horizontal gaze position were linked with fluctuations in subject's attention levels.

Similarly with the above measures, both group and individual analyses were performed for gaze position measures.

3.3.2.1 Group Comparisons

Gaze position in the horizontal (X) and vertical direction (Y) - $Gaze Pos_X$ and $Gaze Pos_Y$ - and also standard deviation of gaze position in X and Y direction - $Std Gaze Pos_X$ and $Std Gaze Pos_Y$ - considering both the prestimulus time windows of 500 and 1000 ms time length were compared between conditions RT_{Q1} , RT_{Q2} , RT_{Q3} and RT_{Q4} . The statistical results for each one of those measures are in table 3.6. It can be observed that none of the gaze position measures analysed showed a statistically significant difference among conditions ($p-value > 0,05$; Repeated Measures ANOVA; two-tailed).

Table 3.6: Group analysis p -values for gaze position measures, considering 500 ms and 1000 ms prestimulus windows and comparisons between conditions RT_{Q1} , RT_{Q2} , RT_{Q3} and RT_{Q4} .

Type of Measure	p -value 4 conditions
$Gaze Pos_X$ 500 ms	0,728
$Gaze Pos_X$ 1000 ms	0,721
$Gaze Pos_Y$ 500 ms	0,460
$Gaze Pos_Y$ 1000 ms	0,421
$Std Gaze Pos_X$ 500 ms	0,657
$Std Gaze Pos_X$ 1000 ms	0,513
$Std Gaze Pos_Y$ 500 ms	0,487
$Std Gaze Pos_Y$ 1000 ms	0,712

In the figures 3.11 and 3.12 are the graphical representations of the mean values across subjects obtained for each condition, for gaze position in the horizontal and vertical directions ($Gaze Pos_X$ and $Gaze Pos_Y$); and for standard deviation of gaze position in both directions ($Std Gaze Pos_X$ and $Std Gaze Pos_Y$), respectively.

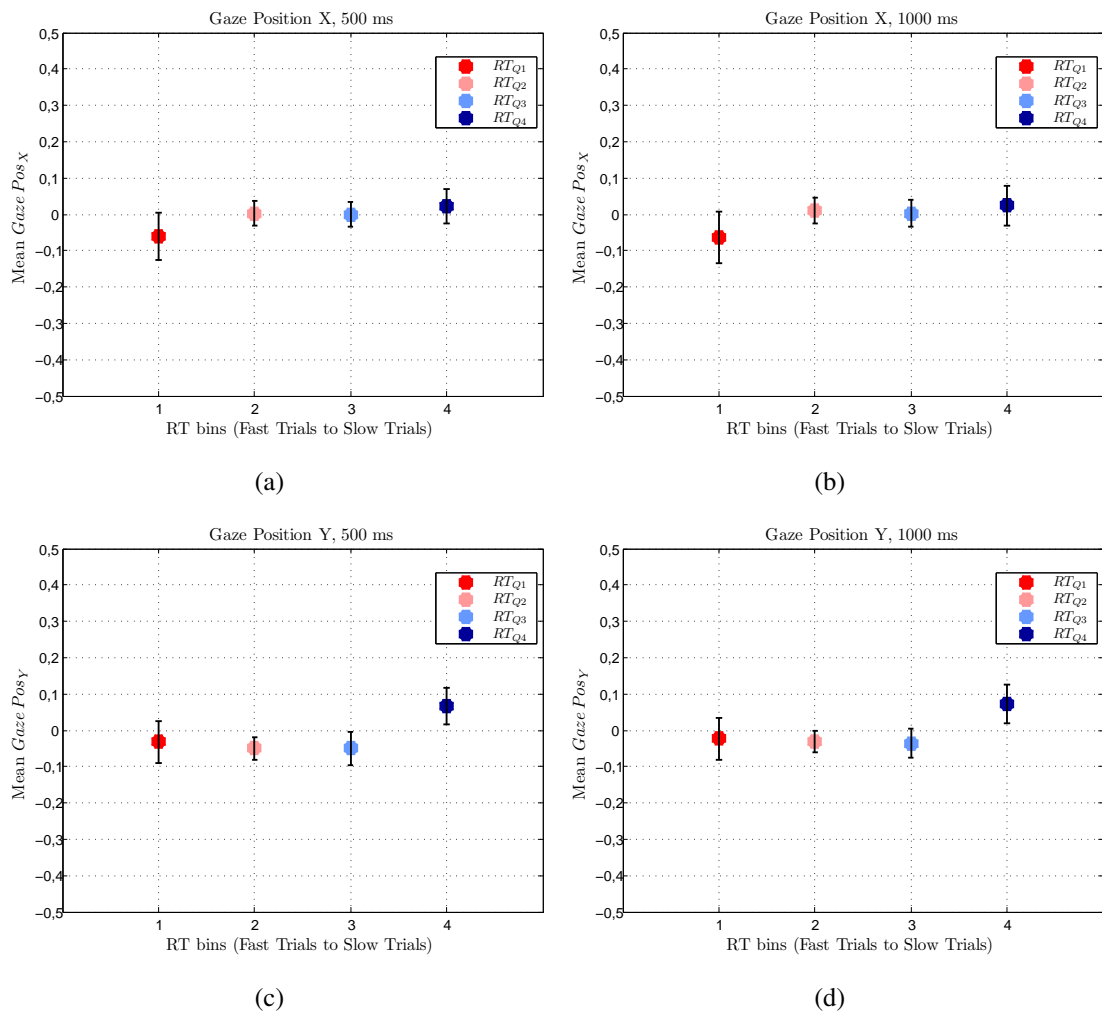


Figure 3.11: Graphical representations of mean values for gaze position regarding the (a) and (b) X and (c) and (d) Y directions across subjects, for each RT bin and for 500 ms and 1000 ms prestimulus windows, considering the group analysis. Gaze position values are in *z-score* units. Graphics (a) and (c) correspond to the 500 ms prestimulus, whereas (b) and (d) to 1000 ms prestimulus time windows. RT_{Q1} and RT_{Q4} represent fast and slow trials, respectively. Error bars represent standard errors.

Visually inspecting, these results revealed differences among conditions for some of the measures considered. However, those differences did not reach the significance level of 0,05 for both the prestimulus windows of 500 and 1000 ms time length, as it can be confirmed by the statistical results obtained (table 3.6). Indeed, for gaze position measures, and comparing the values obtained for the two conditions more extreme - RT_{Q1} and RT_{Q4} , which represent fast and slow trials, respectively - the graphics of the figure 3.11 reveal a deviation of the gaze position relatively to the screen centre in the negative direction of both the axis (X and Y) for fast trials, contrasting with the direction of the

deviation obtained for slow trials, which was positive. Visually, differences are not found between the two intermediate conditions (RT_{Q2} and RT_{Q3}), for gaze position in both the horizontal and vertical directions.

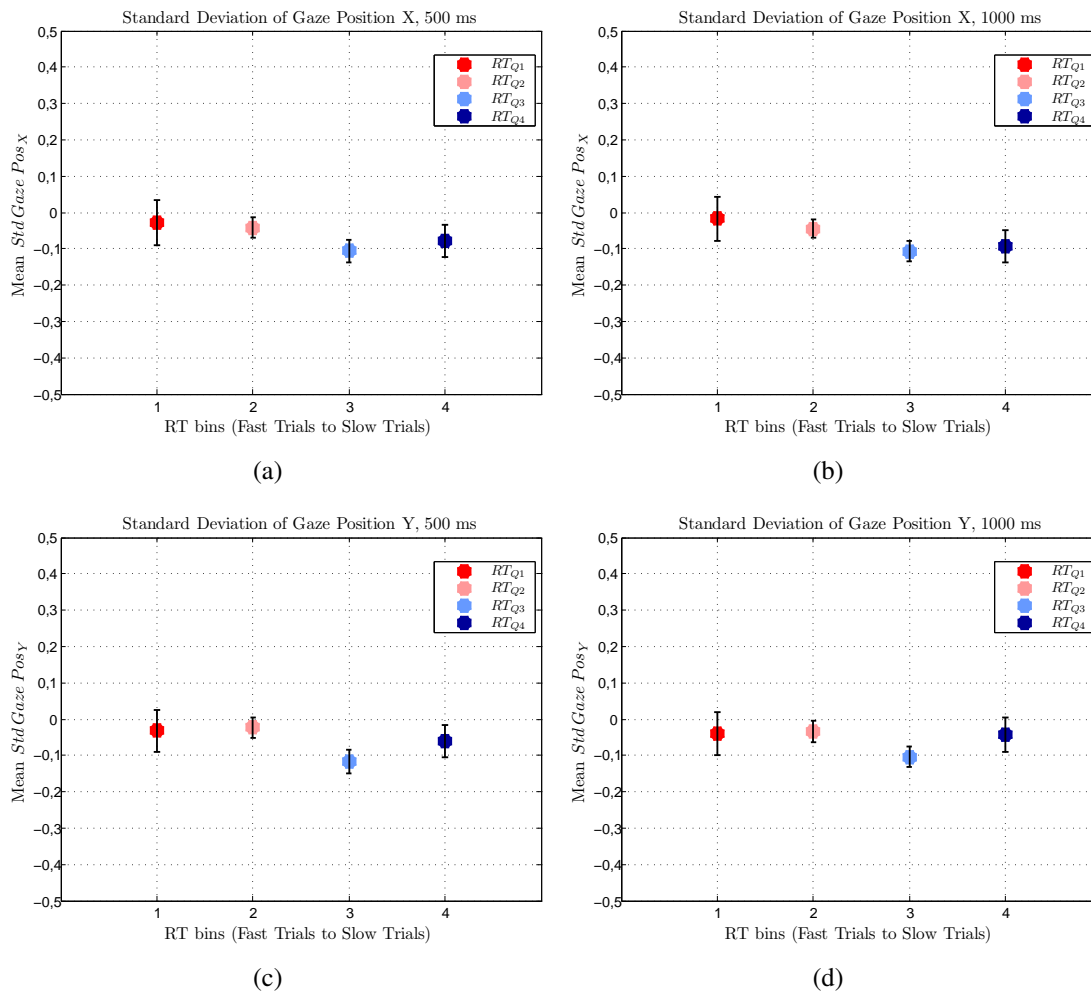


Figure 3.12: Graphical representations of mean values for standard deviation of gaze position in z -score units relatively to (a) and (b) X and (c) and (d) Y directions across subjects, for each RT bin and for 500 ms and 1000 ms prestimulus windows. Error bars represent standard errors.

Regarding the standard deviation of gaze position measures for X and Y directions (figure 3.12), none defined pattern was observed for both prestimulus time windows, suggesting that there is no relation between prestimulus standard deviation of gaze position and RT values.

Globally, it can be concluded that none of the gaze position measures studied above predicted fluctuations in the subject's attention levels, on the group analysis level.

3.3.2.2 Individual Comparisons

Also individual comparisons were made among the conditions RT_{Q1} , RT_{Q2} , RT_{Q3} and RT_{Q4} , ranging from fast to slow trials, in order to determine whether gaze position measures could be used to predict an attention lapse, specifically for each subject. The tables 3.7, 3.8, 3.9 and 3.10 are about the individual results obtained for the gaze position in the horizontal and vertical directions, and standard deviation of gaze position in these two directions, respectively. The tables regarding the gaze position measures, in addition to the *p-value* obtained for the Kruskal Wallis test, also comprise the mean values across trials of the gaze deviation relatively to the screen centre for the two more extreme conditions - RT_{Q1} and RT_{Q4} , which represent fast and slow trials respectively - in order to assess the direction of the gaze deviation during each prestimulus period when each subject has responded faster and slower, accordingly. For the two remaining tables, which correspond to the results obtained for the standard deviation of gaze position measures, additionally to the *p-value* obtained for the Kruskal Wallis test, it is also showed the result of the subtraction between the mean value across trials for fast (RT_{Q1}) and slow trials (RT_{Q4}), for each subject. The results obtained by taking $RT_{Q1} - RT_{Q4}$ are also provided, in order to assess how RT values relate to the variability of the prestimulus gaze position across time.

Taking into account the results obtained for gaze position in the horizontal direction (table 3.7), for both prestimulus time windows, the tendency of horizontal gaze position's deviation relatively to the screen centre with RT values is highly variable from subject to subject, by comparing the mean values regarding the two more extreme conditions (fast and slow trials). Indeed, no defined pattern could be observed in terms of the prestimulus deviation's direction of the gaze position when subjects responded faster relatively when they responded slower. Some subjects shifted more their gaze towards the right relatively to the screen centre for fast trials in comparison with slow trials; whereas others revealed the same tendency between those two conditions (an increased deviation for fast trials than slow trials), but towards the left direction. Additionally, there were also subjects which have shifted more the gaze towards the right for slow trials in comparison with fast trials condition. Moreover, it was also observed the case in which subjects deviated the gaze in different directions for slow or fast trials. These results are controversial relatively to those obtained in the group analysis, because significant differences were not found between conditions as an effect of group. Indeed, a higher number of subjects revealed a significant difference between the four conditions, comparing with the results obtained in the individual analysis for the prestimulus pupil diameter (see table 3.4, in point 3.3.1.2). However, an effect of group was observed for pupil diameter and not for horizontal gaze position. Possibly, those discrepancies between the individual and group

Table 3.7: Individual comparisons for gaze position values relatively to the horizontal direction, considering 500 ms and 1000 ms prestimulus time windows. Numbers in bold indicate values associated with statistically significant differences among the four conditions at the 0,05 level (two-tailed). *Gaze Pos_X*: Mean gaze position in the horizontal direction relatively to the screen centre across each prestimulus time window (500 ms or 1000 ms prior to stimulus onset). px: pixels.

Subject	Gaze Position X, <i>Gaze Pos_X</i>					
	500 ms			1000 ms		
	<i>p</i> -value Kruskal Wallis	<i>RT</i> _{Q1} (px)	<i>RT</i> _{Q4} (px)	<i>p</i> -value Kruskal Wallis	<i>RT</i> _{Q1} (px)	<i>RT</i> _{Q4} (px)
1	0,477	2,208	-15,337	0,322	0,161	-15,502
2	0,103	0,861	-6,195	0,080	-0,016	-6,830
3	0,718	11,059	9,826	0,376	11,549	7,961
4	0,092	144,146	256,476	0,013	129,643	266,772
5	0,951	-69,037	-72,065	0,576	-63,843	-73,700
6	0,000	156,994	71,464	0,000	163,579	78,750
7	0,271	64,303	37,757	0,106	64,384	36,957
8	0,000	-163,820	-41,513	0,000	-165,748	-43,017
9	0,219	3,762	5,584	0,243	4,198	6,209
10	0,402	-70,078	-67,863	0,429	-73,189	-71,693
11	0,604	-1,051	-3,437	0,626	-1,314	-3,461
12	0,004	35,904	7,740	0,001	41,111	8,575
13	0,211	12,868	96,102	0,181	5,039	105,346
14	0,003	48,178	-13,225	0,001	48,016	-15,073
15	0,112	-6,616	-0,045	0,027	-7,805	1,770
16	0,000	-25,806	-6,225	0,000	-25,170	-7,403
17	0,000	14,935	51,240	0,000	15,809	52,344
18	0,007	37,573	69,459	0,000	35,074	72,857
19	0,199	-61,927	51,869	0,167	-70,620	49,433
20	0,091	66,993	182,938	0,011	60,445	190,651

analysis were due to the highly variable results obtained from subject to subject relatively to the tendency of horizontal deviation direction of the gaze position relatively to the screen centre with RT values.

Considering the gaze position in the vertical direction (table 3.8), similarly to the horizontal gaze position analysis, subjects revealed controversial results for the tendency of the gaze deviation's direction with RT values, for both time windows. Indeed, some subjects looked further up relatively to the screen centre for fast than slow trials; whereas one single subject looked further up for slow trials than fast trials condition for both prestimulus time windows. Moreover, differently from those subjects, it was observed also the case in which subjects have looked further down for fast than slow trials. Additionally, one single subject shifted their gaze in opposite directions for fast or slow trials conditions, also for both prestimulus time windows. Indeed, taking into account the number of subjects which demonstrated significant differences for the vertical gaze position among

Table 3.8: Individual comparisons for gaze position values relatively to the vertical direction, considering 500 ms and 1000 ms time windows. Numbers in bold indicate values associated with statistically significant differences among the four conditions at the 0,05 level (two-tailed). *Gaze Pos_y*: Mean gaze position in the vertical direction relatively to the screen centre across each prestimulus time window (500 ms or 1000 ms prior to stimulus onset). px: pixels.

Subject	Gaze Position Y, <i>Gaze Pos_y</i>					
	500 ms			1000 ms		
	<i>p</i> -value Kruskal Wallis	<i>RT</i> _{Q1} (px)	<i>RT</i> _{Q4} (px)	<i>p</i> -value Kruskal Wallis	<i>RT</i> _{Q1} (mm)	<i>RT</i> _{Q4} (px)
1	0,058	-2,670	11,718	0,078	0,012	10,538
2	0,449	20,141	28,534	0,219	20,002	29,427
3	0,835	8,278	7,095	0,811	7,241	7,207
4	0,140	93,014	116,652	0,132	89,068	114,330
5	0,641	76,468	92,654	0,370	78,384	94,963
6	0,002	-154,368	-67,476	0,002	-164,906	-74,017
7	0,068	-64,497	-42,063	0,038	-65,095	-41,498
8	0,000	103,780	26,338	0,000	102,097	27,237
9	0,430	12,851	13,770	0,326	12,394	12,910
10	0,826	-110,615	-160,409	0,678	-96,815	-165,087
11	0,480	-3,380	0,278	0,316	-3,999	1,238
12	0,000	-16,793	5,447	0,000	-18,106	5,874
13	0,014	36,998	99,300	0,004	30,563	101,153
14	0,075	60,723	36,460	0,033	58,622	38,970
15	0,627	25,264	27,082	0,646	25,564	26,326
16	0,194	11,138	25,622	0,095	11,831	33,012
17	0,000	22,106	2,283	0,000	21,966	1,555
18	0,576	-69,931	-83,368	0,472	-64,867	-82,438
19	0,445	57,830	17,475	0,281	90,593	27,712
20	0,839	1,194	1,593	0,359	-5,244	-1,934

conditions, similarly with the previous analysis about the horizontal gaze position, the results obtained for the individual comparisons were discrepant relatively to those obtained in the group analysis. Approximately the same number of subjects has revealed significant differences for the individual analysis in comparison with pupil diameter (see table 3.4, in point 3.3.1.2), but an effect of group was also not verified relatively to vertical gaze position. Probably, the discrepancies for the tendency of the gaze deviation's direction with RT values which were observed among subjects were responsible for an effect of group was not obtained for this measure.

Relatively to the standard deviation of gaze position in the horizontal direction, taking into account the results of the table 3.9, controversial results were also obtained from subject to subject, relatively to how RT values related to standard gaze position in horizontal direction. Indeed, the gaze position in this direction has varied more before fast than slow trials, for five and four subjects, for the prestimulus time windows of 500 and 1000 ms

Table 3.9: Individual comparisons for standard deviation of gaze position values relatively to the horizontal direction, considering 500 ms and 1000 ms time windows. Numbers in bold indicate values associated with statistically significant differences among the four conditions at the 0,05 level (two-tailed). *Std Gaze Pos_X*: Standard deviation of horizontal gaze position relatively to the screen centre across each prestimulus time window (500 ms or 1000 ms prior to stimulus onset). px: pixels.

Subject	Standard Deviation of Gaze Position X, <i>Std Gaze Pos_X</i>			
	500 ms		1000 ms	
	<i>p-value</i> Kruskal Wallis	$RT_{Q1} - RT_{Q4}$ (px)	<i>p-value</i> Kruskal Wallis	$RT_{Q1} - RT_{Q4}$ (px)
1	0,006	-9,585	0,034	-10,069
2	0,669	-0,001	0,537	-1,065
3	0,063	-0,906	0,272	-1,366
4	0,540	-22,877	0,653	-17,516
5	0,741	-6,348	0,482	4,227
6	0,248	32,095	0,298	33,317
7	0,266	0,682	0,565	-0,282
8	0,000	17,435	0,001	17,690
9	0,758	-0,639	0,744	-0,404
10	0,732	-20,848	0,427	-24,039
11	0,575	0,731	0,053	1,615
12	0,029	4,772	0,040	7,013
13	0,558	28,532	0,502	29,605
14	0,000	99,640	0,000	103,840
15	0,208	-3,512	0,437	-2,724
16	0,746	-0,118	0,178	-4,206
17	0,001	-28,419	0,000	-27,680
18	0,000	-14,694	0,000	-15,897
19	0,006	103,516	0,057	79,649
20	0,006	42,371	0,000	54,802

time length, respectively. The opposite pattern was observed for three subjects for both prestimulus time windows. In similarity with the previous two analyses regarding the gaze position in the horizontal and vertical directions, significant differences were not found for the group analysis, despite the number of subjects which demonstrated a significant difference among conditions for the individual analysis was higher relatively to pupil diameter analysis (see table 3.4, in point 3.3.1.2). Possibly, the discrepant results observed between subjects have contributed for different results were obtained for individual and group analysis.

Taking into account the results obtained for the individual analysis of standard deviation of gaze position in the vertical direction (table 3.10), there were also subjects which revealed a higher variability for the vertical gaze position for slow trials than fast trials; whereas others showed the opposite pattern. Probably, as with all the other gaze position measures, an effect of group was not observed due to those controversial results between

subjects.

Table 3.10: Individual comparisons for standard deviation of gaze position values relatively to the vertical direction, considering 500 ms and 1000 ms time windows. Numbers in bold indicate values associated with statistically significant differences at the 0,05 level (two-tailed). *Std Gaze Pos_y*: Standard deviation of vertical gaze position relatively to the screen centre across each prestimulus time window (500 ms or 1000 ms prior to stimulus onset). px: pixels.

Subject	Standard Deviation of Gaze Position Y, <i>Std Gaze Pos_y</i>			
	500 ms		1000 ms	
	<i>p</i> -value Kruskal Wallis	$RT_{Q1} - RT_{Q4}$ (px)	<i>p</i> -value Kruskal Wallis	$RT_{Q1} - RT_{Q4}$ (px)
1	0,029	-4,167	0,127	-3,239
2	0,131	0,385	0,608	0,318
3	0,843	-0,246	0,267	-0,839
4	0,457	-4,015	0,903	-1,011
5	0,857	0,262	0,460	6,619
6	0,251	35,220	0,512	34,904
7	0,350	0,814	0,973	0,240
8	0,000	15,635	0,000	16,738
9	0,867	-0,104	0,474	-0,180
10	0,432	-19,013	0,362	-11,985
11	0,398	0,247	0,047	-0,205
12	0,247	-0,786	0,501	-3,587
13	0,745	-9,352	0,389	-5,744
14	0,000	57,770	0,000	62,157
15	0,819	-1,312	0,188	-1,240
16	0,230	-18,216	0,005	-26,441
17	0,001	-23,974	0,000	-24,965
18	0,005	-24,595	0,000	-32,853
19	0,019	36,519	0,159	22,135
20	0,066	21,497	0,043	17,456

3.4 Classifiers

3.4.1 Simple Classifiers

As it was referred before, one of the main objectives of this work was to develop a classifier specific for each subject, based on the EEG and eye activity features explored above, which could be able to predict attention lapses. Several procedures were taken into account in order to optimize as much as possible each type of classifier developed for each participant of the study. Therefore, because some of the patterns explored in the above statistical analyses showed to be good predictors of fluctuations in attention, three types of unimodal/simple classifiers were developed based on the eye parameters previously

explored, alpha amplitude and temporal phase stability for the beta frequency range measures. As this frequency band was the one which ensured the strongest statistical results in the statistical analyses about phase coherence performed before, other frequency ranges were not considered, in order to avoid the curse-of-dimensionality problem. Three types of classification algorithms were also explored for each one of the three simple classifiers developed - Linear SVM; RBF SVM and KNN - in order to determine the one which ensured the best classification rate in the cross-validation.

Regarding the results obtained for the several types of simple classifiers developed for each subject, in tables 3.11 and 3.12 are the best classification algorithm for each classifier, based on the 5-folds cross-validation method applied; and the accuracy values obtained both in the cross-validation and for the test with the $\sim 10\%$ of the whole data set aside initially, respectively.

By evaluating the results of the table 3.11, the classification algorithm most frequently considered the best across subjects for the classifiers “Eye Parameters (500 ms)”; “Eye Parameters (1000 ms)”; “Alpha Amplitude (500 ms)”; “Alpha Amplitude (1000 ms)” and “Temporal Phase Stability (500 ms)”; are the KNN; KNN; RBF SVM; RBF SVM; and KNN, respectively. The most frequently occurring algorithm among these latter is the KNN.

Table 3.11: Best classification algorithm for each type of unimodal classifier developed, considering each subject individually. Note that it was selected based on the values obtained in the cross-validation method. The names in bold indicate the classification algorithms most frequently considered the best across subjects.

Type of classifier		Eye Parameters		Alpha Amplitude		Temporal Phase Stability
		500 ms	1000 ms	500 ms	1000 ms	500 ms
Subject	1	KNN	KNN	KNN	RBF SVM	KNN
	2	RBF SVM	Linear SVM	KNN	KNN	KNN
	3	KNN	KNN	KNN	RBF SVM	KNN
	4	Linear SVM	KNN	-	-	-
	5	RBF SVM	RBF SVM	KNN	RBF SVM	RBF SVM
	6	KNN	RBF SVM	RBF SVM	RBF SVM	KNN
	7	RBF SVM	RBF SVM	RBF SVM	KNN	RBF SVM
	8	Linear SVM	KNN	RBF SVM	RBF SVM	RBF SVM
	9	RBF SVM	KNN	Linear SVM	RBF SVM	KNN
	10	KNN	KNN	RBF SVM	KNN	KNN
	11	KNN	KNN	KNN	KNN	KNN
	12	RBF SVM	KNN	RBF SVM	Linear SVM	KNN
	13	KNN	Linear SVM	RBF SVM	KNN	KNN
	14	RBF SVM	Linear SVM	RBF SVM	RBF SVM	RBF SVM
	15	KNN	RBF SVM	RBF SVM	KNN	KNN
	16	RBF SVM	KNN	RBF SVM	RBF SVM	RBF SVM
	17	KNN	KNN	RBF SVM	KNN	KNN
	18	KNN	RBF SVM	RBF SVM	RBF SVM	RBF SVM
	19	RBF SVM	RBF SVM	-	-	-
	20	Linear SVM	KNN	KNN	Linear SVM	RBF SVM
Most Frequently		KNN	KNN	RBF SVM	RBF SVM	KNN

Considering the accuracy measures evaluated in this study, the 5-folds cross-validation method should reveal approximately the same results for the classification rate or, eventually, slightly better values than in the test stage with the $\sim 10\%$ of the whole data set “unseen” by the classifier. Indeed, and extrapolating for this specific study, the classification algorithms and corresponding parameters were adjusted only for 90% of the data in the cross-validation, and not for the portion selected to test each classifier, which supposedly contributes to obtain worse results in the test stage. However, if the value obtained for the test with the new set of instances was much higher relatively to the value returned by the cross-validation method, it means that “good” examples for discriminating between the two classes were chosen by chance at the beginning of the classification task. Therefore, both accuracy values (regarding the cross-validation method and the test with the $\sim 10\%$ of the data completely “unknown” by the classifier) were taken into account in the interpretation of the results presented in table 3.12. Globally, comparing the mean accuracy values obtained in the cross-validation method and in the test stage, for each classifier in specific, differences were not observed on average for the five unimodal classifiers evaluated.

A parametric t-test was performed in order to assess if there were statistically significant differences between the accuracy values achieved by each unimodal classifier for both the cross-validation method and test stage (table 3.13). All variables showed to be normally distributed, according with the Shapiro Wilk Normality Test ($p\text{-value} > 0,05$). It can be seen that the classifiers regarding the eye parameters ensured significantly better performance rates in comparison with EEG-based classifiers (see tables 3.12 and 3.13).

Only one subject showed an accuracy value for the cross-validation method higher than 70% (eye parameters classifiers - subject 12). Taking into account the accuracy values obtained in the test stage, seven subjects revealed values higher than 70%, considering all the unimodal classifiers analysed. Although, it is important to emphasize that the accuracy values of subjects 7 and 8 are the values which more deviate from the accuracies obtained in the cross-validation, showing higher values for the test stage in comparison with the latter metric, among those for each classifier considered - “Eye Parameters (500 ms)” for subject 7; and “Eye Parameters (1000 ms)”, for subject 8. This result suggests that, possibly, for those subjects and classifiers, “good” examples for discriminating between the two classes were chosen by chance at the beginning of the classification task.

3.4.2 Hybrid Classifiers

Several recent studies have reported success in applying hybrid procedures [105], mainly by fusing the recognition results at the decision-level based on the outputs of separate unimodal classifiers (decision-level fusion technique). Thus, hybrid classifiers were also developed taking into account the output labels given by the three types of unimodal classifiers developed.

In table 3.14 are presented the combination of classification algorithms that gave the best accuracy values for each subject after combining the output labels given for the three separate classifiers, regarding the $\sim 10\%$ of data set aside at the beginning of the classification task.

Table 3.14: Combination of classification algorithms that gave the best accuracy values for each subject. Each combination was selected based on the best classification accuracy obtained by combining the results at the decision-level based on the outputs of the three separate classifiers for the $\sim 10\%$ of the data set aside at the beginning. When is presented only one name it means that the best classification rate was obtained by implementing the same classification algorithm for the three classifiers. The names in bold indicate the most frequently occurring combination of algorithms among the best across subjects.

Combination of Classifiers	1. Eye Parameters (500 ms) + Alpha Amplitude (500 ms) + Temporal Phase Stability (500 ms)	2. Eye Parameters (500 ms) + Alpha Amplitude (1000 ms) + Temporal Phase Stability (500 ms)	3. Eye Parameters (1000 ms) + Alpha Amplitude (500 ms) + Temporal Phase Stability (500 ms)	4. Eye Parameters (1000 ms) + Alpha Amplitude (1000 ms) + Temporal Phase Stability (500 ms)	
Subject	1	RBF SVM	Linear SVM + KNN + RBF SVM	KNN + Linear SVM + RBF SVM	KNN + RBF SVM + RBF SVM
	2	KNN	KNN	Linear SVM	KNN
	3	RBF SVM	RBF SVM	Linear SVM	Linear SVM
	5	KNN	KNN + RBF SVM + RBF SVM	RBF SVM	RBF SVM
	6	RBF SVM	RBF SVM + Linear SVM + KNN	KNN	KNN
	7	KNN	Linear SVM	RBF SVM	KNN + RBF SVM + Linear SVM
	8	RBF SVM	RBF SVM	KNN + Linear SVM + Linear SVM	Linear SVM
	9	KNN + Linear SVM + KNN	KNN + RBF SVM + KNN	Linear SVM	KNN
	10	KNN	KNN	KNN	KNN + Linear SVM + KNN
	11	RBF SVM	RBF SVM	Linear SVM	KNN
	12	RBF SVM	KNN + RBF SVM + RBF SVM	KNN + KNN + RBF SVM	KNN
	13	KNN	RBF SVM	RBF SVM + KNN + KNN	RBF SVM + Linear SVM + KNN
	14	Linear SVM	Linear SVM + RBF SVM + KNN	KNN	KNN
	15	RBF SVM	RBF SVM + KNN + KNN	RBF SVM + KNN + KNN	KNN
	16	RBF SVM	Linear SVM	KNN	KNN
	17	RBF SVM + RBF SVM + KNN	RBF SVM	KNN + RBF SVM + KNN	KNN
	18	KNN	KNN	Linear SVM	Linear SVM
	20	KNN	KNN + RBF SVM + KNN	RBF SVM	RBF SVM
	Most Frequently	RBF SVM	RBF SVM	Linear SVM	KNN

It can be observed that, for the best combination of classification algorithms, that

RBF SVM is the algorithm that gives the best accuracy across subjects for the hybrid classifiers numbers 1. and 2. of the table 3.14. For the remaining classifiers (numbers 3. and 4. of the table 3.14) Linear SVM and KNN are the classification algorithms applied to each unimodal classifier which ensured the best accuracy in the hybrid classification, respectively.

In table 3.15 are the corresponding accuracy values of the four hybrid classifiers developed.

Table 3.15: Accuracy values for the hybrid classifiers developed for each subject and considering the combination of algorithms of the table 3.14. Accuracy Values 10%: accuracy values regarding the test with the ~10% of data “unknown” by the classifier. The numbers in bold indicate the best accuracy value obtained for each subject. Std. Deviation: standard deviation.

Combination of Classifiers		Accuracy Values 10% (%)				
		1. Eye Parameters (500 ms) + Alpha Amplitude (500 ms) + Temporal Phase Stability (500 ms)	2. Eye Parameters (500 ms) + Alpha Amplitude (1000 ms) + Temporal Phase Stability (500 ms)	3. Eye Parameters (1000 ms) + Alpha Amplitude (500 ms) + Temporal Phase Stability (500 ms)	4. Eye Parameters (1000 ms) + Alpha Amplitude (1000 ms) + Temporal Phase Stability (500 ms)	
Subject	1	36,364	45,455	50,000	50,000	
	2	59,091	68,182	59,091	63,636	
	3	45,455	50,000	59,091	59,091	
	5	61,111	66,667	61,111	72,222	
	6	59,091	68,182	54,545	45,455	
	7	77,273	68,182	68,182	68,182	
	8	40,909	59,091	54,545	54,545	
	9	59,091	54,545	59,091	54,545	
	10	61,111	55,556	72,222	55,556	
	11	45,455	54,545	45,455	45,455	
	12	55,556	88,889	61,111	66,667	
	13	71,429	71,429	71,429	71,429	
	14	50,000	54,545	50,000	50,000	
	15	50,000	72,727	50,000	59,091	
	16	59,091	59,091	59,091	54,545	
	17	68,182	68,182	72,727	77,273	
	18	59,091	54,545	54,545	59,091	
	20	66,667	61,111	66,667	61,111	
	Mean ± Std. Deviation		56,942 ± 10,696	62,274 ± 10,289	59,384 ± 8,236	59,327 ± 9,174

Globally, taking into account the accuracies obtained for the hybrid classification approach (table 3.15), the classifier which ensured the highest mean accuracy across subjects was the “Eye Parameters (500 ms) + Alpha Amplitude (1000 ms) + Temporal Phase Stability (500 ms)” classifier. In table 3.16 are presented the results obtained in the t-test which was conducted in order to assess if there were significant differences for the accuracy values obtained in the test stage for each unimodal classifier versus each hybrid classifier developed. A parametric test was performed because all the variables showed to

be normally distributed, according with the Shapiro Wilk Normality test ($p\text{-value}>0,05$; two-tailed).

Table 3.16: $p\text{-values}$ for the paired t-test conducted in order to compare the accuracy values obtained in the test stage using each unimodal classifier and each hybrid classifier developed. Numbers in bold indicate values associated with statistically significant differences for the accuracy values for each combination of unimodal classifier versus hybrid classifier at the 0,05 level (two-tailed).

$p\text{-values}$ paired t-test X	1.Eye Parameters (500 ms) + Alpha Amplitude (500 ms) + Temporal Phase Stability (500 ms)	2.Eye Parameters (500 ms) + Alpha Amplitude (1000 ms) + Temporal Phase Stability (500 ms)	3.Eye Parameters (1000 ms) + Alpha Amplitude (500 ms) + Temporal Phase Stability (500 ms)	4.Eye Parameters (1000 ms) + Alpha Amplitude (1000 ms) + Temporal Phase Stability (500 ms)
Eye Parameters 500 ms	0,175	0,949	0,367	0,385
Eye Parameters 1000 ms	0,068	0,982	0,308	0,374
Alpha Amplitude 500 ms	0,028	0,008	0,007	0,028
Alpha Amplitude 1000 ms	0,020	0,001	0,000	0,001
Temporal Phase Stability 500 ms	0,114	0,001	0,014	0,008

Despite a higher mean accuracy value was obtained for the second classifier of the table 3.15 (hybrid classifier number 2.) in comparison with the eye parameters classifier for the 500 ms prestimulus time window, a statistically significant difference was not found comparing the results obtained with both the classifiers. Significant differences were also not found between both the eye parameters classifiers and the remaining three hybrid classifiers (numbers 1., 3. and 4. of the table 3.15). There was not a significant improvement in the accuracy of hybrid in comparison with eye unimodal classifiers (see tables 3.12 and 3.15). These results lead to the conclusion that the combination of eye parameters with EEG measures did not significantly improve the classification rate in comparison with the accuracy values achieved by the simple classifiers based on eye activity features. However, significant differences were found for the majority of the combinations between hybrid classifiers versus EEG-based unimodal classifiers (see table 3.16), and higher mean accuracy values were obtained for all the hybrid classifiers developed in comparison with all the unimodal classifiers based on features extracted from EEG signals (see tables 3.12 and 3.15). All these results suggest that the features extracted from the EEG signals could be more noisy and not so good at predicting attention lapses in comparison with eye activity parameters.

Concluding, hybrid classifiers did not significantly improve classification accuracy in comparison with the simple/unimodal classifiers based on eye parameters. However, fusing the outputs given by the three types of unimodal classifiers significantly improved the classification rate relatively to the results obtained with the simple classifiers based on

EEG features. Thus, unimodal classifiers using eye parameters achieved the best accuracy results, not improved by the using of hybrid classifiers.

Chapter 4

Discussion and Conclusions

The main objective of this work was to study fluctuations in task performance, measured as moment-to-moment differences in the response RT to the source stimuli in a choice reaction time task, and to identify patterns in brain and eye activity which could be able to predict those fluctuations. RT variability has been attributed to periodic lapses in attention by several authors, being implemented as an indirect measure of fluctuations in attention levels, specially in studies about the neural correlates of the intra-individual RT variability in ADHD patients [112]. According to several authors, intra-individual behavioural variability refers to moment-to-moment (within subjects) fluctuations in behaviour and task performance during a period of seconds to minutes [112]. Subjects revealed intra-individual inconsistency in the speed of responding to each stimulus during the task. However, not all of the brain and eye activity patterns which were studied here and which have been considered good predictors of attention lapses were able to predict transient fluctuations in performance. In fact, only synchrony in higher frequency bands (beta and gamma) and pupil diameter measurements were capable to predict fluctuations in task performance, according with the results obtained in this study. Alpha amplitude and gaze position did not prove to be reliable predictors of those fluctuations.

In the following paragraphs the main findings of the present work are discussed and confronted with those obtained in previous studies.

Prestimulus Alpha Amplitude Predicted Task Performance For Some Subjects, but Not for the Whole Group

Although prestimulus alpha amplitude within the parietal/parieto-occipital/occipital area was not capable to predict fluctuations in performance for the whole group, it could predict attention fluctuations in a small number of participants (see subsections 3.2.1.1 and 3.2.1.2 in chapter 3, for the results obtained in the group and individual comparisons,

respectively). This finding suggests that, possibly, posterior increased alpha amplitude, makes it hard to maintain visual attention levels, for those subjects.

The negative influence of prestimulus alpha amplitude in subject's visual attention was highlighted in previous works, such as the studies of Van Dijk et al. [2], Hanslmayr et al. [35] and Ergenoglu et al. [69], in which barely visible stimulus were used to study visual attention, through visual discrimination ability. Moments of high alpha amplitude were associated with reduced visual discrimination abilities. The findings reported by these studies provide evidence that alpha activity reflects inhibition, suggesting that lapses in attention could be associated with brain states characterized by high amplitude of posterior alpha oscillations. However, in this work, contrasting with the results obtained in all these studies, a significant difference was not found for prestimulus alpha amplitude between different attention states for the group analysis. Several factors could have contributed for this group effect not being observed. Differently from the present study, the criterion adopted by the above authors to distinguish different states of attention, was based on the detection of a specific stimulus and not considering the response RT values. As was referred before, it is common in this type of studies to employ barely visible stimuli, to which subjects have difficulty to perceive, in order to study lapses in attention. However, the task designed for this work was simple enough for subjects to detect the stimulus in the majority of trials. Possibly, if a less visible stimulus was used, the hit's rate could be used as criterion instead of the response RT, which, according to Van Dijk et al. [2], is not a reliable parameter to assess changes on prestimulus alpha amplitude, and an effect of group could be observed between this latter measure and fluctuations in attention. However, the main objective of the present work was to study if a different type of visual paradigm relatively to the ones already implemented on other studies, could induce fluctuations in task performance, and if they could be predicted by alpha amplitude measurements. Another possible explanation for not finding significant differences between prestimulus alpha amplitude and different states of attention, was the number of trials and/or subjects considered in this analysis, which were probably not large enough to observe this group effect. For example, in their study, Van Dijk et al. [2] ensured that they had at least ~ 130 trials per condition (detected versus undetected stimuli) before artifact removal, for each subject. Ergenoglu et al. [69] considered for analysis ~ 74 trials per condition (perceived versus unperceived trials) after artifact rejection. In this study only ~ 50 trials were used for each one of the four conditions regarding the EEG analyses. Additionally, 35 subjects participated in the study of Hanslmayr et al. [35]; whereas only 18 subjects were considered for EEG analyses in this study. However, it is always important to take into account the inter-subjects variability, which can contribute to obtain inconclusive results regarding the whole group.

In conclusion, this study suggests that the influence of alpha is not detectable when studying differences in RT. However, this seems to vary from subject to subject.

EEG Phase Coherence Between Electrodes/Functional Connectivity Between Brain Areas: Reliable Patterns for Predicting Attention Lapses

One of the main conclusions of this study, regarding the results obtained for the phase coherence group analysis, is that fast responses were linked with increased prestimulus EEG phase coherence in the beta and gamma frequency bands, leading to a better task performance; whereas the opposite pattern was observed for the alpha frequency band (see subsection 3.2.2.1, in chapter 3). These results are in accordance with those obtained by Hanslmayr et al. [35].

The results obtained in this analysis led to the conclusion that increased phase coherence in higher frequency ranges (>20 Hz) reflects states of enhanced attention, which guide visual performance. Indeed, other authors have also concluded that stimulus-induced phase coupling in higher frequency ranges (>15 Hz) is related to perception and binding processes [113, 114], and might indicate the state of attention or expectation. Taking into account the topographical representation of the results obtained here for the phase coherence analysis, mainly fronto-parietal electrode pairs contributed to task performance improvements with increasing prestimulus phase coherence, regarding the beta and gamma frequency bands. Similarly, Gross et al. [113] have concluded that frontal, temporal, and parietal areas play a major role in the attentional control of visual processing, and that communication within the frontal-parieto-temporal attentional network proceeds via transient long-range phase synchronization in the beta frequency band. In their study, they conducted a dual-target task while acquiring MEG signals, in which two visual targets were embedded in streams of distractor letters, being the targets separated in time by a single distractor. This condition is known to lead to a well-studied phenomenon called “attentional blink”, capable of showing the reduced ability to report the second of two targets when an interval <500 ms separates them. They found that beta synchronization is significantly stronger before trials with two targets separated by one distractor where both were detected than trials where the second target was not detected. These results, as the ones reported here, reflect that high levels of synchrony in higher frequency bands are responsible for an improvement on attentional control of visual processing, and this effect can be also observed for the frontal-parietal networks.

By adopting a similar criterion to differentiate between different states of attention to the one adopted in the present study, whereby slower responses were associated with reductions of attention to a relevant stimulus, Prado et al. [115] have also concluded that

variations of RT are mirrored by corresponding variations of functional connectivity between brain regions that support attentional processing. They conducted a BOLD fMRI experiment in which subjects must to identify a centrally presented visual letter, while had to ignore an auditory letter, which was equally likely to be congruent or incongruent with the visual letter. They reported that variations of RT were linked to variations of functional connectivity in a fronto-parietal attentional network and in sensory regions that process relevant stimuli. Indeed, one of their main findings was that slower responses were associated with reductions of functional connectivity (less synchrony) between the anterior cingulate cortex and the right dorsolateral prefrontal cortex; and between the anterior cingulate cortex and bilateral regions of the posterior parietal cortex; regions which work together as part of an attentional work that enables goal-directed behaviour. Such findings reinforce again that reduced functional connectivity within fronto-parietal attentional networks, which correspond to a reduced synchrony of neuronal oscillations within this type of networks, is associated with a disturbance on subject's attention levels, as reported in the present study. Moreover, the findings reported by Prado et al. [115] also enhance the evidence that variations of RT reflect fluctuations in attention, as it was assumed in this study.

Consistent with the theory that increased phase synchrony in higher frequency ranges, specially in the gamma band, is associated with an improvement on visual attention's levels, Gregoriou et al. [116] have reviewed recent physiological evidence which suggests that phase-coupled gamma-frequency oscillations play an important role in communication across brain areas responsible for enhancing and synchronizing visual cortex responses with attention. Those areas are the prefrontal cortex and the posterior parietal cortex. Specifically, the frontal eye field (FEF), an area within the prefrontal cortex and which is part of the dorsal attention network, has been associated with having direct reciprocal connection with visual cortical areas including area V4, which influences visual processing in the context of attention. In order to test whether the FEF might be responsible for the effects of attention on neuronal responses and synchrony in V4, in one of their studies, they recorded spikes and local field potentials simultaneously from FEF and V4, in two monkeys trained in a covert attention task. They reported that enhanced firing rates of FEF can improve detection threshold and increase responses of V4 neurons to a stimulus, associated with an increased synchrony within and between both areas in the gamma frequency range. Other studies have also reported that the posterior parietal cortex, another brain structure that projects to V4, is likely to contribute to the attentional effects on gamma synchrony and firing rates in V4 [116]. Taking into account that neurons in both FEF and V4 showed enhanced firing rates with attention, a phenomenon which has been associated with increased synchrony in the gamma frequency range within and between

both areas, these results are in line with those reported in the present study.

In fact, there is an evidence that increased synchrony in higher frequency ranges (beta and gamma) improves subject's attention state [35, 113–116].

Topographical Representations of the Electrode Pairs for Which Phase Coherence Was Capable to Predict Fluctuations in Attention Differed From Subject to Subject

One of the other main conclusions of the present study is that phase deviation, an equivalent measure for the phase coherence on a single trial basis, can, indeed, predict fluctuations in performance for the three frequency bands (alpha, beta and gamma) - see subsection 3.2.2.2, in chapter 3. The topographical localization of the electrode pairs associated with this correlation varied considerably from subject to subject (see figures 3.6, 3.7 and 3.8). In fact, the results obtained for the individual analysis of phase coherence measures are different, relatively to those obtained in the group analysis. The same electrode pairs did not show a significant improvement on task performance associated with fast responses with decreasing prestimulus phase coherence, from subject to subject, for the alpha frequency band; and the opposite pattern regarding the beta and gamma frequency bands. However, it was frequently observed, that couplings between frontal and frontal, parietal and parietal, and frontal and parietal electrode sites were associated with those effects. These results emphasize again the importance of phase synchrony mainly in frontal-parietal networks, on the attentional control of visual processing. Possibly, a coherent pattern was not obtained from subject to subject due to anatomical differences between them. Based on these results, it can be concluded that alpha, beta and gamma phase coherence can predict the subject's state of attention, from subject to subject.

Pupil Diameter Predicts Disturbances of Attention

Another important finding of this current work, is that pupil diameter can indeed predict fluctuations in subject's attention levels, being the pupil's dilation intrinsically related with increased levels of attention in goal-directed tasks (see point 3.3.1.1, in chapter 3). The results reported showed that fast responses and, therefore, improvements on task performance were predicted by prestimulus increased pupil diameter; whereas slower responses were preceded by smaller pupil diameter values. The findings reported by other studies are in line with those obtained here, although few studies have dedicated to investigate if the pupil diameter could predict phasic disturbances of attention state during goal-directed tasks. Kristjansson et al. [81] suggest that increased mean prestimulus pupil diameter was associated with an increased alertness level. Also in accordance with the

results reported here, Wendt et al. [117] have concluded that increased pupil diameter is closely related with a cognitive effort and refinement on visual attention levels.

Concluding, based on the results reported by the studies cited above and in the present work, there is an increasing evidence towards pupil diameter being a reliable parameter for predicting fluctuations in task performance.

Group and Individual Comparisons Have Revealed Contradictory Results Regarding How Gaze Position is Related With Fluctuations in Task Performance

According with the results reported in this study (regarding the group analysis) gaze position measures, including gaze position in horizontal and vertical directions and standard deviation of gaze position in both directions, were not reliable predictors of fluctuations in subject's task performance (see points 3.3.2.1 and 3.3.2.2, in chapter 3, for group and individual results for gaze position measures, respectively). However, contradictory results were obtained in the individual analysis. In fact, an equal or higher percent of subjects have revealed significant differences between different attention states defined based on RT measurements, in the individual analysis, for gaze position measurements in comparison with pupil diameter (see tables 3.4, 3.7, 3.8, 3.9 and 3.10). However, an effect of group was observed for pupil diameter and not for gaze position measures. This could be explained by the discrepant results which were obtained from subject to subject, relatively to how response RTs related to gaze position measures. Indeed, regarding the pupil diameter, all the subjects which revealed significant differences among different attention levels showed a consistent pattern, revealing a higher prestimulus pupil diameter before responding faster, in comparison when they have responded more slowly. However, contradictory results were obtained for different subjects for all the gaze position measurements. For the gaze position in both horizontal and vertical directions, the subjects which revealed significant differences among conditions, did not show the same tendency relatively to the deviation's direction of the gaze position with response RT values. Regarding the horizontal direction, some subjects have deviated more their gaze towards the left or right directions relatively to the screen centre for fast than slow trials. This inconsistent pattern was also observed for the vertical gaze position. Standard deviation in both directions was used as a measure of variability in gaze position across time. There were also subjects which demonstrated a higher variability for the gaze position for fast trials in comparison with slow trials; whereas others revealed this relation in the opposite direction. Those discrepancies between subjects relatively to all of the gaze position measures might explain why significant differences were not found after averaging those

results across subjects for the group analysis. Possibly, if the gaze's distance from the screen centre was used instead of the horizontal and vertical gaze position measures, an effect of group could be observed. Maybe, the relevant parameters is distance from the screen center and not the exact gaze position.

Few studies have investigated the extent to which gaze position measures could predict disturbances of attention. Both the works of Recarte et al. [10] and He et al. [11] revealed evidence that supports the existence of a correlation between standard deviation of gaze position and task performance. However, these two studies are both about driving tasks, with different conditions from the ones adopted in this study. A driving task considering a simulated or real scenario implies much more variable eye movements in comparison with the simple choice reaction time adopted here, where subjects were instructed to fixate the gaze.

Use of Classifiers For Predicting Attention Lapses

The main goal of the intra-subjects classification approach implemented on this study, was to develop a classifier specific for each subject, for predicting attention lapses. For each subject, several classification algorithms and type of features were explored, in order to optimize the procedure as much as possible. Using two types of metrics for evaluating the performance of each classifier - the accuracy values obtained in both the cross-validation method and in the test stage with the $\sim 10\%$ of data completely "unseen" by the classifiers - a more thorough study could be performed for selecting the most robust option.

Unimodal Classifiers

One of the main findings of this present study is that, taking into account the overall results among subjects for the three unimodal classifiers developed, based on eye parameters, alpha amplitude and temporal phase stability, the eye activity parameters were the features that ensured the best classification rate (see subsection 3.4.1 of chapter 3, tables 3.12 and 3.13). This result suggests that, possibly, the measures regarding the EEG signals are more noisy and not so good at predicting fluctuations in subject's task performance.

Another general conclusion that could be taken is that the best classification algorithm changed from subject to subject (see subsection 3.4.1 of chapter 3, table 3.11). This evidence suggests that it is better to study at first which algorithm's architecture ensures the best classification performance for each subject, although some generalization could be made by observing which algorithm was most frequently considered the best across subjects.

The classification algorithms that showed the best accuracy in the cross-validation was the KNN for the unimodal classifiers developed for eye parameters and temporal phase stability features; and RBF SVM, for alpha amplitude classifiers (see table 3.11).

RBF SVM has already given very good results in EEG-based classification applications [104]. In general, thanks to the margin maximization and the regularization term, SVMs are known to have good generalization properties, to be insensitive to overtraining and to the curse-of-dimensionality problem [104]. Specifically, RBF SVM algorithm tends to obtain more robust results than other kernels [8] as the linear, as was concluded by the results obtained in this study. Indeed, RBF SVM showed to be more frequently the best algorithm together with the KNN, in comparison with Linear SVM, for all the unimodal classifiers tested (see table 3.11). The RBF SVM can nonlinearly map samples into a higher dimensional space. This means that it can handle the cases when the relation between the class labels and corresponding attributes is nonlinear [8]. KNN algorithm can also produce nonlinear decision boundaries. Possibly, this nonlinear relation was verified for the data sets used, for the majority of the subjects.

KNN has been previously implemented on EEG-based classification procedures [118, 119], although SVM algorithms are more frequently used in this context [104]. KNN has been also applied in the prediction of visual attention levels' decrement using eye activity parameters [120]. However, the KNN is known to be very sensitive to the curse-of-dimensionality [104]. As the PCA algorithm was applied, a dimensionality reduction technique and considering that, specifically for the temporal phase stability classifier, the number of features extracted after the PCA was adjusted taking into account the few number of training samples, this latter problem was not a concern in the classification platform developed.

Taking into account other studies which have been conducted in this field, it is always difficult to compare the results obtained between them, including with the results reported here. In the majority of the cases, the classification methodology adopted and the type of features chosen highly differs from study to study [82]. Indeed, no consensus has been reached in the literature related to the best algorithms and features to be used in this type of classification tasks [82]. Factors such as the capability for the classifiers developed to deal with the problems provided by the different head geometry, incorrect electrodes scalp placements, and time-varying stationary of the EEG signals contribute for the variability of results obtained between studies [82]. However, in the following paragraphs, the results obtained in some studies which have focused in same type of features as in the present study are discussed, in terms of their similarities and discrepancies relatively to the results and procedures adopted.

Simple classifiers based on single-trial analysis have been widely used to detect the

spatiotemporal EEG signature of impairments on subject's attention levels [84,121]. However, in several of the classification platforms already developed, the algorithms tested were trained with the data from more than one subject, and tested with the features' vectors from each subject individually, differently from the procedure adopted here. A specific example is the study conducted by Davidson et al. [121]. They developed an algorithm to detect lapses in attention in real-time based on continuous EEG data, collected during a visuomotor pursuit tracking task, which was chosen by its similarity with a driving task. Subjects were asked to keep a cursor as close as possible to a repeating pseudorandom target scrolling down a screen, while EEG and video facial data were recorded. For lapses identification, these authors have adopted a hybrid procedure which took into account the inspection of lapses occurrence by a human expert through the video data acquired; and an algorithm which identified when a subject had stopped moving the cursor in response to a scrolling target, within a fixed interval of time. A lapse in attention was therefore marked when either or both the video inspection procedure and the lapse-detection algorithm have identified a lapse in responsiveness to a target. By calculating the spectral profile of 16 bipolar derivations in seven frequency bands (delta, theta, alpha, low beta, high beta, gamma, and higher frequency ranges) and using neural networks¹, their algorithm achieved a maximum overall accuracy of 84% averaged across subjects. These authors obtained a higher classification rate in comparison with the results achieved in the present study for the classifier using amplitude spectral analysis. However, they have developed a classification platform for identifying "deeper" lapses in attention, in which a subject has completely stopped to responding to a stimulus, differently from the algorithms developed here, which were built for detecting fluctuations in subjects' attention state, using only trials when they have correctly responded to a target, which are much more difficult to predict. Possibly, for this study, if the spectral amplitude in more frequency ranges was explored in addition to the alpha or even if other types of classifiers would be tested, for example, neural networks, more accurate results would be obtained. Note that significant differences between different attention states were not found in the statistical analysis for the alpha frequency range considering the whole group, but only for some specific subjects. Additionally, the neural networks are one of the categories of classifiers mostly used in EEG-based classification platforms [104].

Until now, no study has developed an algorithm based on machine learning techniques for predicting lapses in attention, using phase coherence EEG measurements, during a visual detection task. However, Besserve et al. [122] have conducted a visuomotor experiment in which subjects were requested to continuously manipulate a trackball to

¹**Neural Networks** - A neural network is a type of classification algorithm defined as an assembly of several artificial neurons which enables to produce also nonlinear decision boundaries [104].

compensate the random rotations of a cube projected on a display screen, alternated with periods of resting, while MEG signals were recording. They intended to develop a classifier which could be able to distinguish between visuomotor states from resting state conditions. They explored amplitude and phase coherence features in six frequency bands, obtaining the best accuracy values for the beta frequency range. For the calculation of single-trial phase synchrony measurements, these authors adopted a method similar to the temporal phase stability, which was applied here. They achieved a maximal accuracy in the cross-validation for the beta phase coherence across subjects higher relatively to the one obtained in the present study (85% versus 57,46%, respectively). However, likely to the study mentioned above, distinguishing between visuomotor and resting states is much less demanding than predicting different states of attention, during task performance, taking into account RT variability across trials.

Possibly, in the present study, worse results were obtained for the simple classifier regarding the phase coherence measure in comparison with the eye parameters classifiers, due to the loss of information by retaining the principal components which accounted only for $\sim 68\%$ of the input variance after the PCA algorithm, for further classification, in order to avoid the curse-of dimensionality problem.

Regarding the results obtained for the intra-subjects classification using eye activity parameters, Jin et al. [8] have developed a driver sleepiness detection system based also on eye activity parameters. Their system ensured a mean accuracy value for the intra-subjects classification of 85,41% for the test stage with “unseen” data, which exceeds the mean classification rate obtained in this study (see table 3.12). However, despite these authors have also developed a specific classifier for each subject, distinguishing between alert and sleepy states is different from predicting different states of attention, based on fluctuations in task performance. Moreover, as was referred above, a driving scenario is quite different from the task which was implemented here. However, it is important to emphasize that in addition to specific models based on the information of each subject, they also developed a general model with the data from all the subjects. They concluded that the detecting accuracy of the specific models significantly exceeds the general model. This result shows that individual differences are an important consideration when building detection algorithms for different subjects, which supports the method implemented on this present study. Probably, if a general detection model was developed here, it would not be suitable for all subjects, and worse accuracy values would be obtained. Additionally, taking into account that these authors used the PERCLOS, blink frequency, gaze direction and fixation time as input features for the classifiers developed, possibly if other type of eye activity parameters beyond those related with pupil diameter and gaze position were used, better results regarding the eye parameters classifiers could be obtained for this

study.

Hybrid Classifiers

It has been demonstrated that decisions from multiple unimodal classifiers can be combined to significantly improve the overall classification performance [12].

Contrary to what was expected, there were not found better performance results with hybrid versus unimodal classifiers for this study (see subsection 3.4.2, in chapter 3). Qian et al. [12] obtained better accuracy values by fusing the classification results based on both the features extracted from the EEG signal and pupil measures at the decision level, in comparison with the results obtained with each separate classifier. They implemented a visual target detection, in which participants were instructed to push a button as soon as they detected a target image among several distractors. However, differently from this study, the decision at the fusion level adopted did not take into account the most frequently occurring label among those given by each unimodal classifier separately. Instead, it was determined taking into account a fusion likelihood ratio which accounted with both the probabilities of detection and false alarm for each classifier individually. These authors achieved a significantly better performance for the five subjects which participated on the study with the fusion method, in comparison with the EEG-based and pupil-based classifiers.

Probably, regarding the present study, hybrid classifiers did not significantly improve the classification accuracy relatively to the unimodal classifiers which ensured the best classification rate on average across subjects - the eye parameters classifiers - because the EEG-based classifiers have introduced a high percent of misclassified output labels on the decision fusion rule. By observing the performance results obtained with alpha amplitude and temporal phase stability classifiers alone (see table 3.12), it can be concluded that they are less robust classifiers in comparison with the eye parameters classifiers. Maybe, if a decision rule based also on attributing different weights to the outputs given for each unimodal classifier depending on its individual performance would contribute for obtaining better classification rates for the hybrid approach in comparison with the unimodal classifiers.

General Conclusions

The main findings of this study reveal that EEG signals and eye activity parameters can be used to predict attention lapses. Beta and gamma phase coherence measures were capable of predicting fluctuations in subject's attention levels, being increased frontal-parietal phase coherence values in beta and gamma frequency bands associated with a better task performance. These results are consistent with the theory that the communication within

the attentional networks proceeds via transient long-range phase synchronization in the beta and gamma frequency bands. Relatively to eye measures, the results reported suggest that pupil dilation could be considered as an index of attentional effort and a reliable measure to predict fluctuations in subject's attention levels.

EEG classifiers were not able to consistency discriminate between attention states on a subject by subject basis. Maybe, increasing the number of training trials would lead to better performance results. That could be achieved, for example, by training the developed classifiers with the data from all the participants of the study. Indeed, a general algorithm which could be able to handle with the information from multiple subjects and, at the same time, ensured classification accuracies higher to the subject-specific classifiers, would be preferable for future applications. However, using eye parameters, classification of fluctuations in RT could achieve accuracy values above the chance level.

In summary, fluctuations in attention are related with fluctuations in frontal-parietal phase synchronization and pupil diameter. Future development of classifiers taking into account those features might increase accuracy to a level useful for clinical purposes, such as in the biofeedback therapies' field, for helping children suffering from ADHD or people with neurological disorders; or for the upgrading of the existing alertness management devices.

Appendix A

A.1 Informed Consent

Confidential

Appendix

A.2 Socio-Demographic and Clinical Questionnaire

Ficha de Dados Sócio-Demográficos e Clínicos

Data recrutamento: _____ Cód. Processo: _____

I - Dados Sócio-Demográficos

1. Nome: _____

2. Género: Feminino Masculino

3. Data de Nascimento: _____ 4. Idade: _____

5. E-mail: _____

6. Morada: 6.1. Freguesia: _____

6.2. Concelho: _____

6.3. Distrito: _____

7. Contacto: _____

8. Estado Civil: Casado/União de Facto Divorciado/Separado

Solteiro Viúvo

9. Escolaridade: _____ 10. Atividade Profissional: _____

11. (Se não estudante) Situação Profissional Atual:

- Desempregado A exercer

II – Dados Clínicos

II.1. Historial Clínico

12. Problemas de saúde atuais e/ou passados:

13. História de doença neurológica (ex: epilepsia, AVC, esclerose múltipla) e/ou psiquiátrica (ex: depressão)?

- Sim Não

13.1 Qual(is)? _____

14. Tem alguma(s) doença(s) crónica(s)?

- Sim Não

14.1 Qual(is)? _____

15. História prévia de internamento e/ou coma?

- Sim Não

15.1 Em que circunstâncias?

16. História de Cirurgias?

- Sim Não

16.1. Circunstâncias:

17. História de Lesão Cerebral?

- Sim Não

18. Tem problemas visuais (ex: miopia, ambliopia, etc...)?

- Sim Não

18.1. Qual(is)? _____

18.2. Usa óculos/lentes de contacto para correção?

- Sim Não

19. Tem problemas auditivos?

- Sim Não

19.1. Qual(is)? _____

20. Tem problemas motores? Sim Não

20.1. Qual(is)? _____

21. Toma medicação habitualmente? Sim Não

De que tipo? Antidepressivos Ansiolíticos Estimulantes

Antipsicóticos Antihistamínicos Opióides

Outros: _____

NOTAS: _____

22. História de consumo de substâncias psicoativas?

Álcool Drogas Não

NOTAS: _____

III – Hábitos (preencher se cumpre critérios de inclusão):

23. É fumador? Sim Não

23.1. (Se Sim) Quantos cigarros fuma por dia? _____

23.2. Há quanto tempo fuma? _____

23.3. (Se Não é fumador) Deixou de fumar recentemente?

Há mais de 3 meses Há menos de 3 meses Não

23.4. (Se Não é fumador habitual ou se já foi) É fumador não regular?

Sim Não

23.5. (Se Sim, é fumador não regular) Quantos cigarros fuma por mês, aproximadamente? _____

24. Consome álcool frequentemente? Sim Não

24.1. (Se Sim) Preencha a seguinte tabela. Registe o nº de copos que ingere por dia à semana e ao fim-de-semana, habitualmente:

Tipo de Bebida	Nº de copos por dia: semana (em média)	Nº de copos por dia: fim-de-semana (em média)
Bebidas Brancas (Vodka, Whisky, Gin, Martini, etc)		
Cerveja, cidra e similares		
Vinhos		
Licores		
Outras: _____		

25. Costuma tomar café diariamente? Sim Não

25.1. Quantos cafés toma por dia habitualmente? _____

26. Costuma beber coca-cola diariamente (ou algo do género, p.ex. Ice Tea, Pepsi Cola, etc)?

Sim Não

26.1. (Se Sim) Quantas garrafas de 33 ml consome, em média, por dia (no total, relativamente a todas as bebidas referentes à pergunta anterior)? _____

27. Consome algum tipo de droga? Sim Não

27.1. (Se Sim) Preencha a seguinte tabela, indicando o que consome e o número de vezes:

Droga	Nº de vezes por dia:	Nº de vezes por semana:	Nº de vezes por mês:
Cannabis e similares			
Opiáceos			
Branças (Cocaína, Heroína, etc)			
Alucinogénios			
Esteróides			
Anfetaminas			
Barbitúricos			
Outras: _____			

A.3 Pittsburgh Sleep Quality Inventory

Iniciais do paciente _____ ID _____ Data _____ Hora _____

QUESTIONÁRIO DE PITTSBURGH SOBRE A QUALIDADE DO SONO

INSTRUÇÕES:

As perguntas que se seguem referem-se aos seus hábitos de sono normais apenas ao longo do último mês (últimos 30 dias). As suas respostas devem indicar a opção mais precisa para a maioria dos dias e noites ao longo do último mês. Por favor, responda a todas as perguntas.

1. Ao longo do último mês, normalmente a que horas se deitou, à noite?

HORA DE DEITAR _____

2. Ao longo do último mês, normalmente quanto tempo (em minutos) demorou a adormecer cada noite?

NÚMERO DE MINUTOS _____

3. Ao longo do último mês, normalmente a que horas se levantou de manhã?

HORA DE LEVANTAR _____

4. Ao longo do último mês, quantas horas de sono efectivo dormiu à noite? (pode diferir do número de horas que passou na cama.)

HORAS DE SONO POR NOITE _____

Para cada uma das restantes perguntas, escolha a resposta mais adequada. Por favor, responda a todas as perguntas.

5. Ao longo do último mês, quantas vezes teve problemas relacionados com o sono por . . .

a) ...não conseguir dormir no espaço de 30 minutos

	Menos do		
Não ocorreu no	que uma vez por	Uma ou duas vezes	Três ou mais vezes
último mês _____	semana _____	por semana _____	por semana _____

b) ...acordar a meio da noite ou muito cedo

	Menos do		
Não ocorreu no	que uma vez por	Uma ou duas vezes	Três ou mais vezes
último mês _____	semana _____	por semana _____	por semana _____

c) ...ter de se levantar para ir à casa-de-banho

	Menos do		
Não ocorreu no	que uma vez por	Uma ou duas vezes	Três ou mais vezes
último mês _____	semana _____	por semana _____	por semana _____

d) ...não conseguir respirar comodamente

	Menos do		
Não ocorreu no	que uma vez por	Uma ou duas vezes	Três ou mais vezes
último mês _____	semana _____	por semana _____	por semana _____

e) ...tossir ou ressonar alto

	Menos do		
Não ocorreu no	que uma vez por	Uma ou duas vezes	Três ou mais vezes
último mês _____	semana _____	por semana _____	por semana _____

f) ...sentir demasiado frio

	Menos do		
Não ocorreu no	que uma vez por	Uma ou duas vezes	Três ou mais vezes
último mês _____	semana _____	por semana _____	por semana _____

g) ...sentir demasiado calor

	Menos do		
Não ocorreu no	que uma vez por	Uma ou duas vezes	Três ou mais vezes
último mês _____	semana _____	por semana _____	por semana _____

h) ...ter pesadelos

	Menos do		
Não ocorreu no	que uma vez por	Uma ou duas vezes	Três ou mais vezes
último mês _____	semana _____	por semana _____	por semana _____

i) ...ter dores

	Menos do		
Não ocorreu no	que uma vez por	Uma ou duas vezes	Três ou mais vezes
último mês _____	semana _____	por semana _____	por semana _____

j) ...outra(s) razão/razões; por favor, descreva-a(s) _____

Ao longo do último mês, quantas vezes teve problemas em dormir por esse(s) motivo(s)?

	Menos do		
Não ocorreu no	que uma vez por	Uma ou duas vezes	Três ou mais vezes
último mês _____	semana _____	por semana _____	por semana _____

6. Ao longo do último mês, como classificaria a qualidade geral do seu sono?

Muito boa _____

Moderadamente boa _____

Moderadamente má _____

Muito má _____

7. Ao longo do último mês, quantas vezes tomou medicamentos para o ajudarem a dormir (receitados ou de venda livre)?

	Menos do		
Não ocorreu no	que uma vez por	Uma ou duas vezes	Três ou mais vezes
último mês _____	semana _____	por semana _____	por semana _____

8. Ao longo do último mês, quantas vezes teve problemas em manter-se acordado enquanto conduzia, às refeições ou ao participar em actividades sociais?

	Menos do		
Não ocorreu no	que uma vez por	Uma ou duas vezes	Três ou mais vezes
último mês _____	semana _____	por semana _____	por semana _____

9. Ao longo do último mês, até que ponto foi um problema para si manter o entusiasmo suficiente para realizar as tarefas necessárias?

Nenhum problema _____

Apenas um problema muito ligeiro _____

Algum problema _____

Um problema muito grande _____

10. Partilha a cama ou o quarto com alguém?

Não partilho a cama / o quarto com ninguém _____

Parceiro/a de cama / de quarto noutro quarto _____

Parceiro/a no mesmo quarto mas noutra cama _____

Parceiro/a na mesma cama _____

Se partilha o quarto ou a cama com alguém, pergunte-lhe quantas vezes, ao longo do último mês, você . . .

a) ...ressonou alto

	Menos do		
Não ocorreu no	que uma vez por	Uma ou duas vezes	Três ou mais vezes
último mês _____	semana _____	por semana _____	por semana _____

b) ...fez pausas longas entre respirações enquanto dormia

	Menos do		
Não ocorreu no	que uma vez por	Uma ou duas vezes	Três ou mais vezes
último mês _____	semana _____	por semana _____	por semana _____

c) ...teve contracções musculares ou movimentos bruscos das pernas durante o sono

	Menos do		
Não ocorreu no	que uma vez por	Uma ou duas vezes	Três ou mais vezes
último mês _____	semana _____	por semana _____	por semana _____

d) ...teve episódios de desorientação ou de confusão ao acordar de noite

	Menos do		
Não ocorreu no	que uma vez por	Uma ou duas vezes	Três ou mais vezes
último mês _____	semana _____	por semana _____	por semana _____

e) ...mostrou outros sintomas de desassossego durante o sono; por favor, descreva-os

Não ocorreu no último mês _____	Menos do que uma vez por semana _____	Uma ou duas vezes por semana _____	Três ou mais vezes por semana _____
------------------------------------	---	---------------------------------------	--

A.4 Edinburgh Handedness Inventory

QUESTIONÁRIO DE LATERALIDADE GESCHWIND-OLDFIELD

Data e Local de Avaliação: _____ ID: _____

1. O Sr./Sr^a é: (1) Dextro (2) Canhoto (3) Ambidextro

2. Qual a mão que usa para:

	Sempre Direita (+10)	Quase Sempre Direita (+5)	Uma ou Outra (0)	Quase Sempre Esquerda (-5)	Sempre Esquerda (-10)
1. Escrever	_____	_____	_____	_____	_____
2. Desenhar	_____	_____	_____	_____	_____
3. Atirar uma bola	_____	_____	_____	_____	_____
		Suplementar			
4. Utilizar uma tesoura	_____	_____	_____	_____	_____
5. Escovar os dentes	_____	_____	_____	_____	_____
6. Utilizar uma faca	_____	_____	_____	_____	_____
7. Utilizar uma colher	_____	_____	_____	_____	_____
8. Segurar numa vassoura (mão que está em cima)	_____	_____	_____	_____	_____
9. Acender um fósforo	_____	_____	_____	_____	_____
10. Desenroscar uma tampa	_____	_____	_____	_____	_____
Subtotais	_____	_____	_____	_____	_____

Total: _____

3. Foi sempre: (1) Dextro ou (2) Canhoto?

4. Houve mudança? (1) Sim (2) Não
5. Existem algumas actividades para as quais use a mão não dominante?
(1) Não (2) Sim, _____
6. Qual o **olho** que usa para tirar uma fotografia? (1) Direito (2) Esquerdo
7. Com que **pé** chuta uma bola? (1) Direito (2) Esquerdo

A.5 Sleep Patterns During the Four Days Prior to Testing

Hábitos relativos aos 4 dias anteriores ao teste

Dia: _____ Data: _____ Hora: _____

Nome: _____ Cód. Processo: _____

Questionário sobre a qualidade do sono no dia anterior ao do preenchimento do mesmo.

Sono

1. Quantas horas dormiu esta noite? _____
2. A que horas se deitou a noite passada? _____
3. A que horas se levantou hoje? _____
4. As horas que dormiu foram reconfortantes (qualidade do sono)?
 Sim Não
5. Quanto tempo demorou a adormecer a noite passada? _____
6. Quando acordou hoje de manhã sentiu-se cansado?
 Sim Não
7. Fez alguma pausa durante o dia de ontem para dormir?
 Sim Não
 - 7.1. Se sim, dormiu durante quanto tempo? _____
 - 7.2. A que horas? _____
8. Qual a parte do dia de ontem durante a qual se sentiu mais sonolento?
 Manhã Fim de almoço Tarde Fim de jantar

9. Qual a parte do dia de ontem na qual se sentiu mais cansado/menos atento?

Manhã Fim de almoço Tarde Fim de jantar

10. Teve sono depois de almoço ontem? Sim Não

11. OBSERVAÇÕES (caso tenha algum aspeto importante a relatar sobre o dia/noite de ontem, em termos de sono/cansaço - p. ex. o facto de ter saído à noite; ter tido alguma atividade desportiva muito perto da hora a que se deitou; se teve problemas de insónias; se acordou a meio da noite e teve algum tempo acordado;- etc. -, coloque aqui):

A.6 Sleep Patterns and Caffeine/Alcohol/Nicotine Ingestion On the Day Before and On the Test Day

Hábitos relativos ao dia anterior e dia do teste

Dia: _____ Data: _____ Hora: _____

Nome: _____ Cód. Processo: _____

Questionário sobre qualidade de sono e consumo de substâncias psicoativas (tabaco, café, álcool e outras) no dia anterior ao teste e dia do teste

Sono

1. Quantas horas dormiu esta noite? _____
2. A que horas se deitou a noite passada? _____
3. A que horas se levantou hoje? _____
4. As horas que dormiu foram reconfortantes (qualidade do sono)?
 Sim Não
5. Quanto tempo demorou a adormecer a noite passada? _____
6. Quando acordou hoje de manhã sentiu-se cansado?
 Sim Não
7. Fez alguma pausa durante o dia de ontem para dormir?
 Sim Não
 - 7.1. Se sim, dormiu durante quanto tempo? _____
 - 7.2. A que horas? _____

8. Qual a parte do dia de ontem durante a qual se sentiu mais sonolento?

Manhã Fim de almoço Tarde Fim de jantar

9. Qual a parte do dia de ontem na qual se sentiu mais cansado/menos atento?

Manhã Fim de almoço Tarde Fim de jantar

10. Teve sono depois de almoço ontem? Sim Não

Substâncias Psicoativas

11. Tomou café ontem? Sim Não

11.1. Se sim, quantos? ___ 11.2. A que horas? 1º _____

2º _____

3º _____

4º _____

5º _____

6º _____

7º _____

8º _____

12. Consumiu álcool ontem? Sim Não

12.1. (Se sim) Preencha a seguinte tabela:

Tipo de Bebida	Nº de copos (dia de ontem)	Horário da ingestão
Bebidas Brancas (Vodka, Whisky, Gin, Martini, etc)		
Cerveja, cidra e similares		

Vinhos		
Licores		
Outras: _____		

13. Fumou algum cigarro ontem? Sim Não

13.1. Se sim, quantos? _____

14. Consumiu coca-cola ontem (ou algo similar, p.ex. Ice Tea, Pepsi Cola, etc)?

Sim Não

14.1. (Se Sim) Quantas garrafas de 33 ml bebeu (no total, relativamente a todas as bebidas referentes à pergunta anterior)? _____

15. Consumiu algum tipo de drogas? Sim Não

15.1. (Se Sim) Qual(is)?

Cannabis e similares Opiáceos Alucinogénios

Esteróides Anfetaminas Barbitúricos

Outras: _____

16. Tomou algum tipo de medicação fora do habitual?

Sim Não

16.1. Se sim, qual? _____

16.2. A que horas? _____

DIA DO TESTE – Subst. Psicoativas

17. Tomou café hoje? Sim Não

17.1. Se sim, quantos? ___ 17.2. A que horas? 1º _____

2º _____

3º _____

4º _____

5º _____

6º _____

7º _____

8º _____

18. Consumiu álcool hoje? Sim Não

18.1. (Se sim) Preencha a seguinte tabela:

Tipo de Bebida	Nº de copos (dia de ontem)	Horário da ingestão
Bebidas Brancas (Vodka, Whisky, Gin, Martini, etc)		
Cerveja, cidra e similares		
Vinhos		
Licores		
Outras: _____		

19. Fumou algum cigarro hoje? Sim Não

19.1. Se sim, quantos? _____

20. Consumiu coca-cola hoje (ou algo similar, p.ex. Ice Tea, Pepsi Cola, etc)?

Sim Não

20.1. (Se Sim) Quantas garrafas de 33 ml bebeu (no total, relativamente a todas as bebidas referentes à pergunta anterior)? _____

21. Consumiu algum tipo de drogas no dia de hoje?

Sim Não

21.1. (Se Sim) Qual(is)?

Cannabis e similares Opiáceos Alucinogénios

Esteróides Anfetaminas Barbitúricos

Outras: _____

22. Tomou algum tipo de medicação fora do habitual hoje?

Sim Não

22.1. Se sim, qual? _____

22.2. A que horas? _____

References

- [1] J. Yordanova, B. Albrecht, H. Uebel, R. Kirov, T. Banaschewski, A. Rothenberger, and V. Kolev. Independent oscillatory patterns determine performance fluctuations in children with attention deficit/hyperactivity disorder. *Brain*, 134(6):1740–1750, 2011.
- [2] H. van Dijk, J. M. Schoffelen, R. Oostenveld, and O. Jensen. Prestimulus oscillatory activity in the alpha band predicts visual discrimination ability. *The Journal of Neuroscience*, 28(8):1816–1823, February 2008.
- [3] D. H. Weissman, K. C. Roberts, K. M. Visscher, and M. G. Woldorff. The neural bases of momentary lapses in attention. *Nature Neuroscience*, 9(7):971–978, 2006.
- [4] T. R. Peiris, R. D. Jones, P. R. Davidson, G. J. Carroll, and P. J. Bones. Frequent lapses of responsiveness during an extended visuomotor tracking task in non-sleep-deprived subjects. *Journal of Sleep Research*, 15(3):291–300, 2006.
- [5] C. Anderson, A. W. Wales, and J. A. Horne. PVT lapses differ according to eyes open, closed, or looking away. *Sleep*, 2010.
- [6] K. F. Van Orden, W. Limbert, S. Makeig, and T. Jung. Eye activity correlates of workload during a visuospatial memory task. *Human Factors: The Journal of the Human Factors and Ergonomics Society*, 43(1):111–121, 2001.
- [7] Y. Tsai, E. Viirre, C. Strychacz, B. Chase, and T. Jung. Task performance and eye activity: Predicting behavior relating to cognitive workload. *Aviation, Space, and Environmental Medicine*, 2007.
- [8] L. Jin, Q. Niu, Y. Jiang, H. Xian, Y. Qin, and M. Xu. Driver sleepiness detection system based on eye movements variables. *Advances in Mechanical Engineering*, 2013.
- [9] J. Smallwood, K. S. Brown, C. Tipper, B. Giesbrecht, M. S. Franklin, M. D. Mrazek, J. M. Carlson, and J. W. Schooler. Pupillometric evidence for the decoupling of attention from perceptual input during offline thought. *Plos One*, 6(3), 2011.
- [10] M. A. Recarte and L. M. Nunes. Effects of verbal and spatial-imagery tasks on eye fixations while driving. *Journal of Experimental Psychology: Applied*, 2000.

- [11] J. He, E. Becic, Y. Lee, and J. S. McCarley. Identifying mind-wandering behind the wheel. In *Proceedings of the Human Factors and Ergonomics Society Annual Meeting*, 2009.
- [12] M. Qian, M. Aguilar, K. N. Zachery, C. Privitera, S. Klein, T. Carney, and L. W. Nolte. Decision-level fusion of EEG and pupil features for single-trial visual detection analysis. *Biomedical Engineering, IEEE Transactions on*, 56(7):1929–1937, July 2009.
- [13] M. S. John, M. R. Risser, and D. A. Kobus. Toward a usable closed-loop attention management system: Predicting vigilance from minimal contact head, eye, and EEG measures. *Foundations of Augmented Cognition*, 2006.
- [14] E. Lopez-Larraz, I. Iterate, C. Escolano, I. Garcia, L. Montesano, and J. Minguez. Single-trial classification of feedback potentials within neurofeedback training with an EEG brain-computer interface. In *Engineering in Medicine and Biology Society, EMBC, 2011 Annual International Conference of the IEEE*, August 2011.
- [15] P. M. Matthews and P. Jezzard. Functional magnetic resonance imaging. *Journal of Neurology, Neurosurgery & Psychiatry*, 75(1):6–12, 2004.
- [16] M. Politis and P. Piccini. Positron emission tomography imaging in neurological disorders. *Journal of Neurology*, 259(9):1769–1780, 2012.
- [17] M. E. Raichle, A. M. MacLeod, A. Z. Snyder, W. J. Powers, D. A. Gusnard, and G. L. Shulman. A default mode of brain function. *Proceedings of the National Academy of Sciences*, 98(2):676–682, 2001.
- [18] A. Meyer-Lindenberg. From maps to mechanisms through neuroimaging of schizophrenia. *Nature*, 2010.
- [19] K. Li, L. Guo, J. Nie, G. Li, and T. Liu. Review of methods for functional brain connectivity detection using fMRI. *Computerized Medical Imaging and Graphics*, 33(2):131 – 139, 2009.
- [20] N. K. Logothetis. What we can do and what we cannot do with fMRI. *Nature*, 453(7197):869–878, June 2008.
- [21] C. Asbury. Brain imaging technologies and their applications in neuroscience. *The Dana Foundation*, 2011.
- [22] D. A. Gusnard and M. E. Raichle. Searching for a baseline: Functional imaging and the resting human brain. *Nature Reviews Neuroscience*, 2(10):685–694, 2001.
- [23] D. G. Nair. About being BOLD. *Brain Research Reviews*, 50(2):229 – 243, 2005.
- [24] S. J. Luck. *An Introduction to the Event-Related Potential Technique*. MIT Press, 1st edition, August 2005.

- [25] M. Teplan. Fundamentals of EEG measurement. *Measurement Science Review*, 2002.
- [26] F. L. da Silva. EEG: origin and measurement. In *EEG-fMRI*, pages 19–38. Springer, 2010.
- [27] G. Pfurtscheller and F. H. Lopes da Silva. Event-related EEG/MEG synchronization and desynchronization: basic principles. *Clinical Neurophysiology*, 110(11):1842–1857, November 1999.
- [28] R. G. O’Connell, P. M. Dockree, I. H. Robertson, M. A. Bellgrove, J. J. Foxe, and S. P. Kelly. Uncovering the neural signature of lapsing attention: Electrophysiological signals predict errors up to 20 s before they occur. *The Journal of Neuroscience*, 29(26):8604–8611, July 2009.
- [29] S. Hanslmayr, J. Gross, W. Klimesch, and K. L. Shapiro. The role of alpha oscillations in temporal attention. *Brain Research Reviews*, 67(1–2):331 – 343, 2011.
- [30] R. T. Canolty and R. T. Knight. The functional role of cross-frequency coupling. *Trends In Cognitive Sciences*, 2010.
- [31] J. Malmivuo and R. Plonsey. *Bioelectromagnetism: Principles and Applications of Bioelectric and Biomagnetic Fields*. Oxford University Press, USA, 1st edition, July 1995.
- [32] S. M. Doesburg and L. M. Ward. Synchronization between sources: Emerging methods for understanding large-scale functional networks in the human brain. In J. L. Velazquez and R. Wennberg, editors, *Coordinated Activity in the Brain*, chapter 2, pages 25–42. Springer New York, 2009.
- [33] J. P. Lachaux, E. Rodriguez, J. Martinerie, and F. J. Varela. Measuring phase synchrony in brain signals. *Human Brain Mapping*, 8(4):194–208, 1999.
- [34] A. Delorme and S. Makeig. EEGLAB: an open source toolbox for analysis of single-trial EEG dynamics including independent component analysis. *Journal of Neuroscience Methods*, 2004.
- [35] S. Hanslmayr, A. Aslan, T. Staudigl, W. Klimesch, C. S. Herrmann, and K. H. Bäuml. Prestimulus oscillations predict visual perception performance between and within subjects. *NeuroImage*, 37(4):1465 – 1473, 2007.
- [36] R. Desimone. Visual attention mediated by biased competition in extrastriate visual cortex. *Philosophical Transactions of the Royal Society of London. Series B: Biological Sciences*, 353(1373), 1998.
- [37] J. B. Hopfinger, M. H. Buonocore, and G. R. Mangun. The neural mechanisms of top-down attentional control. *Nature Neuroscience*, 3(3):284–291, 2000.

- [38] S. Kastner, P. De Weerd, R. Desimone, and L. G. Ungerleider. Mechanisms of directed attention in the human extrastriate cortex as revealed by functional MRI. *Science*, 282(5386), 1998.
- [39] M. G. Woldorff, C. J. Hazlett, H. M. Fichtenholtz, D. H. Weissman, A. M. Dale, and A. W. Song. Functional parcellation of attentional control regions of the brain. *Journal of Cognitive Neuroscience*, 16(1):149–165, January 2004.
- [40] X. Wen, L. Yao, Y. Liu, and M. Ding. Causal interactions in attention networks predict behavioral performance. *The Journal of Neuroscience*, 2012.
- [41] G. L. Shulman, J. M. Ollinger, E. Akbudak, T. E. Conturo, A. Z. Snyder, S. E. Petersen, and M. Corbetta. Areas involved in encoding and applying directional expectations to moving objects. *The Journal of Neuroscience*, 19(21), 1999.
- [42] M. Corbetta, J. M. Kincade, J. M. Ollinger, M. P. McAvoy, and G. L. Shulman. Voluntary orienting is dissociated from target detection in human posterior parietal cortex. *Nature neuroscience*, 3(3), 2000.
- [43] S. V. Astafiev, G. L. Shulman, C. M. Stanley, A. Z. Snyder, D. C. Van Essen, and M. Corbetta. Functional organization of human intraparietal and frontal cortex for attending, looking, and pointing. *The Journal of Neuroscience*, 23(11):4689–4699, June 2003.
- [44] G. L. Shulman, M. P. McAvoy, M. C. Cowan, S. V. Astafiev, A. P. Tansy, G. d’Avossa, and M. Corbetta. Quantitative analysis of attention and detection signals during visual search. *Journal of Neurophysiology*, 90(5), 2003.
- [45] J. M. Kincade, R. A. Abrams, S. V. Astafiev, G. L. Shulman, and Corbetta M. An event-related functional magnetic resonance imaging study of voluntary and stimulus-driven orienting of attention. *The Journal of Neuroscience*, 2005.
- [46] S. V. Astafiev, G. L. Shulman, and M. Corbetta. Visuospatial reorienting signals in the human temporo-parietal junction are independent of response selection. *European Journal of Neuroscience*, 23(2), 2006.
- [47] M. Corbetta, G. Patel, and G. L. Shulman. The reorienting system of the human brain: From environment to theory of mind. *Neuron*, 2008.
- [48] D. H. Weissman and J. Prado. Heightened activity in a key region of the ventral attention network is linked to reduced activity in a key region of the dorsal attention network during unexpected shifts of covert visual spatial attention. *NeuroImage*, 61(4):798 – 804, 2012.
- [49] I. G. Meister, M. Wienemann, D. Buelte, C. Grünewald, R. Sparing, N. Dambeck, and B. Boroojerdi. Hemiextinction induced by transcranial magnetic stimulation over the right temporo-parietal junction. *Neuroscience*, 142(1):119 – 123, 2006.

- [50] V. Bonnelle, R. Leech, K. M. Kinnunen, T. E. Ham, C. F. Beckmann, X. De Boissezon, R. J. Greenwood, and D. J. Sharp. Default mode network connectivity predicts sustained attention deficits after traumatic brain injury. *The Journal of Neuroscience*, 31(38):13442–13451, September 2011.
- [51] D. A. Gusnard, E. Akbudak, G. L. Shulman, and M. E. Raichle. Medial prefrontal cortex and self-referential mental activity: Relation to a default mode of brain function. *Proceedings of the National Academy of Sciences*, 98(7):4259–4264, 2001.
- [52] M. F. Mason, M. I. Norton, J. D. Van Horn, D. M. Wegner, S. T. Grafton, and C. N. Macrae. Wandering minds: The default network and stimulus-independent thought. *Science*, 315(5810):393–395, 2007.
- [53] P. Hagmann, L. Cammoun, X. Gig, R. Meuli, C. J. Honey, and V. J. Wedeen. Mapping the structural core of human cerebral cortex. *PLOS Biology*, 2008.
- [54] M. Greicius. Resting-state functional connectivity in neuropsychiatric disorders. *Current Opinion in Neurology*, 2008.
- [55] M. E. Raichle. Two views of brain function. *Trends in Cognitive Sciences*, 14(4), 2010.
- [56] L. Q. Uddin, A. M. Kelly, B. B. Biswal, F. X. Castellanos, and M. P. Milham. Functional connectivity of default mode network components: Correlation, anti-correlation, and causality. *Human Brain Mapping*, 30(2):625–637, 2009.
- [57] D. Navon. Forest before trees: The precedence of global features in visual perception. *Cognitive Psychology*, 9(3):353 – 383, 1977.
- [58] S. J. Broyd, C. Demanuele, S. Debener, S. K. Helps, C. J. James, and E. J. S. Sonuga-Barke. Default-mode brain dysfunction in mental disorders: A systematic review. *Neuroscience and Biobehavioral Reviews*, 33(3):279 – 296, 2009.
- [59] M. D. Fox, A. Z. Snyder, J. L. Vincent, M. Corbetta, D. C. Van Essen, and M. E. Raichle. The human brain is intrinsically organized into dynamic, anticorrelated functional networks. *Proceedings of the National Academy of Sciences of the United States of America*, 102(27):9673–9678, 2005.
- [60] J. S. Durmer and D. F. Dinges. Neurocognitive consequences of sleep deprivation. *Seminars in Neurology*, 25(01):117–129, March 2005.
- [61] M. W. Chee, J. C. Tan, H. Zheng, S. Parimal, D. H. Weissman, V. Zagorodnov, and D. F. Dinges. Lapsing during sleep deprivation is associated with distributed changes in brain activation. *The Journal of Neuroscience*, 28(21):5519–5528, May 2008.
- [62] F. Indlekofer, M. Piechatzek, M. Daamen, C. Glasmacher, R. Lieb, H. Pfister, O. Tucha, K. W. Lange, H. U. Wittchen, and C. G. Schütz. Reduced memory and

- attention performance in a population-based sample of young adults with a moderate lifetime use of cannabis, ecstasy and alcohol. *Journal of Psychopharmacology*, 2008.
- [63] P. J. Bushnell, E. D. Levin, R. T. Marrocco, M. F. Sarter, B. J. Strupp, and D. M. Warburton. Attention as a target of intoxication: Insights and methods from studies of drug abuse. *Neurotoxicology and Teratology*, 22(4):487 – 502, 2000.
- [64] M. Raznahan, E. Hassanzadeh, A. Houshmand, L. Kashani, M. Tabrizi, and S. Akhondzadeh. Change in frequency of acute and subacute effects of ecstasy in a group of novice users after 6 months of regular use. *Psychiatria Danubina*, 2013.
- [65] C. M. Thiel, K. Zilles, and G. R. Fink. Nicotine modulates reorienting of visuospatial attention and neural activity in human parietal cortex. *Neuropsychopharmacology*, January 2005.
- [66] B. Hahn, M. Shoaib, and I. Stolerman. Nicotine-induced enhancement of attention in the five-choice serial reaction time task: the influence of task demands. *Psychopharmacology*, 162(2):129–137, 2002.
- [67] S. J. L. Einöther and T. Giesbrecht. Caffeine as an attention enhancer: reviewing existing assumptions. *Psychopharmacology*, 225(2):251–274, 2013.
- [68] K. A. Fleming, B. D. Bartholow, J. Sable, and M. Pearson. Effects of alcohol on sequential information processing: evidence for temporal myopia. *Psychology of Addictive Behaviors*, 2013.
- [69] T. Ergenoglu, T. Demiralp, Z. Bayraktaroglu, M. Ergen, H. Beydagi, and Y. Uresin. Alpha rhythm of the EEG modulates visual detection performance in humans. *Cognitive Brain Research*, 20(3):376 – 383, 2004.
- [70] K. E. Mathewson, M. Fabiani, G. Gratton, D. M. Beck, and A. Lleras. Rescuing stimuli from invisibility: Inducing a momentary release from visual masking with pre-target entrainment. *Cognition*, 115(1):186 – 191, 2010.
- [71] C. Kranczioch, S. Debener, A. Maye, and A. K. Engel. Temporal dynamics of access to consciousness in the attentional blink. *NeuroImage*, 37(3):947 – 955, 2007.
- [72] S. Sadaghiani, G. Hesselmann, K. J. Friston, and A. Kleinschmidt. The relation of ongoing brain activity, evoked neural responses, and cognition. *Frontiers in Systems Neuroscience*, 4(20), 2010.
- [73] T. Eichele, S. Debener, V. D. Calhoun, K. Specht, A. K. Engel, K. Hugdahl, D. Y. von Cramon, and M. Ullsperger. Prediction of human errors by maladaptive changes in event-related brain networks. *Proceedings of the National Academy of Sciences*, 105(16):6173–6178, 2008.

- [74] D. Ress, B. T. Backus, and D. J. Heeger. Activity in primary visual cortex predicts performance in a visual detection task. *Nature Neuroscience*, 2000.
- [75] L. Johnson, B. Sullivan, M. Hayhoe, and D. Ballard. Predicting human visuomotor behaviour in a driving task. *Philosophical Transactions of the Royal Society B: Biological Sciences*, 2014.
- [76] L. M. Rowland, M. L. Thomas, D. R. Thorne, H. C. Sing, J. L. Krichmar, H. Q. Davis, S. M. Balwinski, R. D. Peters, E. Kloeppe-Wagner, D. P. Redmond, E. Alicandri, and G. Belenky. Oculomotor responses during partial and total sleep deprivation. *Aviation, Space, and Environmental Medicine*, 76(7):C104–C113, 2005.
- [77] M. Russo, M. Thomas, D. Thorne, H. Sing, D. Redmond, L. Rowland, D. Johnson, S. Hall, J. Krichmar, and T. Balkin. Oculomotor impairment during chronic partial sleep deprivation. *Clinical Neurophysiology*, 114(4):723 – 736, 2003.
- [78] M. B. Russo, A. P. Kendall, D. E. Johnson, H. C. Sing, D. R. Thorne, S. M. Escolas, S. Santiago, D. A. Holland, S. W. Hall, and D. P. Redmond. Visual perception, psychomotor performance, and complex motor performance during an overnight air refueling simulated flight. *Aviation, space, and environmental medicine*, 76(Supplement 1):C92–C103, 2005.
- [79] J. Beatty and B. Lucer-Wagoner. The pupillary system. In J. T. Cacioppo, L. G. Tassinary, and G. G. Berntson, editors, *Handbook of Psychophysiology*, pages 142–162. Cambridge University Press, Cambridge, MA, 2nd edition, 2000.
- [80] J. Klingner, B. Tversky, and P. Hanrahan. Effects of visual and verbal presentation on cognitive load in vigilance, memory, and arithmetic tasks. *Psychophysiology*, 48(3):323–332, 2011.
- [81] S. D. Kristjansson, J. A. Stern, T. B. Brown, and J. W. Rohrbaugh. Detecting phasic lapses in alertness using pupillometric measures. *Applied Ergonomics*, 40(6):978 – 986, 2009.
- [82] G. Borghini, L. Astolfi, G. Vecchiato, D. Mattia, and F. Babiloni. Measuring neurophysiological signals in aircraft pilots and car drivers for the assessment of mental workload, fatigue and drowsiness. *Neuroscience & Biobehavioral Reviews*, 2012.
- [83] J. Fu, M. Li, and B. Lu. Detecting drowsiness in driving simulation based on EEG. In B. Mahr and S. Huanye, editors, *Autonomous Systems – Self-Organization, Management, and Control*, pages 21–28. Springer Netherlands, 2008.
- [84] V. Lawhern, S. Kerick, and K. Robbins. Detecting alpha spindle events in EEG time series using adaptive autoregressive models. *BMC Neuroscience*, 14(1):101, 2013.
- [85] M. Simon, E. A. Schmidt, W. E. Kincses, M. Fritzsche, A. Bruns, C. Aufmuth, M. Bogdan, W. Rosenstiel, and M. Schrauf. EEG alpha spindle measures as indicators of driver fatigue under real traffic conditions. *Clinical Neurophysiology*, (6):1168 – 1178, 2011.

- [86] A. Sonnleitner, M. Simon, W. E. Kincses, A. Buchner, and M. Schrauf. Alpha spindles as neurophysiological correlates indicating attentional shift in a simulated driving task. *International Journal of Psychophysiology*, 83(1):110 – 118, 2012.
- [87] J. L. Cantero, M. Atienza, and R. M. Salas. Human alpha oscillations in wakefulness, drowsiness period, and rem sleep: different electroencephalographic phenomena within the alpha band. *Neurophysiologie Clinique/Clinical Neurophysiology*, 32(1):54–71, 2002.
- [88] M. K. Wali, M. Murugappan, and B. Ahmad. Subtractive fuzzy classifier based driver distraction levels classification using EEG. *Journal of Physical Therapy Science*, 25(9):1055–8, 2013.
- [89] NeuroSky. NeuroSky’s eSense™ meters and detection of mental state. 2009.
- [90] J. He, S. Roberson, B. Fields, J. Peng, S. Cielocha, and J. Coltea. Fatigue detection using smartphones. *Journal of Ergonomics*, 2013.
- [91] D. H. Brainard. The psychophysics toolbox. *Spatial Vision*, 10:433–436, 1997.
- [92] R. Mancini and B. Carter. *Op Amps for everyone*. Newnes, 2009.
- [93] R. C. Oldfield. The assessment and analysis of handedness: The Edinburgh inventory. *Neuropsychologia*, 9(1):97–113, March 1971.
- [94] D. J. Buysse, C. F. Reynolds III, T. H. Monk, S. R. Berman, and D. J. Kupfer. The pittsburgh sleep quality index: A new instrument for psychiatric practice and research. *Psychiatry Research*, 28(2):193 – 213, 1989.
- [95] SensoMotoric Instruments. iView X™ Manual. 2011.
- [96] B. J. Roach and D. H. Mathalon. Event-related EEG time-frequency analysis: An overview of measures and an analysis of early gamma band phase locking in schizophrenia. *Schizophrenia Bulletin*, 34(5):907–926, 2008.
- [97] N. I. Fisher. *Statistical Analysis of Circular Data*. Cambridge University Press, January 1996.
- [98] P. Berens. CircStat: a MATLAB toolbox for circular statistics. *Journal of Statistical Software*, 31(10):1–21, 2009.
- [99] D. Alnæs, M. H. Sneve, T. Espeseth, T. Endestad, S. H. P. van de Pavert, and B. Laeng. Pupil size signals mental effort deployed during multiple object tracking and predicts brain activity in the dorsal attention network and the locus coeruleus. *Journal of Vision*, 14(4), 2014.
- [100] Y. Benjamini and D. Yekutieli. The control of the false discovery rate in multiple testing under dependency. *Annals of Statistics*, 29:1165–1188, 2001.
- [101] D. M. Groppe, T. P. Urbach, and M. Kutas. Mass univariate analysis of event-related brain potentials/fields II: Simulation studies. *Psychophysiology*, 2011.

- [102] B. Jones. MATLAB Statistics Toolbox, User's Guide, The MathWorks, 1997.
- [103] J. M. de Sá. *Pattern Recognition: Concepts, Methods and Applications*. Springer Berlin Heidelberg, 2012.
- [104] F. Lotte, M. Congedo, A. Lécuyer, F. Lamarche, and B. Arnaldi. A review of classification algorithms for EEG-based brain-computer interfaces. *Journal of Neural Engineering*, 4(2):R1, 2007.
- [105] M. Petrakos, J. A. Benediktsson, and I. Kanellopoulos. The effect of classifier agreement on the accuracy of the combined classifier in decision level fusion. *Geoscience and Remote Sensing, IEEE Transactions on*, 39(11):2539–2546, November 2001.
- [106] Y. Wang, B. Hong, X. Gao, and S. Gao. Phase synchrony measurement in motor cortex for classifying single-trial EEG during motor imagery. In *Engineering in Medicine and Biology Society; 28th Annual International Conference of the IEEE*, 2006.
- [107] S. Valle, W. Li, and S. J. Qin. Selection of the number of principal components: The variance of the reconstruction error criterion with a comparison to other methods. *Industrial Engineering & Chemistry Research*, 38(11):4389–4401, 1999.
- [108] Y. Liu and Y. F. Zheng. FS_SFS: A novel feature selection method for support vector machines. *Pattern Recognition*, 39(7):1333 – 1345, 2006.
- [109] J. S. Raikwal and K. Saxena. Performance evaluation of SVM and K-Nearest Neighbor algorithm over medical data set. *International Journal of Computer Applications*, 50(14), 2012.
- [110] V. Franc and V. Hlavac. *Statistical Pattern Recognition Toolbox for Matlab. Prague, Czech: Center for Machine Perception, Czech Technical University*, 2004.
- [111] R. Kohavi. A study of cross-validation and bootstrap for accuracy estimation and model selection. In *IJCAI'95 Proceedings of the 14th international joint conference on Artificial intelligence*, volume 14, pages 1137–1145, 1995.
- [112] M. J. Kofler, M. D. Rapport, D. E. Sarver, J. S. Raiker, S. A. Orban, L. M. Friedman, and E. G. Kolomeyer. Reaction time variability in ADHD: A meta-analytic review of 319 studies. *Clinical Psychology Review*, 33(6):795–811, 2013.
- [113] J. Gross, F. Schmitz, I. Schnitzler, K. Kessler, K. Shapiro, B. Hommel, and A. Schnitzler. Modulation of long-range neural synchrony reflects temporal limitations of visual attention in humans. *Proceedings of the National Academy of Sciences of the United States of America*, 101(35):13050–13055, August 2004.
- [114] E. Rodriguez, N. George, J. Lachaux, J. Martinerie, B. Renault, and F. J. Varela. Perception's shadow: long-distance synchronization of human brain activity. *Nature*, 397(6718):430–433, February 1999.

- [115] J. Prado, J. Carp, and D. H. Weissman. Variations of response time in a selective attention task are linked to variations of functional connectivity in the attentional network. *NeuroImage*, 54(1):541–549, 2011.
- [116] G. G. Gregoriou, S. J. Gotts, H. Zhou, and R. Desimone. Long-range neural coupling through synchronization with attention. 176:35 – 45, 2009.
- [117] M. Wendt, A. Kiesel, F. Geringswald, S. Purmann, and R. Fischer. Attentional adjustment to conflict strength: Evidence from the effects of manipulating flanker-target SOA on response times and prestimulus pupil size. *Experimental Psychology*, 2013.
- [118] X. Li, Q. Zhao, L. Liu, H. Peng, Y. Qi, C. Mao, Z. Fang, Q. Liu, and B. Hu. Improve affective learning with EEG approach. *Computing and Informatics*, 29(4):557–570, 2012.
- [119] T. Lan, A. Adami, D. Erdogmus, and M. Pavel. Estimating cognitive state using EEG signals. *Journal of Machine Learning*, 4:1261–1269, 2003.
- [120] A. Borji, D. N. Sihite, and L. Itti. Computational modeling of top-down visual attention in interactive environments. In *Proceedings of the British Machine Vision Conference*, pages 1–12. BMVA Press, 2011.
- [121] P. R. Davidson, R. D. Jones, and M. T. R. Peiris. EEG-based lapse detection with high temporal resolution. *Biomedical Engineering, IEEE Transactions on*, 54(5):832–839, 2007.
- [122] M. Besserve, K. Jerbi, F. Laurent, S. Baillet, J. Martinerie, and L. Garnero. Classification methods for ongoing EEG and MEG signals. *Biological Research*, 40(4):415–437, 2007.